12-2012

Energy and Spectral Efficient Wireless Communications

Guoqing Zhou
University of Arkansas, Fayetteville

ENERGY AND SPECTRAL EFFICIENT WIRELESS COMMUNICATIONS

ENERGY AND SPECTRAL EFFICIENT WIRELESS COMMUNICATIONS

A Dissertation submitted in partial fulfillment
of the requirements for the degree of
Doctor of Philosophy in Electrical Engineering

By

Guoqing Zhou
Shandong University of Science and Technology
Bachelor of Science in Electrical Engineering, 2002
Soongsil University
Master of Science in Electrical Engineering, 2008

December 2012
University of Arkansas

Abstract

Energy and spectrum are two precious commodities for wireless communications. How to improve the energy and spectrum efficiency has become two critical issues for the designs of wireless communication systems. This dissertation is devoted to the development of energy and spectral efficient wireless communications. The developed techniques can be applied to a wide range of wireless communication systems, such as wireless sensor network (WSN) designed for structure health monitoring (SHM), medium access control (MAC) for multi-user systems, and cooperative spectrum sensing in cognitive radio systems.

First, to improve the energy efficiency in SHM WSN, a new ultra low power (ULP) WSN is proposed to monitor the vibration properties of structures such as buildings, bridges, and the wings and bodies of aircrafts. The new scheme integrates energy harvesting, data sensing, and wireless communication into a unified process, and it achieves significant energy savings compared to existing WSNs.

Second, a cross-layer collision tolerant (CT) MAC scheme is proposed to improve energy and spectral efficiency in a multi-user system with shared medium. When two users transmit simultaneously over a shared medium, a collision happens at the receiver. Conventional MAC schemes will discard the collided signals, which result in a waste of the precious energy and spectrum resources. In our proposed CT-MAC scheme, each user transmits multiple weighted replicas of a packet at randomly selected data slots in a frame, and the indices of the selected slots are transmitted in a special collision-free position slot at the beginning of each frame. Collisions of the data slots in the MAC layer are resolved by using multiuser detection (MUD) in the PHY layer. Compared to existing schemes, the proposed CT-MAC

scheme can support more simultaneous users with a higher throughput.

Third, a new cooperative spectrum sensing scheme is proposed to improve the energy and spectral efficiency of a cognitive radio network. A new Slepian-Wolf coded cooperation scheme is proposed for a cognitive radio network with two secondary users (SUs) performing cooperative spectrum sensing through a fusion center (FC). The proposed scheme can achieve significant performance gains compared to existing schemes.

This dissertation is approved for recommendation
to the Graduate Council.

Dissertation Director:

Dr.Jingxian Wu

Dissertation Committee:

Dr. Jia Di

Dr. Scott C. Smith

Dr. Jing Yang

Dissertation Duplication Release

I hereby authorize the University of Arkansas Libraries to duplicate this dissertation when needed for research and/or scholarship.

Agreed _____

Guoqing Zhou

Refused _____

Guoqing Zhou

Acknowledgements

This dissertation could not been done without the support and help from many people. I would like to express my grateful thanks to them in this acknowledgment.

First, I would like to express my deepest gratitude to my dedicated supervisor, Dr. Wu. Without his patient guidance, I can not finish this dissertation. At the first year of my Ph.D. study, he gave me many good training projects, which leads me to the area of wireless communication. In the following three years, he offered me many valuable ideas, guidance and criticisms with his broad knowledge and rich research experience. Besides, he always puts first priority on students and is willing to discuss with me about my research at anytime when he is available. I would like to keep all of his kindness and teaching in my heart forever.

Second, I am also extremely grateful to my dissertation committee members, Dr. Scott C. Smith, Dr. Jing Yang and Dr. Jia Di, who spent their valuable time to serve in my dissertation committee. Their invaluable suggestions and comments are indispensable to the completion of this dissertation.

Moreover, I wish to extend my thanks to current and previous group members. Special thanks should go to Mr. Michael Jamal Isteevan, Mr. Gang Wang, Mrs. Qing Guo, Mrs. Ning Sun, Mr. Michael Walker and Mr. Qi Yang, for their friendship and cooperations.

Last but not least, I would like to thank my family for their support all the way through my Ph.D. study. For my parents, I am thankful to them for their understandings and encouragement. For my wife, Ning Sun, she is always with me to work through all the difficulties, not only in the study but also in the daily life. Without her scarification, it is

impossible for me to obtain this degree.

Contents

List of Figures

List of Papers

- **Chapter 2**, Guoqing Zhou and Jingxian Wu, "Unifying energy harvesting, sensing, and communication for ultra-low power structure health monitoring," Submitted to *IEEE Trans. Aerospace and Electronic Systems*, May 2012.

- **Chapter 3**, Jingxian Wu and Guoqing Zhou, "Cross-layer collision-tolerant MAC with message passing detection", to appear in *Proc. IEEE Global Commun. Conf. GLOBECOM'12*, Dec. 2012.

- **Chapter 4**, Guoqing Zhou, Jingxian Wu, Gang Wang, and Geoffrey Ye Li, "Collision-tolerant media access control with asynchronous users," Submitted to *IEEE Trans. Wireless Commun.*, Oct. 2012.

- **Chapter 5**, Guoqing Zhou, Jingxian Wu, and Kazem Sohraby "Cooperative spectrum sensing with a progressive MAP detection algorithm,", in *Proc. IEEE Global Commun. Conf. GLOBECOM'11*, Dec. 2011.

- **Chapter 6**, Ning Sun, Guoqing Zhou, and Jingxian Wu "Cooperative spectrum sensing with Slepian-Wolf coded cooperations", in *Proc IEEE Intern. Conf. Commun ICC'12*, vol.1, pp. 1512-1516, June 2012.

Chapter 1

Introduction

1.1 Background and Motivation

The most precious commodities for wireless communications are energy and spectrum. With the rapid growth of high data rate applications, more and more energy and spectrum resources are required in wireless communications to maintain the quality of service (QoS). At the mean time, ultra-low power (ULP) consumption is one of the most formidable challenges faced by the development of wireless sensor networks (WSN). Furthermore, in recent years, with the increasing demand in wireless services, there is a dramatic increase in the requirement of radio spectrum. Unfortunately, most of the spectrums have been already allocated and it is extremely hard to find vacant bands to deploy new services. Hence, the efficient utilization of the existing precious spectrum is critical for the long term evolution of communication. Therefore, how to improve the energy and spectral efficiency have become two critical issues for the design of the next generation wireless communications.

Energy efficient communication in WSN: WSN has a wide range of applications such as environmental monitoring, structure health monitoring (SHM), biomedical sensing, and military applications. The sensor nodes in a WSN are usually expected to operate

uninterrupted over a long period of time, under the constraints of extremely limited battery capacity or very small energy scavenging devices. Therefore, one of the most formidable challenges faced by the design of the WSNs is how to develop ULP wireless communication technologies that can work over an extended period of time with limited energy sources. In WSNs, a large number of sensor nodes are densely deployed to sense the physical properties of the phenomenon and the neighbor nodes are often very close to each other. As a result, the densely deployed sensors coupled with the physical properties of the sensing phenomenon introduce correlations in both spatial and temporal domains. Hence, the spatio-temporal correlation can be utilized in WSNs to improve the energy efficiency.

Energy and spectral efficient communication in multi-user system: Media access control (MAC) protocols are critical to the efficient operations of wireless networks designed to support multiple simultaneous users. In conventional MAC schemes such as slotted ALOHA (SA) or carrier sensing multiple access (CSMA), signals collided at a receiver will be discarded and retransmitted. This results in a waste of the precious spectrum and energy resources. However, the signals collided at the receiver still contain salient information that can be utilized to facilitate the detection. The signal collision can be resolved by resorting to cross layer design techniques. The methodology of cross layer design has emerged to improve the system performance as well as energy efficiency. The cross layer design between the physical (PHY) and MAC layer is particular important because there are rich interactions between these two layers due to the unique properties of wireless communication systems. CT-MAC coupled with PHY-MAC cross layer designs has the potential to yield significant performance gains over conventional MAC schemes.

Energy and Spectral efficient communication in cognitive radio network: Cognitive radio (CR), which provides flexible spectrum accesses by dynamically sensing and adapting to the surrounding radio environment, is quickly emerging as one of the most promising technologies for improving the utilization of the precious spectrum resources. The primary user (PU) is the licensed user in the network, which has the first priority to use the network. Secondary users (SUs) are the unlicensed ones, which need to detect the spectrum holes in the time-frequency plane and avoid interference to the licensed or primary PUs. Hence, spectrum sensing, which detects the spectrum holes in the time and frequency domains, is a key function of cognitive radio to avoid the harmful interference to the licensed users. In reality, the performance of spectrum sensing is negatively affected by factors such as multi-path fading, shadowing, and noise. To overcome these problems, cooperative spectrum sensing has emerged to improve the detection performance by exploiting spatial diversity. By cooperation, CR users make a combined decision based on their shared sensing information, which is more accurate than each individual local decision.

1.2 Objectives

The primary goal of this dissertation is to develop new wireless communication techniques and system structures, which can efficiently utilize the precious energy and spectrum resources in wireless communication systems. The specific objectives leading to this goal are as follows. First, in order to realize the energy efficient communication in WSNs, we propose a ULP structure health monitoring systems by unifying energy harvesting, sensing, and communication into a unified process. The spatio-temporal correlations among the deployed

sensors are fully utilized to improve the system performance. As a result, considerable improvement in energy efficiency is achieved with the proposed scheme. Second, new cross-layer CT-MAC schemes are developed by exploiting the interactions between the MAC layer and PHY layer. The CT-MAC scheme can effectively extract the salient information from the signals collided in the PHY layer by utilizing signal processing technologies in the PHY layer. The new CT-MAC schemes lead to significant improvement in terms of both energy efficiency and spectral efficiency. Third, new cooperative spectrum sensing techniques are developed for a CR network, where multiple SUs cooperate with each other to detect whether the PU is active or not. The proposed scheme aims to maximize the probability of detecting the PUs while maintain a certain level of false alarm probability. The cooperation among the SUs is achieved through distributed coding techniques. As a result, the interferences from the unlicensed users to the licensed users are minimized and the utilization of the spectrum efficiency is improved.

1.3 Dissertation Outline

The outline of this dissertation is presented as follows.

Chapter 2: In this chapter, a ULP WSN is proposed to monitor the vibration properties of critical structures such as buildings, bridges, and the wings and bodies of aircrafts. The new scheme integrates energy harvesting, data sensing, and wireless communication into a unified process, and it is fundamentally different from all the existing WSNs.

Chapter 3: A cross-layer CT MAC scheme is proposed in this chapter. In the MAC layer, each user transmits multiple weighted replicas of a packet at randomly selected data slots in a frame. Collisions of the data slots in the MAC layer are resolved by using multiuser detection

(MUD) in the PHY layer. The MUD is performed by employing a modified message passing (MP) algorithm.

Chapter 4: A frequency-domain cross-layer CT-MAC is proposed for the up-links of a broadband wireless networks with asynchronous users. The collision tolerance is achieved with a frequency-domain on-off accumulative transmission (FD-OOAT) scheme, where the frequency selective spectrum is divided into a large number of orthogonal sub-channels, and each symbol is transmitted over a small subset of the sub-channels to reduce the probability of collision.

Chapter 5: In this chapter, a new cooperative spectrum sensing algorithm is proposed for a cognitive radio network with multiple SUs sharing spectrum with one or more PUs. Unlike most previous spectrum sensing algorithms that do not consider the time domain traffic statistics of the PU, the algorithm in this chapter is developed by exploiting the statistical properties of the PU's transmission pattern, which is modeled with a Markov chain with two states: busy (1) and idle (0). Each SU performs energy detection based on an observation of the Markov chain, and the detection results are forwarded to a fusion center (FC) through a noisy channel. The FC recovers the decisions of the SUs by using a new progressive maximum *a posteriori* (MAP) algorithm, where the *a priori* probability essential to the MAP detection is obtained by progressively estimating the transition probabilities of the Markov chain.

Chapter 6: A new Slepian-Wolf coded cooperation scheme is proposed for a cognitive radio network with two SUs performing cooperative spectrum sensing through a FC. Instead of making a hard decision based on the local sensing results, the SUs quantize the measured energy statistics with a Lloyd-Max quantizer, and forward the quantized information to the FC.

Chapter 7: The main contributions of this dissertation are summarized and several new future research directions are discussed in this chapter.

Chapter 2

Unifying Energy Harvesting, Sensing, and Communication for Ultra-low Power Structure Health Monitoring

2.1 Abstract

A new ultra-low power (ULP) wireless sensor network (WSN) is proposed to monitor the vibration properties of critical structures such as buildings, bridges, and the wings and bodies of aircrafts. The new scheme integrates energy harvesting, data sensing, and wireless communication into a unified process, and it is fundamentally different from all the existing WSNs. In the new WSN, self-powered sensors are employed to harvest vibration energy and measure vibration intensity simultaneously, by utilizing the fact that *the harvested energy accumulated through time is proportional to the vibration amplitude and frequency.* Once the harvested energy reaches a threshold, it is released as an impulse with a wireless transmitter. An estimate of the structure vibration intensity can then be obtained by measuring the number of binary impulses in a unit time. Such an approach does not require complicated analog-to-digital conversion or signal processing, and it can achieve an ULP performance unrivaled by existing technologies. Optimum and sub-optimum impulse density estimation algorithms are proposed to take advantage of the spatial correlation among signals from

the sensors. Analytical and simulation results demonstrate that the proposed scheme can efficiently operate at a low signal-to-noise ratio (SNR).

keywords

Wireless sensor network, structure health monitoring, energy harvesting, maximum *a posteriori* (MAP) detection

2.2 Introduction

Wireless sensor network (WSN) designed for structure health monitoring (SHM) is expected to operate uninterrupted over a long period of time, under the constraints of extremely limited battery capacity or very small energy scavenging devices. Ultra-low power (ULP) consumption is one of the most formidable challenges faced by the development of wireless sensor networks (WSN) for the autonomous monitoring of critical structures, such as bridges, buildings, [1], and aircrafts and spacecrafts [2]. Hence, an extremely stringent power budget is required to power the operation of a wireless sensor, which transmits the measured data to a fusion center (FC) through a wireless link.

Recently there have been considerable efforts devoted to the development of WSN for SHM systems [1] – [6]. Most of the sensing systems are built with commercial-off-the-shelf (COTS) wireless sensor nodes, such as Mica-Z Mote [3], [4], Mica-2 Mote [5], and iMote [6], etc. Even though these modules are designed with low power consumption as one of the design objectives, their structures still follow a conventional sensing framework, which includes sensing, analog-to-digital conversion (ADC), digital signal processing (DSP), and wireless transmission. These modules are designed separately, and they do not directly take

advantage of the unique features of SHM systems. In order to achieve ULP performance, we need to break free from the conventional sensing frameworks, and seek fundamentally new WSN structures. SHM possess many unique features that can be exploited to facilitate the ULP design. Many of the structures, such as bridges, have very slow changing rate, e.g., new data might only need to be collected once every few seconds or minutes. As a result, SHM have long latency tolerance with ultra-low data rate. In addition, Data collected by spatially distributed sensors often contain redundancy [10], [16], which can be used to achieve better power efficiency.

In this chapter, we propose a new type of battery-free ULP WSN by integrating energy harvesting, data sensing, and wireless communication into a unified process. The system is designed to monitor the structure vibration intensity, such as vibration amplitude and frequency, which provides useful information about the local stress intensity and the dynamic behaviors of the structure [7]. Vibration generates energy that can be harvested by a sensor with piezoelectric devices [8], [9]. The harvested energy is expected to power the operations of the entire sensor node. However, due to the low efficiency of current piezoelectric materials, the harvested energy level is usually much lower compared to that required to perform any regular sensing, ADC, DSP, or communication functions. Therefore, conventional sensing or communication techniques can no longer be applied in such a system.

We propose to address this problem by utilizing the correlation between energy and vibration, *i.e.*, the harvested energy accumulated through time is proportional to the local vibration amplitude and frequency. Once the harvested energy reaches a predefined threshold, the energy is released in the form of an impulse. The receiver can then obtain an estimate of the vibration intensity by observing the impulse density, *i.e.*, the number of

impulses in unit time. Such an integrated harvesting, sensing, and communication (IHSC) process exploits the unique features of SHM systems, and it is fundamentally different from conventional sensing schemes.

The impulses from the sensors are detected at the FC through an optimum multi-node maximum *a posteriori* (MAP) detector, which exploits the spatial correlation among the signals from the sensors. It should be noted that the proposed multi-node MAP detector needs to detect the presence of impulses from different sensors, and this is different from the decentralized detection in the literature [11] - [15], where the FC only needs to detect the presence of a single event by collecting the noise-free or noisy local detections from a number of sensors. The multi-node MAP detector requires the *a priori* probabilities of the impulses, which are not readily available at the receiver. We propose an iterative method to estimate the *a priori* probability of the impulses at the FC. Simulations show that the iterative method usually converges in less than 5 iterations. The theoretical mean square error (MSE) of the estimated impulse density is derived for a system operating in a Rayleigh fading channel. Both analytical and simulation results show that the proposed IHSC scheme can operate at a very low signal-to-noise ratio (SNR) by effectively utilizing the spatial signal correlation.

The remainder of this chapter is organized as follows. A new WSN structure with integrated harvesting, sensing and communication is presented in Section 2.3. The optimum impulse density estimation algorithms and the corresponding theoretical analysis are proposed in Section 2.4. Simulation results are given in Section 2.5, and Section 2.6 concludes the chapter.

2.3 A New WSN Structure with Integrated Harvesting, Sensing, and Communication

Consider a WSN consisting of a large number of low cost battery-free wireless sensor nodes uniformly distributed over the monitored structure. As illustrated in Fig. 2.1, each sensor node is equipped with a self-powered nanowire sensor [8] for energy harvesting and data sensing, and a simple radio frequency (RF) transmitter, such as a simple resistor-capacitor (RC) oscillator. The sensor performs the IHSC operation described as follows.

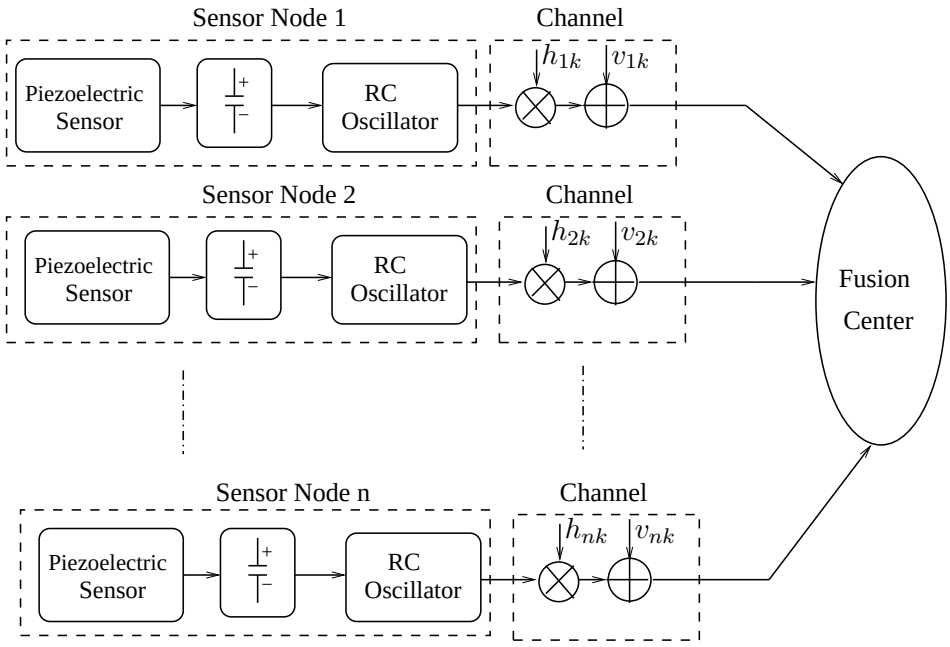

Figure 2.1: The block diagram of the wireless sensor network structure with integrated harvesting, sensing, and communication.

Definition 2.1: *(IHSC)*: The energy collected by the nanowire piezoelectric sensor is used to charge a capacitor. Once the harvested energy reaches a predefined threshold, E_{TH}, the energy is released as a single impulse through the RF transmitter. Then the receiver can obtain an estimate of the structure vibration intensity by measuring the impulse density. ■

In the above IHSC procedure, it is assumed that the energy harvesting rate, *i.e.*, the

energy harvested in unit time, is proportional to the structure vibration intensity, *i.e.*, vibration amplitude and frequency. As a result, the amount of time required for the harvested energy to reach E_{TH} is inversely proportional to the vibration intensity. Therefore, the structure vibration information is carried in the form of the time delay between two consecutive impulses, or the number of impulses in unit time. The proposed IHSC scheme utilizes the correlation among structure vibration, energy, and time to get an estimate of the structure vibration intensity.

Given the fact that the structure vibration is highly correlated across the spatial domain, the density information collected by spatially distributed sensors is correlated. Such correlation information can be exploited by the FC to increase the estimation accuracy even at an extremely low SNR. Optimum and sub-optimum impulse density estimation algorithms will be developed in the next section to exploit the spatial correlation among sensors.

To facilitate analysis, we have the following assumptions regarding the statistical properties of the structure vibration.

A.1) The amount of time for the harvested energy to reach E_{TH} is an exponentially distributed random variable (RV) with mean μ. A higher vibration intensity yields a smaller μ.

A.2) The time is discretized into small intervals with duration $T_s << \mu$. For each interval, the receiver performs detection to find whether there is an impulse in the interval. Define a RV, x_{nk}, where $x_{nk} = 1$ represents an impulse is transmitted by the node n at the k-th detection interval and 0 otherwise. Based on Assumption A.1), it can be easily shown that

x_{nk} is a Bernouli RV with the parameter

$$p = P(x_{nk} = 1) = 1 - e^{-\frac{T_s}{\mu}}. \tag{2.1}$$

A.3) Data collected from different sensor nodes are correlated. The vibration correlation is translated to the correlation among the Bernouli RVs, $\{x_{nk}\}_{n=1}^{N}$. The normalized covariance coefficient between x_{mk} and x_{nk} is

$$\phi_{mn} \triangleq \frac{\mathbb{E}\{[x_{mk} - \bar{x}_{mk}][x_{nk} - \bar{x}_{nk}]\}}{\sqrt{\sigma_m^2 \sigma_n^2}} = \theta^{|m-n|}, \tag{2.2}$$

where $\theta \in [0, 1]$ is the spatial correlation coefficient, $\bar{x}_{mk}$ is the mean of x_{mk}, σ_m^2 is the variance of x_{mk} and $\mathbb{E}(\cdot)$ is the expectation operator.

A.4) Sensors deliver the impulses to the FC through an orthogonal media access control (MAC) scheme, such as the frequency division multiplexing access (FDMA), to achieve a collision-free communication at the FC.

With the above assumptions, the signal received by the FC from the n-th sensor at the k-th interval can be represented as

$$y_{nk} = \sqrt{E_{\mathrm{TH}}} \cdot h_{nk} \cdot x_{nk} + v_{nk} \tag{2.3}$$

where $\sqrt{E_{\mathrm{TH}}}$ is the amplitude of the transmitted signal, h_{nk} is the gain of the channel, and v_{nk} is the additive white Gaussian noise (AWGN) with double-sided power spectral density $N_0/2$.

Based on the model in (2.3), define the average impulse density of the n-th sensor node over a duration of KT_s as

$$V_n = \frac{\sum_{k=1}^{K} x_{nk}}{KT_s}. \tag{2.4}$$

With the proposed IHSC scheme, the impulse density is proportional to the vibration intensity of the monitored structure, thus it can be used as an important indicator of the health condition of the structure.

2.4 Optimum Impulse Density Estimation

In this section we present an optimum receiver for the estimation of the impulse density, V_n, in a multi-node system employing the IHSC scheme.

2.4.1 Iterative Impulse Density Estimation

To utilize the spatial data correlation, we will jointly estimate the data from all the nodes, $\mathbf{x}_k = [x_{1k}, \cdots, x_{nk}]^T \in \mathcal{B}^{N\times 1}$, based on the received signal vector, $\mathbf{y}_k = [y_{1k}, \cdots, y_{Nk}]^T \in \mathcal{C}^{N\times 1}$, where $(\cdot)^T$ represents matrix transpose, and $\mathcal{C}$ is the set of complex numbers. At the detection interval k, the multi-node MAP detection of $\mathbf{x}_k$ is

$$\hat{\mathbf{x}}_k = \underset{\mathbf{b}\in\mathcal{B}^N}{\operatorname{argmax}}\, p(\mathbf{y}_k|\mathbf{x}_k = \mathbf{b})P(\mathbf{x}_k = \mathbf{b}), \tag{2.5}$$

where $p(\mathbf{y}_k|\mathbf{x}_k{=}\mathbf{b})$ takes the form of a multi-variant Gaussian probability density function (pdf) with the mean vector $\mathbf{b}$ and the covariance matrix $N_0\mathbf{I}_N$, with $\mathbf{I}_N$ being a size-N identity matrix,

$$p(\mathbf{y}_k|\mathbf{x}_k{=}\mathbf{b}){=}\frac{1}{(\pi N_0)^N}\exp\left\{-\frac{1}{N_0}\sum_{n=1}^{N}\left|y_{nk}{-}\sqrt{E_{\mathrm{TH}}}h_{nk}b_n\right|^2\right\}. \tag{2.6}$$

It should be noted that $\mathbf{x}_k$ are mutually correlated with the normalized correlation coefficient defined in (2.2).

The MAP detection rule described in (2.5) requires the knowledge of $p_{\mathbf{b}} \triangleq P(\mathbf{x}_k = \mathbf{b})$,

which is unknown at the receiver. To solve this problem, we propose to perform joint estimation of $p_{\mathbf{b}}$ and $\mathbf{x}_k$ with an iterative method.

At the beginning of the iteration, it is assumed that the data from all the nodes are uncorrelated, and the initial value of the *a priori* probability is $p_{\mathbf{b}}^{(0)} = 0.5^N$. During the i-th iteration, we apply $p_{\mathbf{b}}^{(i-1)}$ from the $(i-1)$-th iteration to (2.5), and get the estimates $\hat{\mathbf{x}}_k^{(i)}$, for $k = 1, \cdots, K$. The estimated values are then used to obtain an estimate of $p_{\mathbf{b}}$ as

$$p_{\mathbf{b}}^{(i)} = \frac{1}{K} \sum_{k=1}^{K} \delta(\hat{\mathbf{x}}_k^{(i)} - \mathbf{b}), \quad \forall \mathbf{b} \in \mathcal{B}^{N \times 1} \tag{2.7}$$

where the indicator function $\delta(\mathbf{0}) = 1$, and $\delta(\mathbf{x}) = 0$ if $\mathbf{x} \neq \mathbf{0}$. It should be noted that the estimation of the *a priori* probability in (2.7) implicitly takes into consideration of the mutual correlation among the data in $\mathbf{x}_k$.

The iteration will be terminated if $\max_{\mathbf{b}} \{p_{\mathbf{b}}^{(i)} - p_{\mathbf{b}}^{(i-1)}\} < \epsilon$, or the number of iterations exceeds a predefined threshold. At the end of the iteration, we can get an estimate of the impulse density of the n-th node as

$$\hat{V}_n = \frac{1}{KT_s} \sum_{k=1}^{K} \hat{x}_{nk}. \tag{2.8}$$

Simulation results demonstrate that the proposed iteration method usually converges after less than 5 iterations.

The optimum MAP detection requires the exhaustive search of the space $\mathcal{B}^N$, and the complexity grows exponentially with the node number, N. In a practical environment, the correlation between two nodes decreases as their distance increases. Therefore, joint detection of two nodes that are further apart would render very small performance gains over the case that they are detected separately.

In recognition of this fact, when N is large, we propose to divide the N nodes into G groups. Each group contains up to $N_g = \lceil \frac{N}{G} \rceil$ adjacent nodes. The iterative MAP algorithm can then be applied to each group separately. Such a method features a tradeoff between complexity and performance. The optimum performance is obtained by setting $N_g = N$ with the highest complexity. The complexity can be reduced by decreasing N_g, at the cost of slightly decreased performance. Our simulation results show that the performance at $N_g = 4$ is very similar to its optimum counterpart for a wide range of correlation coefficient.

2.4.2 Performance Analysis

The MSE of the estimated impulse density in a multi-node system with correlated information is presented in this section.

To facilitate analysis, define $U_n = \sum_{k=1}^{K} x_{nk}$, and $\hat{U}_n = \sum_{k=1}^{K} \hat{x}_{nk}$. Then both U_n and $\hat{U}_n$ are binomial RVs, *i.e.*, $U_n \sim B(K, p)$, and $\hat{U}_n \sim B(K, q(N, \theta))$, with $p = P(x_{nk} = 1)$ and $q(N, \theta) = P(\hat{x}_{nk} = 1 | N, \theta)$. Then the MSE can be written as $\sigma^2 = \frac{1}{(KT_s)^2} \mathbb{E}\left(|U_n - \hat{U}_n|^2 \right)$, and it can be calculated from the following proposition.

Proposition 2.1: For a multi-node system that employs the optimum multi-node MAP detection, the MSE of the estimated impulse density for each sensor node can be calculated by

$$\sigma^2 = \frac{1}{KT_s^2} \left\{ (K-1)[p - q(N,\theta)]^2 + p + q(N,\theta) - 2\alpha(N,\theta) \right\}. \tag{2.9}$$

where $\alpha(N, \theta) = \mathbb{E}[x_{nk} \hat{x}_{nk} | N, \theta]$ is the cross-correlation between x_{nk} and $\hat{x}_{nk}$.

Proof: The proof is in Appendix 2.7.1. ■

The calculation of the MSE requires the knowledge of $q(N,\theta)$ and $\alpha(N,\theta)$. The analytical evaluations of the two parameters for arbitrary N are quite tedious. Here we only give the analytical expressions for $N=1$, *i.e.*, the information from each node is detected independently, thus $q(1,\theta)=q(1)$ because the correlation θ is not used during the detection.

Lemma 2.1: The value of $q(1)=P(\hat{x}_{nk}=1|N=1)$ in a Rayleigh fading channel is given as follows

$$q(1)=p(1-P_m)+(1-p)P_f, \tag{2.10}$$

where

$$P_m{=}P\{\hat{x}_{nk}{=}0|x_{nk}{=}1\}{=}\int_0^\infty Q\left(\frac{E_{\mathrm{TH}}\cdot x-\eta_{10}}{\sqrt{2N_0\cdot E_{\mathrm{TH}}\cdot x}}\right)\exp(-x)dx, \tag{2.11a}$$

$$P_f{=}P\{\hat{x}_{nk}{=}1|x_{nk}{=}0\}{=}\int_0^\infty Q\left(\frac{E_{\mathrm{TH}}\cdot x+\eta_{10}}{\sqrt{2N_0\cdot E_{\mathrm{TH}}\cdot x}}\right)\exp(-x)dx, \tag{2.11b}$$

are the probabilities of missing detection and false alarm, respectively,

$Q(x)=\frac{1}{\sqrt{2\pi}}\int_x^\infty \exp\left(-\frac{u^2}{2}\right)du$ is the Gaussian-Q function, and $\eta_{10}=N_0\log\frac{1-p}{p}$.

Proof: The proof is in Appendix 2.7.2 ■

The cross-correlation $\alpha(1)=\alpha(1,\theta)$ can be evaluated as $\alpha(1)=P(\hat{x}_{nk}=1,x_{nk}=1)=(1-P_m)p$.

The probability expressions of missing and false alarm given in Lemma 2.1 involve integrations over infinite limits, which might cause instability during numerical evaluations. We propose to calculate the results in Lemma 2.1 by using the Laguerre's method [20]

$$\int_0^\infty f(a)\exp(-a)da=\sum_{i=1}^{M}w_i f(a_i)+R_M, \tag{2.12}$$

where a_i is the i-th zeros of the Lagueree polynomials $L_I(a)$, weights w_i is defined as $w_i=\frac{a_i}{(M+1)^2[L_{I+1}(a_i)]^2}$, and R_M is the remainder term.

Based on (2.12), P_m and P_f in a Rayleigh fading channel can be represented as,

$$P_m \approx \sum_{i=1}^{M} w_i Q\left(\frac{E_{\mathrm{TH}} \cdot x_i - \eta_{10}}{\sqrt{2N_0 \cdot E_{\mathrm{TH}} \cdot x_i}}\right),$$
$$P_f \approx \sum_{i=1}^{M} w_i Q\left(\frac{E_{\mathrm{TH}} \cdot x_i + \eta_{10}}{\sqrt{2N_0 \cdot E_{\mathrm{TH}} \cdot x_i}}\right). \tag{2.13}$$

When $N > 1$, the value of $q(N, \theta)$ and $\alpha(N, \theta)$ can be evaluated through numerical simulations, the results of which can then be substituted into (2.9) to obtain the MSE.

2.5 Simulation Results

Simulation results are presented in this section to verify the performance of the proposed ULP IHSC scheme and the optimum and sub-optimum impulse density estimation algorithms.

In the simulation, it is assumed that the mean, μ, of the exponentially distributed energy harvesting time is 1 s. The detection duration is $T_s = 10$ ms. The correlated Bernoulli RVs, x_{nk}, are generated by using the method described in [21]. The iterative impulse density detection is performed over 100 s, which corresponds to $K = 10^4$ detection intervals. The average SNR is calculated as $\nu = \frac{E_{\mathrm{TH}} T_s}{N_0 \mu}$. Unless otherwise stated, the receiver does not have any *a priori* knowledge of the probability, $P(\mathbf{x}_k)$, or spatial correlation coefficient, θ.

Fig. 2.2 shows the MSE of the estimated impulse density for a one-node and a two-node system with the optimum MAP detection at the FC. The simulation results obtained from systems with both known and unknown *a priori* probability at the receiver are plotted in the figure for comparison. The spatial correlation coefficient of the two-node system is $\theta = 0.9$. We have the following observations of the results. First, the system can operate at extremely low SNR due to the low duty cycle and the innovative IHSC scheme. When SNR $= 0$ dB, an MSE of 2×10^{-4} and 3×10^{-3} is achieved by the one-node and two-node systems,

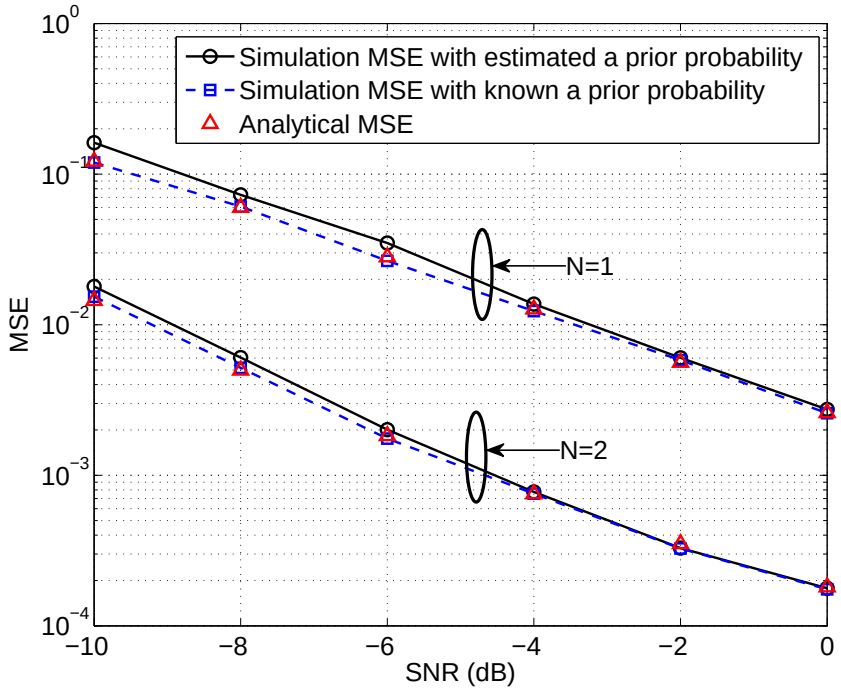

Figure 2.2: MSE for systems with optimum impulse density estimation.

respectively. Second, when SNR > -4 dB, the iterative estimation methods with unknown *a priori* probability can achieve a performance that is almost identical to that of a system with known *a priori* probability. This demonstrates the effectiveness of the proposed iterative estimation method. Third, the analytical results match very well with the simulation results when the SNR > -4 dB. Fourth, at MSE $= 10^{-2}$, the two-node system outperforms the one-node system by 5.5 dB. The performance improvement is contributed by the utilization of the spatial node correlation.

The impact of the spatial correlation coefficient, θ, on the MSE performance is shown in Fig. 2.3 for a two-node system. As expected, the MSE performance improves consistently as θ increases. At MSE $= 10^{-3}$, the system with $\theta = 1$ outperforms that with $\theta = 0.5$ by 6.3 dB. The results demonstrate that the proposed algorithm can effectively utilize the spatial correlation between the nodes. Meanwhile, it shows that the stronger the spatial correlation,

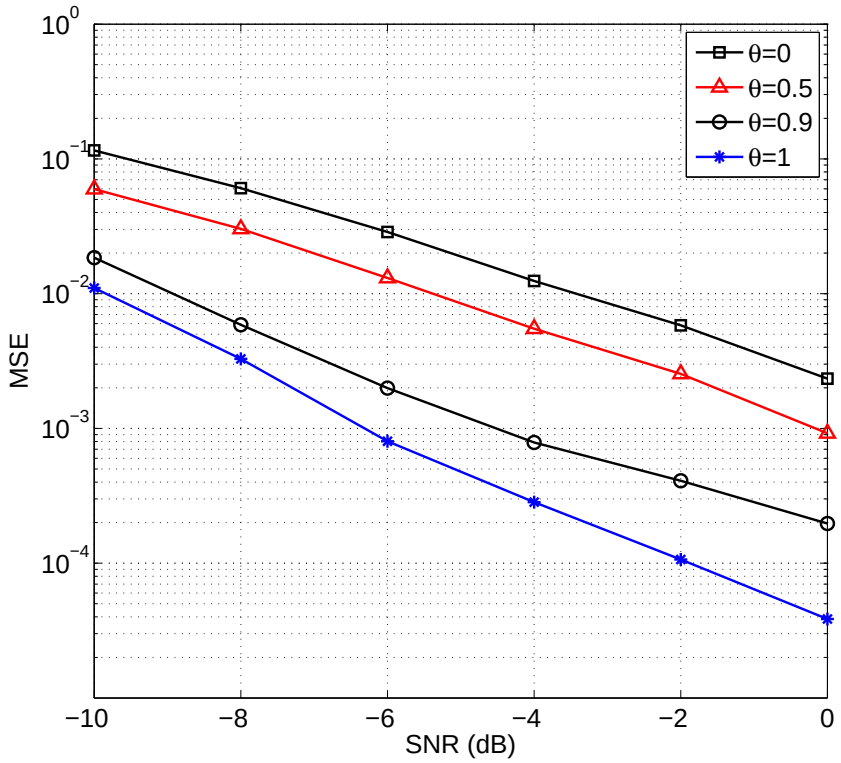

Figure 2.3: MSE with different values of spatial correlation coefficient, θ.

the better performance can be obtained.

In Fig. 2.4, the MSE of estimated impulse density is shown for a multi-node system using MAP detection scheme with different group size at the FC. The SNR is -10 dB. As expected, the performance improves as the group size increases. Most of the performance gains are achieved when $N_g < 4$, and they gradually diminish as $N_g \geq 4$, for all the systems considered in this example. Based on the results, a window size of 4 yields the best tradeoff between complexity and performance for a wide range of the correlation coefficient, θ.

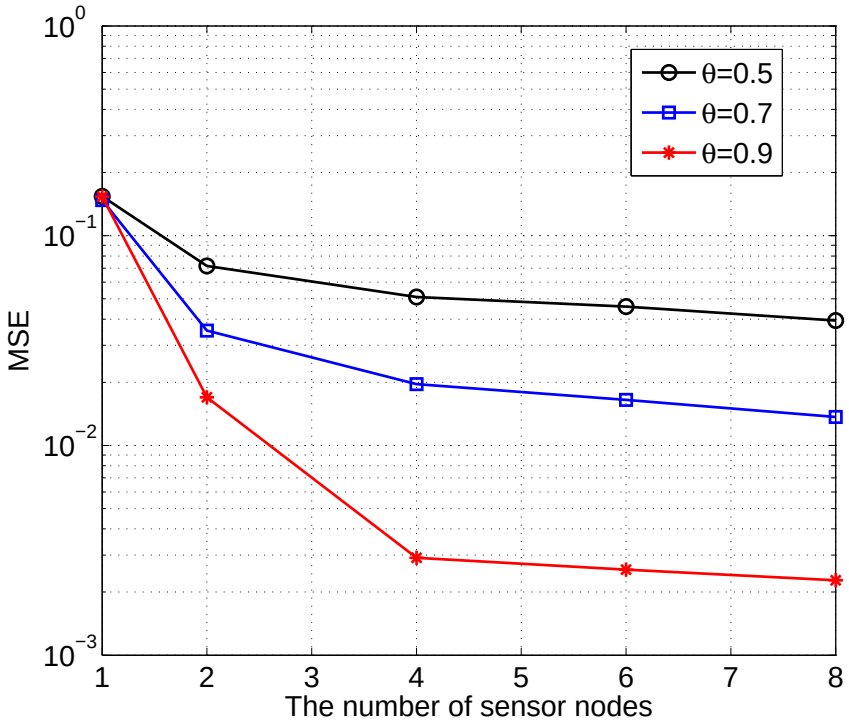

Figure 2.4: MSE for systems with the sub-optimum impulse density estimation.

2.6 Conclusions

A new paradigm of integrated harvesting, sensing, and communication scheme was proposed for ultra-low power structure health monitoring. The IHSC scheme was designed by exploiting the correlation between the harvested energy and vibration intensity. The structure vibration information is carried as the densities of the impulses generated by the sensors. An optimum multi-node MAP detector with iterative *a priori* probability estimation was developed to estimate the impulse densities from the spatially distributed sensor nodes. The theoretical MSE of the estimated impulse density was derived for a one-node system operating in a Rayleigh fading channel. Both the theoretical and simulation results indicated that the proposed algorithm can effectively utilize the spatial correlation among the sensors. The system can operate effectively at a SNR as low as -10 dB without battery or external energy

sources.

2.7 Appendix

2.7.1 Proof of Proposition 2.1

The MSE can be written as $\sigma^2 = \frac{1}{(KT_s)^2}\left[\mathbb{E}(U_n^2) - 2\mathbb{E}(U_n\hat{U}_n) + \mathbb{E}(\hat{U}_n^2)\right]$. Since U_n and $\hat{U}_n$ are binomial RVs, we have $\mathbb{E}(U_n^2) = Kp(Kp - p + 1)$, and $\mathbb{E}(\hat{U}_n^2) = Kq(N,\theta)[Kq(N,\theta) - q(N,\theta) + 1]$.

Based on the definition of U_n and $\hat{U}_n$, we have

$$\mathbb{E}(U_n\hat{U}_n) = \sum_{\substack{j,k=1 \\ j\neq k}}^{K} pq(N,\theta) + \sum_{k=1}^{K}\mathbb{E}[x_{nk}\hat{x}_n(k)]. \tag{2.14}$$

Combining the above equations leads to (2.9).

2.7.2 Proof of Lemma 2.1

When $N = 1$, the MAP detector in (2.5) decides $\hat{x}_{nk} = \hat{b}$ given that $x_{nk} = b$ was transmitted when

$$\left|y_{nk} - \sqrt{E_{\mathrm{TH}}}\cdot h_{nk}\cdot\hat{b}\right|^2 - \left|y_{nk} - \sqrt{E_{\mathrm{TH}}}\cdot h_{nk}\cdot b\right|^2 < \eta, \tag{2.15}$$

where $\eta = N_0\cdot\log\frac{P(x_{nk}=\hat{b})}{P(x_{nk}=b)}$, and $b,\hat{b}\in\mathcal{B}$. The decision rule in (2.15) can be alternatively written as

$$\mathbf{Z} < \eta - E_{\mathrm{TH}}|h_{nk}|^2, \tag{2.16}$$

where $\mathbf{Z} = 2\Re\{\sqrt{E_{\mathrm{TH}}}\cdot h_{nk}\cdot d\cdot v_{nk}\}$, $d = b - \hat{b}$. The decision variable $\mathbf{Z}$ conditioned on h_{nk} and d is a Gaussian random variable with 0 mean and variance $\sigma_{\mathbf{Z}}^2 = 2N_0\cdot E_{\mathrm{TH}}\cdot|h_{nk}|^2$. Then

the conditional probability

$$P\left\{\hat{x}_{nk}=\hat{b}|x_{nk}=b,h_{nk}\right\}=P\left(\mathbf{Z}<\eta-E_{\mathrm{TH}}|h_{nk}|^2\right)=Q\left(\frac{E_{\mathrm{TH}}|h_{nk}|^2-\eta}{\sqrt{2N_0\cdot E_{\mathrm{TH}}\cdot|h_{nk}|^2}}\right), \quad (2.17)$$

In a Rayleigh fading channel, $f_{|h_{nk}|^2}(x)=\exp(-x), \text{for } x\geq 0$. Then the unconditional probability is

$$P\left\{\hat{x}_{nk}=\hat{b}|x_{nk}=b\right\}=\int_0^\infty Q\left(\frac{E_{\mathrm{TH}}\cdot x-\eta}{\sqrt{2N_0\cdot E_{\mathrm{TH}}\cdot x}}\right)\exp(-x)dx. \quad (2.18)$$

The results in (2.10) and (2.11) can then be obtained by substituting (2.18) into $P(\hat{x}_{nk}=1)=pP(\hat{x}_{nk}=1|\hat{x}_{nk}=1)+(1-p)P(\hat{x}_{nk}=1|\hat{x}_{nk}=0)$.

2.8 References

[1] J. P. Lynch and K. J. Loh, "A summary review of wireless sensors and sensor networks for structural health monitoring," *The Shock and Vibration Digest*, Vol. 38, No. 2, pp. 91 128, Mar. 2006.

[2] C. Escriba, J. Fourniols, "New real-time structural health monitoring microsystem for aircraft propeller blades," *IEEE Trans. Aerospace and Electronic Systems*, vol. 27, pp. 29 - 41, Feb. 2012.

[3] K. Chintalapudi, T. Fu, J. Paek, N. Kothari, S. Rangwala, J. Caffrey, R. Govindan, E. Johnson, and S. Masri, "Monitoring civil structures with a wireless sensor network," in *IEEE Internet Computing*, vol. 10, pp. 26 - 34, Apr. 2006.

[4] S. Kim, S. Pakzad, D. Culler, and J. Demmel, "Health monitoring of civil infrastructures using wireless sensor networks," in *Proc. 6th Intern. Sym. Information Processing in Sensor Networks*, pp. 254 - 263, Apr. 2007.

[5] R. Cardell-Oliver, K. Smettem, M. Kranz, and K. Mayer, "Field testing a wireless sensor network for reactive environmental monitoring," in *Proc. IEEE Conf. Intelligent Sensors, Sensor Networks and Information Processing*, pp. 7 - 12, Dec. 2004.

[6] J. Beutel, "Fast-prototyping Using the BTnode Platform," in *Proc. Conf. Design, Automation Test in Europe*, 2006.

[7] S. Liu, M. Tomizuka and G. UlsoyS, "Strategic issues in sensors and smart structures," *Structural Control Health Monitoring*, vol. 13, pp. 946-957, 2006.

[8] S. Xu, Y. Qin, C. Xu, Y. Wei, R.Yang and Z. Wang, "Self-Powered nanowire devices," *Nature Nanotechnology*, vol. 5, pp. 366-373, Mar. 2010.

[9] S. Roundy, P. K. Wright and J. Rabaey, "A study of low level vibrations as a power source for wireless sensor nodes," *Journal of Computer Commu.*, vol. 26, pp. 1131-1144, 2003.

[10] J. Wu and N. Sun, "Optimal sensor density in a distortion-tolerant linear wireless sensor network," in *Proc. IEEE Global Telecommun. Conf.*, Dec. 2010.

[11] F. Li, J. Evans and S. Dey, "Design of distributed detection schemes for multiaccess channels," *IEEE Trans. Aerospace and Electronic Systems*, vol. 48, pp. 1552 - 1569, Apr. 2012.

[12] T. M. Duman and M. Salehi, "Decentralized detection over multiple-access channels," *IEEE Trans. Aerospace and Electronic Systems*, vol. 34, pp. 469 - 476, Apr. 1998.

[13] J. J. Xiao and Z. Q. Luo, "Universal decentralized detection in a bandwidth-constrained sensor network," *IEEE Trans. Signal Processing*, vol. 53, pp. 2617-2623, Aug. 2005.

[14] G. Ferrari, M. Martalo and R. Pagliari, "Decentalized detection in clustered sensor networks," *IEEE Trans. Aerospace and Electronic Systems*, vol. 47, pp. 959 - 973, Apr. 2011.

[15] G. Ferrari and R. Pagliari, "Decentalized binary detection with noisy communication links," *IEEE Trans. Aerospace and Electronic Systems*, vol. 42, pp. 1554 - 1562, Oct. 2008.

[16] J. Wu and G. Zhou, "A new Ultra-low power wireless sensor network with integrated energy harvesting, data sensing, and wireless communication," in *Proc. IEEE Inter. Conf. on Commu.*, June 2011.

[17] X. Wang and H. V. Poor, "Iterative (Turbo) soft interference cancellation and decoding for coded CDMA," *IEEE Trans. Commun.*, vol. 47, pp. 1046-1061, July 1999.

[18] P. Li, "Approximate MMSE-APP estimation for linear systems with binary inputs," *IEEE Commun. Letters*, vol. 9, pp. 172-174, Feb. 2005.

[19] J. Wu and Y. R. Zheng, "Low complexity soft-input soft-output block decision feedback equalization," *IEEE J. Selected Areas Commun.*, vol. 26, pp. 281-289, Feb. 2008.

[20] M. Abramowitz and I. A. Stegun, "Handbook of mathematical functions with formulas, graphs and mathematical tables," *Dover*, 9th Ed., 1972.

[21] A. D. Lunn, "A note on generating correlated binary variables," *Biometrika*, vol. 85, pp. 487-490, 1998.

Chapter 3

Cross-Layer Collision-Tolerant MAC with Message Passing Detection

3.1 Abstract

A cross-layer collision-tolerant (CT) media access control (MAC) scheme is proposed in this paper. In the MAC layer, each user transmits multiple weighted replicas of a packet at randomly selected data slots in a frame, and the indices of the selected slots are transmitted in a special collision-free position slot at the beginning of each frame. Collisions of the data slots in the MAC layer are resolved by using multiuser detection (MUD) in the physical (PHY) layer. The MUD is performed by employing a modified message passing (MP) algorithm, which treats the MAC structure as a bipartite graph, with each unique packet denoted as a message node (MN), and each slot denoted as a slot node (SN). The graph is simplified by removing the nodes with 0 or 1 connection to reduce the complexity of the MP algorithm. Simulation results demonstrate that the proposed CT-MAC achieves significant performance gains over existing cross-layer MAC schemes. It can support as many as $N = 2.4M$ simultaneous users for a system with M slots per frame, yet most existing schemes can only operate with $N \leq M$.

keywords

Collision-tolerant media access control, message passing, cross layer design, and wireless sensor network

3.2 Introduction

Media access control (MAC) protocols are critical to the efficient operations of wireless networks. In conventional MAC schemes such as slotted ALOHA (SA) or carrier sensing multiple access (CSMA), signals collided at a receiver will be discarded and retransmitted. This results in a waste of the precious spectrum and energy resources.

Various collision-tolerant (CT) MAC protocols have been proposed in the literature by resorting to cross-layer designs [1]–[7]. The concept of multi-packet reception (MPR) is proposed in [1] and [2], where it is assumed that a fraction of the collided signals can be correctly detected with physical (PHY) layer signal processing. In most MPR related works, the effects of channel and PHY layer operations are abstracted into a group of parameters P_{nk}, the probability that k packets can be recovered when there are $n \geq k$ packets in the collision. They do not specify how the collisions can be resolved. An iterative interference cancellation (IC) method is employed in a contention-resolution diversity SA (CRDSA) scheme [3] to achieve MPR. In CRDSA, each packet is transmitted twice at two random slots in a frame. If one of the packet is detected, then it can be used to subtract the interference caused by its twin replica. The IC process is performed iteratively. The performance of CRDSA is further improved with an irregular repetition SA (IRSA) scheme [4] and [5], where the number of repetitions for each packet is determined by a probability distribution, and a coded

SA (CSA) scheme [6], where linear block code across the packets is used to replace simple repetitions. All these schemes work well under low offered loads. However, the throughput drops dramatically once the normalized offered load exceeds a saturation point. The sharp drop is due to the fact that there are so many collisions such that the iterative IC process cannot be properly initiated. A CT-MAC with an on-off accumulative transmission (OOAT) is proposed in [7], where a sub-optimum block decision feedback equalizer (BDFE) is used for multiuser detection (MUD).

In this paper, we propose to develop a new cross-layer CT-MAC scheme by employing an iterative message passing (MP) algorithm for MUD. In the MAC layer, each user transmits multiple weighted replicas of a packet over randomly chosen slots in a frame. Such a transmission scheme can be represented as a bipartite graph, where each unique packet can be represented as a message node (MN), and each slot in a frame can be represented as a slot node (SN). The n-th MN is connected to the m-th SN if the n-th user transmits a packet at the m-slot. The indices of the occupied slots of each user is transmitted at a special collision-free slot at the beginning of each frame, so the receiver can construct the graph. We propose to perform MUD by exchanging soft log-likelihood information between the MNs and SNs with a modified MP algorithm. The MP algorithm was originally developed for the decoding of graph-based codes [8] and [9], or iterative IC in single-user systems [10] and [11]. It is extended here for the simultaneous detection in a multi-user network. The graph is simplified by removing some of the nodes that will not benefit from the iterative process, and the soft information collected from the removed nodes is used as *a priori* information for the nodes connected to them. The performance and convergence of the modified MP algorithm is analyzed with the extrinsic information transfer (EXIT) chart [12]. Simulation results

demonstrate that the proposed cross-layer MAC with MP detection can achieve significant performance gains over existing MAC schemes, and it can support as many as $N = 2.4M$ simultaneous users in a frame with M slots.

3.3 System Model

Consider a wireless network with N users transmitting to the same receiver through a shared channel. Each MAC frame is divided into M slots, and the duration of each slot contains K symbols. One packet has K symbols and can thus be transmitted in one slot. Each packet is transmitted in the form of R weighted replicas on R randomly selected slots in a frame. Denote $\mathcal{A}(m)$ as the set of users that transmit their respective packets on the slot m. The signal observed by the receiver at the slot m can then be described as

$$y_{mk} = \sum_{n \in \mathcal{A}(m)} h_{mn} w_{mn} x_{nk} + z_{mk}, \text{ for } k = 1, \cdots, K \tag{3.1}$$

where h_{mn} is the fading coefficient experienced by the signal from the n-th user at the m-th slot, w_{mn} is a weight coefficient used by the n-th user on the m-th slot, $x_{nk} \in \mathcal{S}$ is the k-th symbol in the packet from the n-th user, with $\mathcal{S}$ being the modulation constellation set with cardinality $S = |\mathcal{S}|$, and y_{mk} and z_{mk} are the received sample vector and noise sample, respectively. The weight coefficients are used to improve the numerical stability of the MUD. In this paper, we choose $w_{mn} = \frac{1}{\sqrt{R}} \exp\left[-j2\pi \frac{nm}{\max(N,M)}\right]$.

When $R = 1$ and $w_{mn} = 1$, the system degrades to the SA scheme. When $R = 2$ and $w_{mn} = 1$, the system at the transmitter is similar to the CRDSA scheme, where each packet is transmitted exactly twice in a frame. When R varies from user to user based on a certain probability distribution, and $w_{mn} = 1$, the system at the transmitter is similar to the IRSA

scheme. None of these systems can operate when the normalized offered load, $G = \frac{N}{M}$, is greater than 1.

In order to perform the joint detection of the information from all the users, the receiver requires the knowledge of the indices of the slots on which a user transmits its packets. To meet this requirement, we propose to prefix a position slot that contains NM bits at the beginning each frame. Each user transmits an M-bit vector, $\mathbf{p}_n = [p_{n1}, \cdots, p_{nM}]^T \in \{0,1\}^M$, to notify the receiver the indices of the slots on which it will transmit in this frame, with $p_{nm} = 1$ if a packet will be transmitted in the m-th slot and $p_{nm} = 0$ otherwise. Because of the importance of the position slot to the final detection, the M-bit position vectors of the N users are transmitted in a deterministic time division manner in a slot of MN bits such that there is no collision. In addition, the position slot can be transmitted with a relatively higher signal-to-noise ratio to improve the reliability of the information.

Given M and R, the position vector is randomly generated by each user and is updated for each frame. For a given frame, define the collision order of the system as $N_c = \max_m A_m$, where A_m is the cardinality of the set $\mathcal{A}_m$. Each received sample is thus the superposition of up to N_c transmitted symbols, and the receiver has up to R observations of each transmitted symbol. Therefore the system can be represented as a multiple-input multiple-output (MIMO) system with N_c inputs and R outputs. The receiver can recover the N_c-dimension input by using the R-dimension output. The weight coefficients are used to ensure the MIMO matrix has a rank of $\min(N_c, R)$,

3.4 Collision Resolution with a Modified Message Passing Algorithm

A modified MP algorithm is proposed in this section to achieve collision tolerance in the MAC layer by performing the MUD in the PHY layer.

The MAC scheme with weighted packet repetitions can be represented as a bipartite graph as shown in Fig. 3.1(a) for a system with $N = 5$ users, $M = 10$ slots, and $R = 2$ repetitions. In the graph, the MN represents a unique packet from a user and it is shown as a circle. The SN represents the observed signal in a given slot at the receiver, and it is represented as a square. The n-th MN is connected to the m-th SN if user n transmits a packet at the m-th slot. In the full graph, there are N MNs and M SNs. In a message passing algorithm, the MN and the SN iteratively exchange soft log-likelihood information to achieve performance improvement.

Define the set of SNs that are connected to the n-th MN as $\mathcal{B}_n$. The set of MNs that are connected to the m-th SN is denoted as $\mathcal{A}_m$. The number of connections that each node has is defined as the order of the node. Therefore, the order of the m-th SN is A_m, and the order of the n-th MN is $B_n = |\mathcal{B}_n|$. For the proposed scheme, $B_n = R$, $\forall n$, and $|\mathcal{A}_m| \leq N_c$.

3.4.1 Graph Simplification and Initialization

The graph shown in Fig. 3.1(a) can be simplified by removing some of the MNs and SNs that will not benefit from the iterative message passing process.

The order-0 nodes do not contribute to the detection process, thus can be removed from the graph.

For those order-1 SNs, there is no collision at the corresponding slot. In this case, these

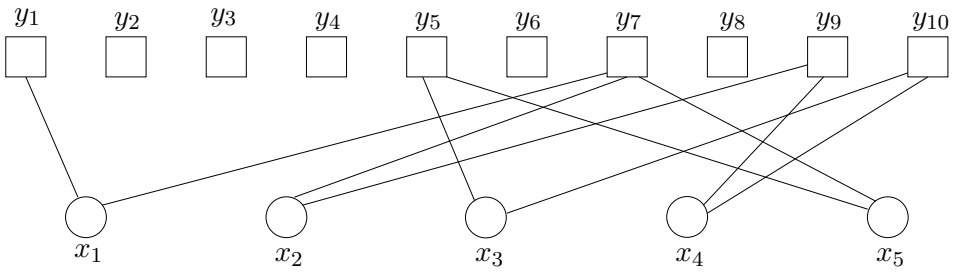

(a) The complete graph

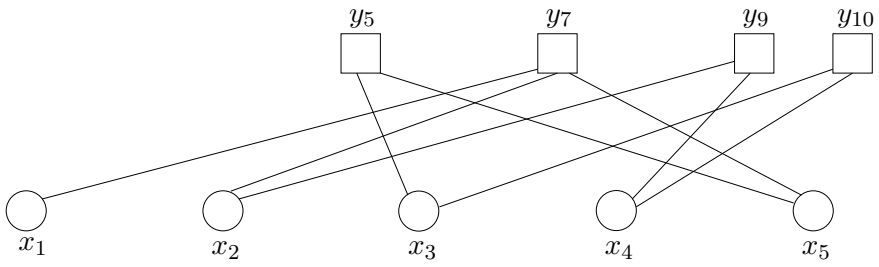

(b) The simplified graph

Figure 3.1: Graph representations of a CT-MAC system with $N = 5$ users, $M = 10$ slots, and $R = 2$ repetitions.

nodes will not benefit from the iterations of the message passing algorithm. Therefore, we can calculate the log-likelihood information at the order-1 nodes at the beginning of the iteration as *a priori* initial conditions, and remove the order-1 nodes from the actual iteration process. Assume SN m is an order-1 node connected to the n-th MN, as $\mathcal{A}_m = \{n\}$. The log-likelihood function (LLF) for the k-th symbol transmitted at the m-th slot, $\mu_{nk}^{(m)}(x_s) = \log P(y_{mk}|x_{nk} = \chi)$, can be calculated by

$$\mu_{nk}^{(m)}(\chi) = C_{nk1} - \frac{1}{\sigma_z^2}|y_{mk} - h_{mn}w_{mn}\chi|^2, \text{ for } \chi \in \mathcal{S}, \text{ if } \mathcal{A}_m = \{n\},$$

where $\chi \in \mathcal{S}$, σ_z^2 is the noise variance, and C_{nk1} is a normalization constant to make $\sum_{\chi\in\mathcal{S}} \exp\left[\mu_{nk}(\chi)\right] = 1$.

For the SNs with order greater than 1, no *a priori* information is available and initialize the log-likelihood information as

$$\mu_{nk}^{(m)}(\chi) = \log \frac{1}{S}, \ \forall n \in \mathcal{A}_m, \text{ if } A_m > 1 \tag{3.2}$$

If all the SNs connected to the n-th MN are order-1 nodes, then we can directly get an estimate of x_{nk} as

$$\hat{x}_{nk} = \underset{\chi \in \mathcal{S}}{\operatorname{argmax}} \sum_{m \in \mathcal{B}_n} \mu_{nk}^{(m)}(\chi) \tag{3.3}$$

Therefore node n can be removed from the graph if $A_m = 1$, $\forall m \in \mathcal{B}_n$.

After the removal of the nodes, a simplified graph is obtained. Fig. 3.1(b) shows the simplified graph with only 4 SNs and 5 MNs.

Before the iteration, assign the symbols on each remaining MN an *a priori* LLF as

$$\lambda_{nk}(\chi) = C_{nk2} + \sum_{m \in \mathcal{B}_n} \mu_{nk}^{(m)}(\chi), \tag{3.4}$$

where C_{nk2} is a normalization constant.

The *a priori* LLF for the SNs in the simplified graph can be calculated from the channel measurements as

$$\mu_{mk}(\mathbf{x}_m) = C_{nk3} - \frac{1}{\sigma_z^2} |y_{mk} - \sum_{n \in \mathcal{A}_m} h_{mn} w_{mn} x_{nk}|^2 \tag{3.5}$$

where $\mathbf{x}_m = [x_{nk}]_{n \in \mathcal{A}_m}^T$ is a length-A_m vector containing one possible realization of the A_m symbols that collide at the slot m. Since there are S^{A_m} such vectors, each MN is associated with a set of S^{A_m} initial LLFs.

3.4.2 Message Passing

The MNs and SNs iteratively exchange soft information to recover the information collided at the receiver.

Denote the message from the m-th SN to the n-th MN about the k-th symbol x_{nk} as $\alpha_{nk}^{(m)}(\chi)$, for $\chi \in \mathcal{S}$, $n \in \mathcal{A}_m$, and $k = 1, \cdots, K$. Similarly, denote the message from the n-th MN to the m-th SN about the k-th symbol x_{nk} as $\beta_{nk}^{(m)}(\chi)$.

1) SN → MN: $\alpha_{nk}^{(m)}(\chi)$.

Each SN collects the soft information from all of its connected MNs, and combine these soft information to get an update of the LLF of the received symbols.

The likelihood function of x_{nk} at the m-th slot can be calculated as

$$P(y_{mk}|x_{nk} = \chi) = \sum_{\boldsymbol{\chi}_m \in \mathcal{S}^{A_m-1}} P(\mathbf{x}_{mk\backslash n} = \boldsymbol{\chi}_m) \times P(y_{mk}|x_{nk} = \chi, \mathbf{x}_{mk\backslash n} = \boldsymbol{\chi}_m) \quad (3.6)$$

where $\boldsymbol{\chi}_m \in \mathcal{S}^{A_m-1}$ contains one possible realization of a length-(A_m-1) vector with elements from $\mathcal{S}$, $\mathbf{x}_{mk\backslash n} = [x_{uk}]_{u\in\mathcal{A}_m, u\neq n}^T$ is a length-(A_m-1) vector containing all but x_{nk} related to $\mathcal{A}_m$.

The *a priori* probability $P(\mathbf{x}_{mk\backslash n} = \boldsymbol{\chi}_m)$ can be obtained by combining the soft information from the MNs as

$$\log P(\mathbf{x}_{mk\backslash n} = \boldsymbol{\chi}_m) = \prod_{\chi_u \in \boldsymbol{\chi}_m} \beta_{nk}^{(m)}(\chi_u) \quad (3.7)$$

where χ_u is an element in $\boldsymbol{\chi}_m$.

The sequence-based LLF in (3.6) can be obtained from the initial LLF as in (3.5). Combining (3.5), (3.6), and (3.7), the LLF delivered from the m-th SN to the n-th MN, $\alpha_{nk}^{(m)}(\chi) = \log P(y_{mk}|x_{nk} = \chi)$, can be calculated as

$$\alpha_{nk}^{(m)}(\chi) = \underset{\boldsymbol{\chi}_m \in \mathcal{S}^{A_m-1}}{\text{logsum}} \left[\prod_{\chi_u \in \boldsymbol{\chi}_m} \beta_{nk}^{(m)}(\chi_u) + \mu_{mk}(x_{nk} = \chi, \mathbf{x}_{mk\backslash n} = \boldsymbol{\chi}_m) \right], \quad (3.8)$$

where

$$\underset{n\in[1,\cdots,N]}{\text{logsum}} [a_n] = \max(\mathbf{a}) + \log \left\{ \sum_{n=1}^{N} \exp\left[a_n - \max(\mathbf{a})\right] \right\}, \quad (3.9)$$

with $\max(\mathbf{a})$ returning the maximum value in the vector $\mathbf{a} = [a_1, \cdots, a_N]^T$. The log-domain operations in (3.8) and (3.9) can avoid the numerical instability caused by overflowing during the iterations.

The LLR sent from the SN to the MN as calculated in (3.8) incorporates the initial LLFs from the channel measurements, and the soft messages from all but the n-th SN connected to the m-th MN.

2) MN $\rightarrow$ SN: $\beta_{nk}^{(m)}(\chi)$.

The message from the n-th MN to the m-th SN with $m \in \mathcal{B}_n$ about x_{nk} is

$$\beta_{nk}^{(m)}(\chi) = \sum_{m' \in \mathcal{B}_n \backslash m} \alpha_{nk}^{(m')}(\chi) + \lambda_{nk}(\chi), \tag{3.10}$$

where $\mathcal{B}_n \backslash m$ is obtained by removing the element m from $\mathcal{B}$.

The soft message to the m-th SN contains the message from all but the m-th SN connected to the n-th MN, and the initial LLF defined in (3.4). Removing the information from the SN m in the soft message to the SN m can avoid numerical instability caused by positive feedback.

3) Hard Decision.

The iteration terminates if the parity check or cyclic redundancy check is satisfied in all the packets, or if the maximum number of iterations is reached. At the end of the iteration, a hard decision can be made based on the soft information as

$$\hat{x}_{nk} = \underset{\chi \in \mathcal{S}}{\operatorname{argmax}} \sum_{m \in \mathcal{B}_n} \alpha_{nk}^{(m)}(\chi) + \lambda_{nk}(\chi) \tag{3.11}$$

The complexity of the message passing algorithm is proportional to S^{N_c}. The number of packets in a given slot follows a Poisson distribution with parameters N and $\frac{R}{M}$. Thus the average number collisions is $\frac{NR}{M}$. On average, the complexity of the message passing algorithm is on the order of $\mathcal{O}(N_I S^{\frac{NR}{M}})$, where N_I is the maximum number of iterations.

The complexity of the optimum exhaustive search is on the order of $\mathcal{O}(S^N)$. Since R is

usually far less than M, the complexity of the message passing algorithm is usually much lower than the optimum search algorithm.

3.5 EXIT Chart Analysis

The convergence of the modified MP algorithm developed for the CT-MAC is studied in this section with the EXIT chart [12], which traces the evolution of mutual information between the data and the soft information through iterations.

The EXIT chart analysis is performed by tracing the evolution of the log-likelihood ratio (LLR) of the binary data. Assume that the binary vector, $\mathbf{b}_{nk} = [b_{nk1}, \cdots, b_{nk\log_2 S}]^T \in \mathcal{B}^{\log_2 S}$, with $\mathcal{B} = \{-1, 1\}$, is mapped to the symbol $x_{nk} \in \mathcal{S}$ through modulation. Define the LLR of b_{nkq} as

$$L(b_{nkq}) = \frac{\sum_{\chi \in \mathcal{S}_q^+} \log P(x_{nk} = \chi)}{\sum_{\chi \in \mathcal{S}_q^-} \log P(x_{nk} = \chi)} \tag{3.12}$$

where $\mathcal{S}_q^+$ contains all the symbols in $\mathcal{S}$ with the q-th bit in the demodulated vector being 1, and $\mathcal{S}_q^- = \mathcal{S} \backslash \mathcal{S}_q^+$. For the message passed from the m-th SN to the n-th MN, $\log P(x_{nk} = \chi) = \alpha_{nk}^{(m)}(\chi)$; for the message passed from the n-th MN to the m-th SN, $\log P(x_{nk} = \chi) = \beta_{nk}^{(m)}(\chi)$.

The EXIT chart analysis is based on the assumption that the LLRs are independent and identically distributed (i.i.d.) with a conditional pdf, $p_L(l|b)$, given by

$$p_L(l|b) = \frac{1}{\sqrt{2\pi}\sigma_L} \exp\left[-\frac{\left(l - b\sigma_L^2/2\right)^2}{2\sigma_L}\right], \tag{3.13}$$

where $b \in \mathcal{B}$, σ_L is the variance of the random variable $L(b)$. The conditional pdf given in (3.13) is a Gaussian pdf with a single parameter σ_L.

With the pdf of the LLR given in (3.13), define the mutual information between a bit b and its LLR $L(b)$ as

$$I = \frac{1}{2} \sum_{b \in \mathcal{B}} \int_{-\infty}^{+\infty} p_L(l|b) \log_2 \frac{2p_L(l|b)}{p_L(l|1) + p_L(l|-1)} dl. \tag{3.14}$$

Note that $I = 0$ implies no information about the bit, while $I = 1$ means ideal information. Since the conditional pdf $p_L(l|b)$ is a function of a single parameter σ_L, the mutual information I is completely determined by σ_L.

The MN or SN can be modeled as a mutual information transfer device, *i.e.*, given mutual information at the input, the MN or SN generates a new mutual information at the output by exploring the graph structure. Usually the output mutual information is larger than the input one due to the improvement of reliability achieved through the MP detection.

The values of the mutual information at the output of the MN or SN can be obtained through numerical simulations. For a given input mutual information I, the value of σ_L can be obtained through the mapping in (3.13) and (3.14). An ensemble of random input LLRs, $\{L_I(b)\}$, can then be generated following the conditional pdf in (3.13) and the value of σ_L. Feeding these random LLRs to (3.8) or (3.10) leads to an ensemble of LLRs at the output of the SN or MN, respectively. Denote the output LLRs as $\{L_O(b)\}$. An empirical histogram, or probability mass function (PMF), of the output LLRs, $P_{L_O}(l|b)$, can then be numerically generated provided that the number of random samples is large enough.

Fig. 3.2 depicts the EXIT chart of the modified MP by placing the mutual information transfer curves of the MN and the SN in the same figure. The horizontal axis is the mutual information at the input to the SN (the LLR of bits corresponding to $\beta_{nk}^{(m)}(\chi)$), and the vertical axis is the mutual information at the input to the MN (the LLR of bits corresponding

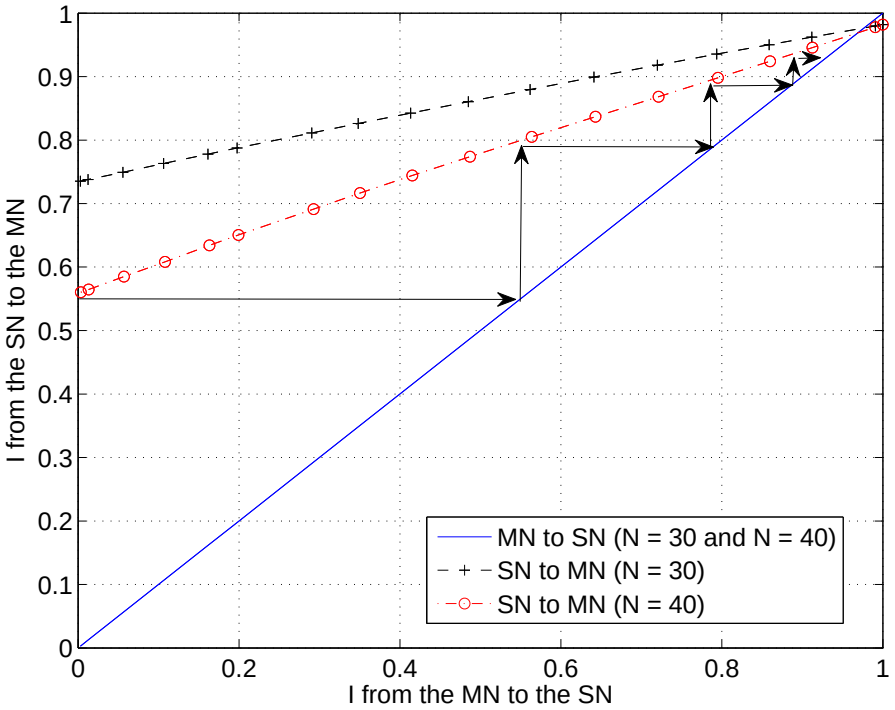

Figure 3.2: EXIT chart of a system with $M = 12$ slots and $R = 2$ repetitions.

to $\alpha_{nk}^{(m)}(\chi)$). The curves are obtained from systems with $M = 12$ and $R = 2$, at $E_b/N_0 = 10$ dB. The trajector traces visualizes the evolution of the mutual information by following the guide of the "tunnel" between the transfer curves. All transfer curves terminate at $I_O = 1$, which means they can generate ideal outputs. The transfer curve for the MN has a slope 1 when $R = 2$ because in this case a MN simply forwards the message from one SN to the other SN, and there is no further mutual information gain. The transfer curve of the SN has a larger slope when N is small, which means it can converge with less iterations.

3.6 Simulation Results

Simulation results are presented in this section to demonstrate the performance of the proposed cross layer MAC with the modified MP algorithm.

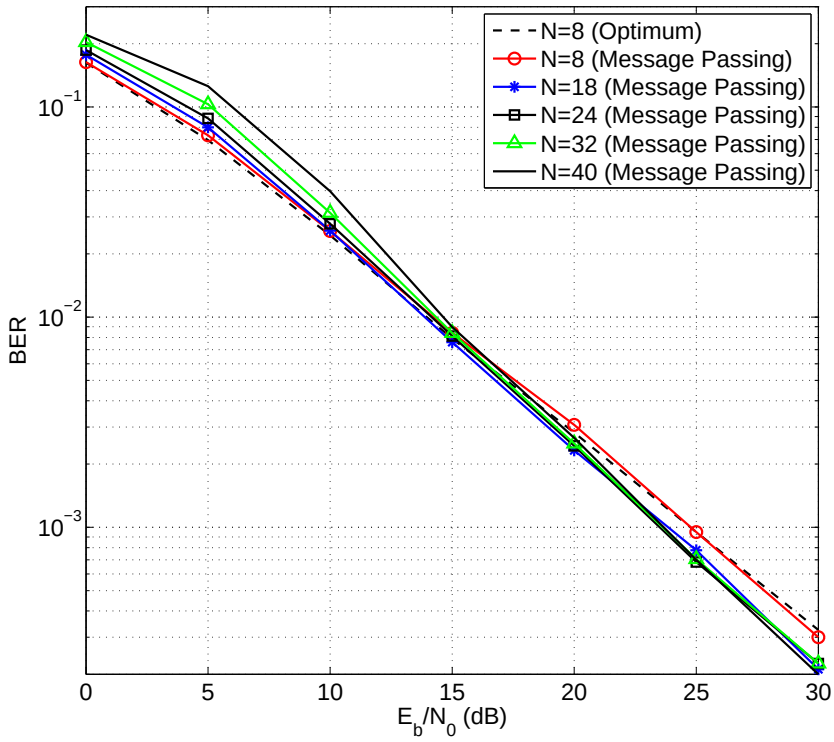

Figure 3.3: BER performance of the system with $M = 12$ slots, $R = 2$ repetitions, and the message passing algorithm.

Fig. 3.3 shows the bit error rate (BER) of the proposed system with various number of users N. There are $M = 12$ slots per frame, and each packet is repeated $R = 2$ times. The maximum iteration is set to 6. For comparison, the BER performance with optimum maximum likelihood sequence detection with exhaustive search for $N = 8$ is also shown in the figure. It can be seen that the modified MP can achieve a performance that is almost identical to its optimum counterpart. In addition, it is interesting to note that the BER performance improves slightly as N increases at high SNRs. This can be explained by the fact that more users means a more diverse channel conditions and more node interactions, which contribute positively to the detection process. Therefore, the collision-tolerant MAC with MP detection can support a large number of simultaneous users.

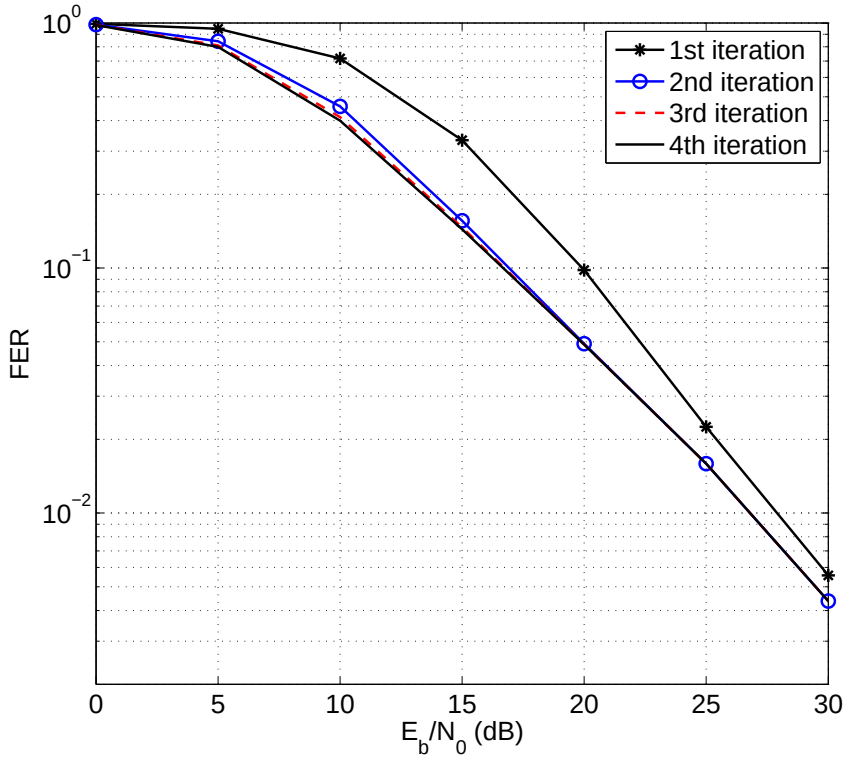

Figure 3.4: FER performance of the system with $M = 10$ slots, $N = 20$ users, $R = 2$ repetitions, and the message passing algorithm.

The effect of the number of iterations on the frame error rate (FER) is shown in Fig. 3.4. There are $N = 20$ active users, $M = 10$ slots per frame, and $R = 2$ repetitions. The largest performance gain is achieved at the second iteration. The performance converges at the 4th iteration, which corroborates the EXIT chart in Fig. 3.2.

Fig. 3.5 shows the normalized throughput as a function of the normalized offered load for various MAC schemes. The SA, CRDSA and IRSA achieve their respective peak throughputs when $G \leq 1$, and the throughputs drop dramatically when $G > 1$. The throughput of the proposed scheme achieves the maximum throughput 1.3 at $G = 2.4$ due to the MUD with the modified MP algorithm.

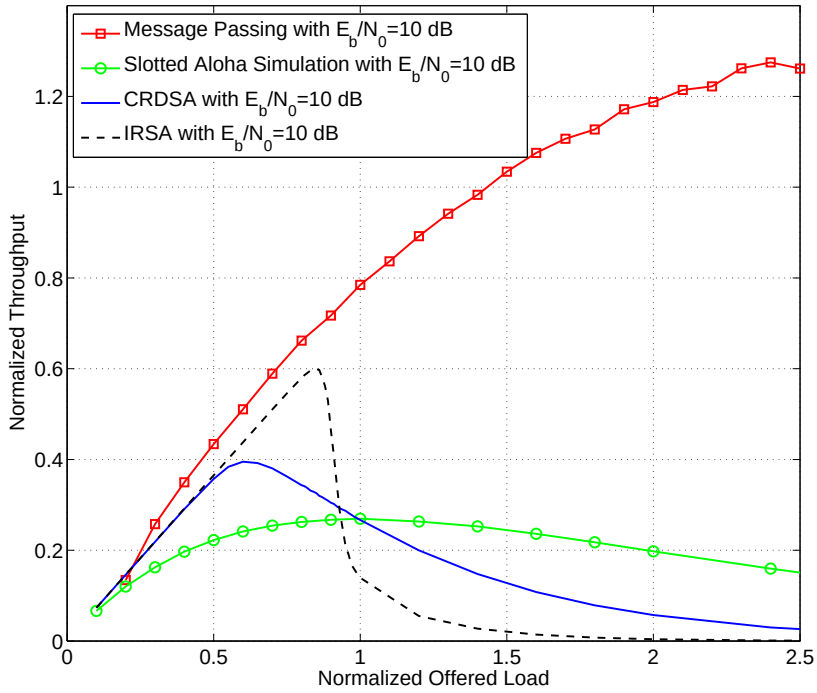

Figure 3.5: Normalized throughput v.s. normalized offered load.

3.7 Conclusions

A cross-layer CT-MAC scheme was proposed in this paper. In the MAC layer, each packet was transmitted in the form of multiple weighted replicas at randomly selected slots in a frame, and the positions of the occupied slots were specified in a collision-free position slot at the beginning of each frame. The collisions in the MAC layer were resolved by using a modified MP algorithm in the PHY layer, which operated on a simplified bipartite graph of the MAC structure. Simulation results demonstrated that the modified MP algorithm can achieve a performance that was almost identical to the optimum maximum likelihood detection, but with a much lower complexity. In addition, the proposed CT-MAC scheme could support up to $N = 2.4M$ simultaneous user for a system with M slots per frame, whereas most existing cross-layer MAC schemes can only support $N \leq M$ users.

3.8 References

[1] G. Mergen and L. Tong, "Receiver controlled medium access in multihop ad hoc networks with multipacket reception," in *Proc. IEEE Military Commun. Conf. MILCOM 2001*, vol. 2, pp. 1014 - 1018, 2001.

[2] L. Tong, V. Naware, and P. Venkitasubramaniam, "Signal processing in random access," *IEEE Sig. processing Mag.*, vol. 21, pp. 29 - 39, Sept. 2004.

[3] E. Casini, R. De Gaudenzi, and O. del Rio Herrero, "Contention resolution diversity slotted ALOHA (CRDSA): an enhanced random access scheme for satellite access packet networks," *IEEE Trans. Wireless Commun.*, vol. 6, pp. 1408 - 1419, Apr. 2007.

[4] G. Liva, "A slotted ALOHA scheme based on bipartite graph optimization," in *Proc. Intern. ITG Conf. Source and Channel Coding SCC'10*, Jan. 2010.

[5] G. Liva, "Graph-based analysis and optimization of contention resolution diversity slotted ALOHA," *IEEE Trans. Commun.*, vol. 59, pp. 477 - 487, Feb. 2011.

[6] E. Paolini, G. Liva, and M. Chiani, "High throughput random access via codes on graphs: coded slotted ALOHA," in *Proc. Intern. Conf. Commun. ICC'11*, June. 2011.

[7] J. Wu and Y. Li, "Cross-layer design of random on-off accumulative transmission with iterative detections," in *Proc. Global Telecommun. Conf. Globecom'11*, Dec. 2011.

[8] T. J. Richardson, M. A. Shokrollahi, and R. L. Rubanke, "Design of capacity-approaching irregular low-density parity-check codes," *IEEE Trans. Info. Theory*, vol. 47, pp. 619 - 637, Feb. 2001.

[9] A. Shokrollahi, "Raptor code," *IEEE Trans. Info. Theory*, vol. 52, pp. 2551 - 2567, June 2006.

[10] M. H. Taghavi, and P. H. Siegel, "Equalization on graphs: linear programming and message passing," in *Proc. IEEE Intern. Symp. on Infor. Theory ISIT'07*, pp. 2551 - 2555, June. 2007.

[11] C. W. Huang, P. A. Ting, and C. C. Huang, "A novel message passing based MIMO-OFDM Data detector with a progressive parallel ICI canceller," *IEEE Trans. Wireless Commun.*, vol. 4, pp. 1260 - 1268, APr. 2011.

[12] S. t. Brink, "Designing iterative decoding schemes with the extrinsic information transfer chart", *AEU Int. J. Electron. Commun.*, vol. 54, pp. 389–398, Nov. 2000.

Chapter 4

Collision-Tolerant Media Access Control with Asynchronous Users

4.1 Abstract

A frequency-domain cross-layer *collision-tolerant* (CT) *media access control* (MAC) scheme is proposed for the up-links of broadband wireless networks with asynchronous users. The collision tolerance is achieved with a *frequency-domain on-off accumulative transmission* (FD-OOAT) scheme, where the frequency-selective spectrum is divided into a large number of orthogonal sub-channels, and each symbol is transmitted over a small subset of the sub-channels to reduce the probability of collision. Such a configuration renders a special signal structure that enables *multi-user detection* (MUD) in the physical layer to resolve the collisions at the MAC layer. Most MUDs in the literature require precise symbol level synchronizations among the users. The proposed scheme, on the other hand, can operate with asynchronous users. By employing oversampling in the time domain and detection in the frequency domain, the proposed scheme is insensitive to the timing phase offset between the sampling clocks at the transmitter and receive. In addition, oversampling in the time domain and spreading the signal in the frequency domain enable multipath diversity that further improves the system performance. Theoretical analysis are performed to quantify the impacts

of multipath diversity and relative user delays on the system performance. Both analytical and simulation results demonstrated that significant performance gains are achieved with the proposed scheme, in terms of both the number of users supported and the normalized throughput.

keywords

Collision-tolerant media access control, asynchronous users, timing phase offset, cross layer design, and oversampling

4.2 Introduction

Medium access control (MAC) coordinates the access of the shared wireless medium among multiple synchronous or asynchronous users. It is critical for the efficient operations of multi-user wireless communication systems, such as the up-links of cellular networks, satellite communications, and wireless sensor networks with multiple sensors transmitting to the same information sink. In many conventional MAC schemes such as slotted ALOHA or *carrier sensing multiple access* (CSMA), signals collided at a receiver will be discarded and retransmitted. This results in a waste of the precious energy and spectrum resources.

Various *collision-tolerant* (CT) MAC protocols have been proposed to extract the salient information contained in the collided signals by resorting to cross-layer designs [1]–[10]. The concept of *multi-packet reception* (MPR) is proposed in [1]–[4], where it is assumed that a fraction of the collided signals can be correctly detected with *physical* (PHY) layer signal processing. In most MPR related works, the effects of channel and PHY layer operations are abstracted into a group of parameters P_{nk}, the probability that k packets can be recovered

when there are $n \geq k$ packets in the collision. They do not specify how the collisions can be resolved. Iterative *interference cancellation* (IC) methods are employed to resolve multi-user collisions in a *contention-resolution diversity slotted ALOHA* (CRDSA) [5] and an *irregular repetition slotted ALOHA (IRSA)* scheme [6] and [7]. In the CRDSA and IRSA schemes, each packet is transmitted multiple times at random slots in a frame. If one of the packet is detected, then it can be used to subtract the interference caused by its replicas. The IC process is performed iteratively. These schemes work well under low offered loads. However, the throughput drops dramatically once the normalized offered load exceeds a saturation point. The sharp drop is due to the fact that the IC schemes used in CRDSA or IRSA require at least one collision-free signal at the receiver in order to initiate the iterative IC process. This is difficult to achieve under a heavy load with high collision probabilities. In addition, all of the above MAC techniques rely on perfect synchronization among the users, which is difficult, if not impossible, to achieve in practical systems.

The limitations of iterative IC can be partly solved by using *multi-user detection* (MUD), which performs simultaneous detection of signals from two or more users collided at the receiver. MUD in the PHY layer can be combined with MAC techniques to improve the spectrum and energy efficiency in wireless networks [8]–[10]. MUD techniques are often designed with multi-dimensional signals in the PHY layer, such as *code-division multiple access* (CDMA) [8] or *orthogonal frequency division multiplexing* (OFDM) [9]. An *on-off accumulative transmission* (OOAT) scheme is proposed in [10] for systems operating in frequency flat fading. The OOAT scheme can support more simultaneous users than the dimension of the signals by repeating the same signal multiple times and using silence periods between two consecutive repetitions to reduce collisions.

The proper operations of all the above cross-layer MAC schemes require perfect symbol level synchronization. In a multi-user system, two types of synchronizations are needed: the synchronization among the users (denoted as *multi-user synchronization*, or MUS), and the synchronization of the sampling phase between the transmitter and receiver clocks (denoted as *sampling phase synchronization*, or SPS). The SPS is usually achieved by performing correlation between a specially designed training sequence and the signals at the receiver [10], [14] and [15]. In multi-user systems, the *base station* (BS) can first estimate the relative delays of all the users with techniques from SPS. The estimated timing information can either be used to assist the detection process [10], or fed back to the users through a down-link control channel to achieve MUS [16]. All these schemes can only achieve synchronization up to a certain level of precision, and there will always be residual timing offsets or synchronization errors. MUS errors could cause additional *multiple access interference* (MAI) and/or destroy the special signal structure that is critical for MUD [11]. SPS errors introduce timing phase offset that will increase *inter-symbol interference* (ISI) and degrade *signal-to-noise ratio* (SNR) at the receiver [12] and [13]. If the users in a multi-user system are not perfectly aligned in the time domain, then SPS for one user might create timing phase offset for other users.

In this paper, we propose a new cross-layer CT-MAC scheme that operates in frequency-selective fading, does not require either MUS or SPS, and is insensitive to timing phase offsets. The collision tolerance is achieved by employing a *frequency-domain OOAT* (FD-OOAT). The OOAT technique was originally proposed for time domain operations [10], and it can only operate in frequency flat fading channels, so as many other CT-MAC schemes in the literature [5]–[7]. Spectral efficient wide-band communications dictate an operation

environment of frequency-selective fading, which imposes additional challenges to the design of CT-MAC techniques. In the FD-OOAT, the frequency-selective channel is divided into multiple orthogonal sub-channels in the frequency domain with the help of OFDM. Different from conventional OFDM, each symbol is transmitted over multiple sub-channels by following a certain on-off pattern in our scheme. Consequently, the proposed scheme can not only deal with frequency-selectivity of wide-band wireless channels as OFDM, but also exploit frequency diversity since each symbol is spread to several sub-channels. The FD-OOAT converts the relative transmission delays among the users in the time domain into phase shifts in the frequency domain, such that the sub-channels from different users are perfectly aligned in the frequency domain. Therefore, the frequency-domain operation eliminates the need for precise MUS, and it allows us to carefully plan the on-off patterns employed by different users to minimize the number of users colliding on each sub-channel.

Without time-domain MUS, there will always be non-negligible timing phase offsets because the receiver can only synchronize with the sampling phase of at most one user at a time. To mitigate the negative impacts of timing phase offsets, we propose to perform time-domain oversampling of the received signals. It has been shown in [13] through theoretical analysis that time-domain oversampling can effectively remove the effects of timing phase offset for a single-user single-carrier system operating in frequency-selective fading. We will show in this paper through both theoretical analysis and simulation that this is also true for multi-user multi-carrier systems. The performance of the proposed FD-OOAT with the time-domain oversampling is insensitive to the absolute sampling phase used at the receiver. Therefore, the proposed scheme can operate in an asynchronous environment without incurring additional interferences or SNR degradation. In addition, it has been shown in [10]

that time-domain oversampling can benefit the performance of a multi-carrier system by introducing additional frequency diversity gains. Based on the special signal structure of the FD-OOAT with time domain oversampling, optimum and sub-optimum MUDs are developed to effectively collect the frequency diversity gain, and to resolve the collisions among the users. An analytical matched filter bound is derived to quantify the performance of the proposed scheme and the impacts of timing delays. Simulation results demonstrate that the proposed CT-MAC can achieve significant performance gains over existing CT-MAC schemes.

The remainder of this paper is organized as follows. The FD-OOAT scheme with time-domain oversampling is presented in Section 4.3. The optimum and sub-optimum detection methods that can resolve collisions and collect the diversity gains are described in Section 4.4. In Section 4.5, theoretical studies are performed to quantify the impacts of multipath diversity gain and timing phase offset. Simulation results are given in Section 4.6, and Section 4.7 concludes the paper.

4.3 Frequency-Domain OOAT with Time-Domain Oversampling

4.3.1 Proposed System Structure

Consider a wireless network with N users transmitting to the same receiver through a shared channel. Each MAC frame contains K symbols. To achieve collision tolerance in the MAC layer, users employ the FD-OOAT in the physical layer as shown in Fig. 4.1.

The entire available bandwidth, B, is divided into KM sub-channels, with a bandwidth $B_0 = \frac{B}{KM}$ each. Each symbol uses M sub-channels uniformly spread over the entire frequency

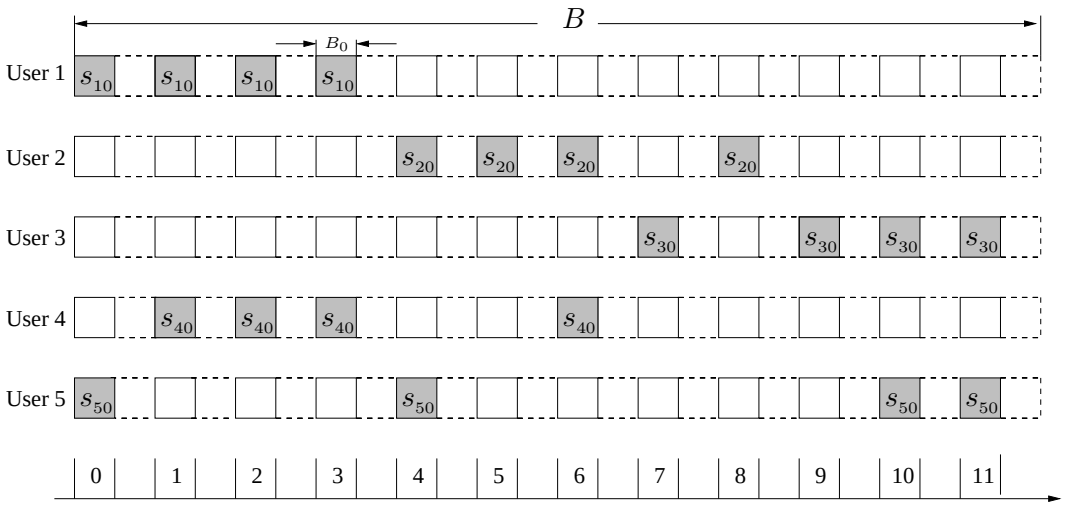

Figure 4.1: A frequency-domain OOAT system with $N = 5$ users, $R = 4$ sub-channels occupied out of $M = 12$ sub-channels for each symbol.

band. If sub-channels are indexed as $0, 1, \cdots, KM-1$, then the M sub-channels with indices, $\{mK + k\}_{m=0}^{M-1}$, are assigned for the k-th symbol in the frame, for $k = 0, \cdots, K-1$. During each transmission, only R randomly-chosen sub-channels from the M ones are occupied. The indicator vector of the occupied sub-channels for the n-th user can be represented by a binary vector of length M, $\mathbf{p}_n = [p_n(0), \cdots, p_n(M-1)]^T \in \mathcal{B}^{M\times 1}$, where $\mathcal{B} = \{0, 1\}$, with $p_n(m) = 1$ if the k-th symbol is transmitted at the $\{mK+k\}$-th sub-channel, and $p_n(m) = 0$ otherwise. All symbols from the n-th user use the same transmission pattern $\mathbf{p}_n$. With such a scheme, each symbol is repeated over R sub-channels (accumulative transmission), and the utilization of the sub-channels are determined by an on-off transmission pattern $\mathbf{p}_n$. In the example shown in Fig. 4.1, there are $N = 5$ users, $M = 12$ available sub-channels per symbol, and $R = 4$ out of the 12 available sub-channels are occupied.

Based on the above description, the signal transmitted on the m-th sub-channel of the n-th user can be represented as

$$d_n(m) = p_n(i_m)s_{nk_m}, \tag{4.1}$$

where $i_m = \lfloor \frac{m}{K} \rfloor$ with $\lfloor a \rfloor$ being the largest integer smaller than or equal to a, s_{nk} is the k-th symbol from user n, and $k_m = [m]_K$ with $[m]_K = m - i_m K$ being the modulo K operator. Consequently, the signal vector of the n-th user can be expressed as

$$\mathbf{d}_n = [d_n(0), d_n(1), \cdots, d_n(KM-1)]^T \in \mathcal{S}_+^{L\times 1}, \tag{4.2}$$

where $L = KM$, $\mathcal{S}_+ = \{\mathcal{S}, 0\}$, and $\mathcal{S}$ is the modulation constellation set with a cardinality $S = |\mathcal{S}|$.

The signal vector, $\mathbf{d}_n$, is converted to the time domain by applying an L-point *inverse discrete Fourier transform* (IDFT) as

$$\mathbf{x}_n = \mathbf{F}_{_L}^H \cdot \mathbf{d}_n, \tag{4.3}$$

where $\mathbf{x}_n = [x_n(0), x_n(1), \cdots, x_n(L-1)]^T$ is the time-domain signal vector, and $\mathbf{F}_{_L} \in \mathcal{C}^{L\times L}$ is the L-point discrete Fourier transform (DFT) matrix with the $(r+1, c+1)$-th element being

$$[\mathbf{F}_{_L}]_{r,c} = \frac{1}{\sqrt{L}} \exp\left[-j2\pi \frac{r\cdot c}{L}\right], \quad r, c = 0, 1, \cdots, L-1.$$

Before transmission, a length-l_{cp} *cyclic prefix* (CP) is added to the time-domain signal $\mathbf{x}_n$ to avoid interference between consecutively transmitted frames. The time domain signals pass through a transmit filter, $p_1(t)$, and then transmitted over a quasi-static frequency-selective fading channel with impulse response $g_n(t)$. In a quasi-static channel, the fading is constant inside a frame, and varies independently from frame to frame. At the receiver, the received signals pass through a receive filter, $p_2(t)$. Define the *composite impulse response* (CIR) of the channel as

$$h_{nc}(t) = p_1(t) \odot g_n(t) \odot p_2(t), \tag{4.4}$$

where $\odot$ is the convolution operator. The CIR, $h_{nc}(t)$, includes the effects of the physical channel and the transmit and receive filters.

The output of the receive filter is

$$y_c(t) = \sum_{n=1}^{N} \sum_{l=-\infty}^{+\infty} \sqrt{\frac{E_s}{R}} x_n(l) h_{nc}(t - lT_1 - \tau_n) + z_c(t), \tag{4.5}$$

where E_s is the energy per symbol, $x_n(l)$ is the l-th time-domain sample from the n-th user with a sample period T_1, $z_c(t) = p_2(t) \odot v_c(t)$ is the noise component at the output of the receive filter, with $\odot$ denoting convolution and $v_c(t)$ the *additive white Gaussian noise* (AWGN) with one-sided power spectral density N_0.

The output of the receive filter is sampled at the time instant $t = iT_2$, where $T_2 = T_1/u$ is the sampling period at the receiver, with the oversampling factor, u, being an integer. Denote the relative delays among the users as $\tau_n = l_n T_2 + \tau_{n0}$, where l_n represents the mis-alignment among the users in terms of receive samples, and $\tau_{n0} \in [0, T_2]$ is the timing phase offset between the sampling clocks at the transmitter and receiver. The discrete-time samples are

$$y_{_T}(i) = \sum_{n=1}^{N} \sum_{l=0}^{ul_c-1} \sqrt{\frac{E_s}{R}} x_{_{nT}}(i - l - l_n) h_{_{nT}}(l) + z_{_T}(i), \tag{4.6}$$

where $y_{_T}(i) = y_c(iT_2)$ and $z_{_T}(i) = z_c(iT_2)$ are the T_2-spaced samples of the received signals and noise components, respectively, $h_{_{nT}}(l) = h_{nc}(lT_2 - \tau_{n0})$ is the sampled version of the continuous-time CIR $h_{nc}(t)$, and $x_{_{nT}}(i)$ is the oversampled version of $x_n(i)$ as $x_{_{nT}}(i) = x_n(i/u)$, if i/u is an integer, and 0 otherwise. It is assumed that the length of the CIR, ul_c, is an integer multiple of u, with l_c being the length of the CIR without oversampling. This condition can always be met by appending zeros to the CIR. The timing phase offset τ_{n0} is incorporated in the discrete-time CIR $h_{_{nT}}(l)$. We will study in Section 5.4.2 through

frequency-domain analysis the impacts of τ_{n0} on the statistical properties of the channel coefficients and the system performance.

With the discrete-time system model given in (4.6), the length of the CP should satisfy $l_{cp} \geq l_c + l_d/u - 1$, where $l_d = \max\{l_n\}$ is the maximum relative transmission delay among the users. It should be noted that the proposed method can work for arbitrary value of l_d, and a larger l_d means a longer CP. To achieve better spectral and energy efficiency, it is assumed in the simulation that $l_d \in [0, uK)$.

Due to the time span of the transmit and receive filters, the CIR coefficients, $h_{_{nT}}(l)$, are correlated, even though the underlying channel might undergo uncorrelated scattering. The correlation coefficient, $c_n(k_1, k_2) = \mathbb{E}\left[h_{_{nT}}(k_1)h^*_{_{nT}}(k_2)\right]$, can be calculated as [18, eqn. (17)].

$$c_n(k_1, k_2) = \int_{-\infty}^{+\infty} R_{P_1P_2}(k_1T_2 - \tau_{n0} - \tau)R^*_{P_1P_2}(k_2T_2 - \tau_{n0} - \tau)\zeta(\tau)d\tau, \tag{4.7}$$

where $\zeta(\tau)$ is the power delay profile of the physical channel, and $R_{P_1P_2}(t)$ is the convolution of the transmit and receive filters.

After the removal of the CP, the received symbols can be written in a matrix form as

$$\mathbf{y}_{_T} = \sqrt{\frac{E_s}{R}} \sum_{n=1}^{N} \mathbf{H}_{_{nT}} \cdot \mathbf{x}_n + \mathbf{z}_{_T}, \tag{4.8}$$

where $\mathbf{y}_{_T} = [y_{_T}(0), \cdots, y_{_T}(uL-1)]^T \in \mathcal{C}^{uL\times 1}$, $\mathbf{z}_{_T} = [z_{_T}(0), \cdots, z_{_T}(uL-1)]^T \in \mathcal{C}^{uL\times 1}$, $\mathbf{H}_{_{nT}} = [\mathbf{h}_{n,1}, \mathbf{h}_{n,u+1}, \cdots, \mathbf{h}_{n,(L-1)u+1}] \in \mathcal{C}^{uL\times L}$, with $\mathbf{h}_{n,k} \in \mathcal{C}^{uL\times 1}$ being the k-th column of a circulant matrix $\mathbf{H}_n \in \mathcal{C}^{uL\times uL}$. The first column of $\mathbf{H}_n \in \mathcal{C}^{uL\times uL}$ is $\mathbf{h}_{n,1} = [\mathbf{0}^T_{l_n}, h_{nT}(0), h_{nT}(1), \cdots, h_{nT}(ul_c - 1), \mathbf{0}^T_{uL-l_n-ul_c},]^T$, and $\mathbf{0}_a$ is a length-a all-zero vector. Due to the time span of the receive filter and the oversampling operation, the time domain noise vector is also correlated. The vector, $\mathbf{z}_{_T}$, is zero mean complex Gaussian distributed with a covariance matrix $\mathbf{R}_{\mathbf{z}_{_T}} = \mathbb{E}(\mathbf{z}_{_T}\mathbf{z}^H_{_T}) = N_0\mathbf{R}_p$, where $\mathbf{R}_p$ is defined in [19, Lemma 2].

The uL-point DFT is applied to the vector $\mathbf{y}_{T}$ to convert the signal to the frequency domain as

$$\mathbf{y}_{F} = \sqrt{\frac{E_s}{R}} \sum_{n=1}^{N} \mathbf{H}_{nF} \cdot \mathbf{d}_n + \mathbf{z}_{F}, \tag{4.9}$$

where $\mathbf{y}_{F} = \mathbf{F}_{uL}\mathbf{y}_{T}$ and $\mathbf{z}_{F} = \mathbf{F}_{uL}\mathbf{z}_{T}$ are the frequency-domain signal vector and noise vector, respectively, and $\mathbf{H}_{nF} = \mathbf{F}_{uL}\mathbf{H}_{nT}\mathbf{F}_{L}^{H} \in \mathcal{C}^{uL\times L}$ is the frequency-domain channel matrix. Due to the correlation among the noise samples in the time domain, they are still correlated in the frequency domain. The covariance matrix of $\mathbf{z}_{F}$ is $\mathbf{R}_{\mathbf{z}_{F}} = N_0\mathbf{F}_{uL}\mathbf{R}_p\mathbf{F}_{uL}^{H}$. It should be noted that due to the on-off transmission, only RK out of the $L = MK$ elements in $\mathbf{d}_n$ are non-zero.

The matrix $\mathbf{H}_{nF}$ can be partitioned into a stack of u sub-matrices as $\mathbf{H}_{nF} = [\mathbf{G}_{n0}^{T}, \cdots, \mathbf{G}_{n(u-1)}^{T}]^{T}$, where $\mathbf{G}_{nv} \in \mathcal{C}^{L\times L}$. The matrix, $\mathbf{G}_{nv}$, is a diagonal matrix, with the $(m+1)$-th diagonal element being [19, Corollary 1]

$$G_{nv}(m) = \frac{\exp\left[-j2\pi\frac{l_n\cdot(vL+m)}{uL}\right]}{\sqrt{u}} \sum_{l=0}^{ul_c-1} h_{nT}(l) \exp\left[-j2\pi\frac{(vL+m)\cdot l}{uL}\right]. \tag{4.10}$$

Even though the signals transmitted by the different users are mis-aligned in the time domain, the FD-OOAT symbols from different users are perfectly aligned in the frequency domain as shown in (4.9), (4.10) and Fig. 4.1. The relative delay, l_n, in the time domain is converted to a phase shift, $\exp\left[-j2\pi\frac{l_n\cdot(vL+m)}{uL}\right]$, in the frequency domain.

With the model given in (4.9) and (4.10), each $d_n(m)$ is equivalently transmitted over u sub-carriers with coefficients $\{G_{nv}(m)\}_{v=0}^{u-1}$. Since each symbol is repeated R times, each modulated symbol, s_{nk}, is equivalently transmitted over uR sub-carriers in the frequency domain. Therefore, frequency diversity is achieved with the proposed FD-OOAT scheme.

The uR sub-carriers spread over the entire frequency band to maximize the frequency diversity. We will quantify the frequency diversity order by resorting to a matched filter bound in Section 4.5.

4.3.2 Collision Tolerance

With the frequency-domain system representation in (4.9), the received information at the m-th sub-channel at the BS is the superposition of the set of signals, $\{d_n(m)\}_{n=1}^{N}$. The value of $d_n(m)$ is 0 if $p_n(i_m) = 0$. Therefore, only a subset of the users will collide at the m-th sub-channel. Define the collision order at the m-th sub-channel as $N_c(m) = \sum_{n=1}^{N} p_n(i_m)$. The collision order of the network is then defined as $N_c = \max_m N_c(m)$. We have $N_c = 2$ for the system shown in Fig. 4.1.

The FD-OOAT system with time-domain oversampling can be equivalently represented as an N_c-input uR-output system. In practice, to ensure collision tolerance and system performance, it is desirable to have a system with $N_c \leq uR$. Due to the perfect alignment of the users in the frequency domain, given N, M, and R, we can choose a subset of position vectors to minimize N_c. The subset of position vectors can be constructed by exhaustively searching over the set of all the $\binom{M}{R}$ possible patterns. This task only needs to be done once during the system design, so the high complexity incurred by the exhaustive search will not affect the actual operation of the network.

The oversampled FD-OOAT scheme contributes to the performance improvement of the wireless network from the following perspectives. First, the on-off transmission across the sub-channels will reduce the collision order. Second, the transmission of R identical sub-symbols with oversampling results in a uR-dimensional received signal in the frequency

domain, which can be used for the detection of the N_c-dimensional signal in the space domain. Third, frequency diversity is achieved by transmitting the k-th symbol in uR sub-channels. Fourth, the OOAT signals from different users are perfectly aligned in the frequency domain even if they are asynchronous in the time domain, and this enables the precise control of the collision order by carefully selecting the transmission patterns for all the users.

4.4 Collision Resolution with Optimum Detection and Sub-optimum Detection

In this section, optimum and sub-optimum detectors are developed for the oversampled FD-OOAT system to resolve the collisions among the users and to collect the inherent frequency diversity.

4.4.1 Optimum Detection with Maximum Likelihood Detector

Since all the FD-OOAT symbols are perfectly aligned in the frequency domain as shown in Fig. 4.1, the k-th symbol from one user will only interfere the k-th symbol from the other users. This is different from the time-domain OOAT [10], where the k-th symbol from one user might interfere the $(k-1)$-th, k-th, and the $(k+1)$-th symbols from the other users due to the signal mis-alignment in the time domain.

The k-th symbols from all the N users, $\{s_{nk}\}_{n=1}^{N}$, can be jointly detected by using a block of uM received signal samples $\mathbf{r}_k = [\mathbf{y}_0^T, \cdots, \mathbf{y}_{u-1}^T]^T \in \mathcal{C}^{uM\times 1}$ with $\mathbf{y}_v = [y_{_F}(vL + k), y_{_F}(vL + K + k), \cdots, y_{_F}(vL + (M-1)K + k)]^T \in \mathcal{C}^{M\times 1}$. The vector $\mathbf{r}_k$ defined above is obtained by extracting uM elements from the frequency domain vector $\mathbf{y}_{_F}$. It can be alternatively represented as $\mathbf{r}_k = \mathbf{B}_k\mathbf{y}_{_F}$, where $\mathbf{B}_k \in \mathcal{B}^{uM\times uL}$ is obtained by extracting uM rows from a size-uL identity matrix $\mathbf{I}_{uL}$. The indices of the extracted rows are $vL+mK+k$,

for $v = 0, \cdots, u-1$ and $m = 0, \cdots, M-1$.

From (4.9), we have

$$\mathbf{r}_k = \sqrt{\frac{E_s}{R}}\mathbf{H}_k \cdot \mathbf{s}_k + \mathbf{w}_k, \tag{4.11}$$

where $\mathbf{s}_k = [s_{1k}, s_{2k}, \cdots, s_{Nk}]^T \in \mathcal{S}^{N\times 1}$ and $\mathbf{w}_k = \mathbf{B}_k\mathbf{z}_F \in \mathcal{C}^{uM\times 1}$ are the modulation symbol vector and noise vector, respectively, $\mathbf{H}_k = [\mathbf{G}_0^T, \cdots, \mathbf{G}_{u-1}^T]^T$, and $\mathbf{G}_v \in \mathcal{C}^{M\times N}$ is the frequency-domain channel matrix with the $(m+1, n)$-th element being $p_n(m)G_{nv}(mK+k)$.

Since the elements of $\mathbf{w}_k$ are extracted from $\mathbf{z}_F$, they are mutually correlated with the covariance matrix $\mathbf{R}_{\mathbf{w}_k} = N_0\mathbf{B}_k\mathbf{F}_{uL}\mathbf{R}_p\mathbf{F}_{uL}^H\mathbf{B}_k^H$. The covariance matrix might be rank deficient. Define the pseudo-inverse of $\frac{1}{N_0}\mathbf{R}_{\mathbf{w}_k}$ as

$$\mathbf{\Phi}_k = \mathbf{V}_k\mathbf{\Omega}_k^{-1}\mathbf{V}_k^H \in \mathcal{C}^{uM\times uM}, \tag{4.12}$$

with

$$\mathbf{V}_k = [\mathbf{v}_{k1}, \mathbf{v}_{k2}, \cdots, \mathbf{v}_{ku_k}] \in \mathcal{C}^{uM\times u_k} \tag{4.13a}$$

$$\mathbf{\Omega}_k = \mathrm{diag}[\omega_{k1}, \omega_{k2}, \cdots, \omega_{ku_k}] \in \mathcal{C}^{u_k\times u_k}, \tag{4.13b}$$

where u_k is the number of non-zero eigenvalues of $\frac{1}{N_0}\mathbf{R}_{\mathbf{w}_k}$, $\mathbf{\Omega}_k$ is a diagonal matrix, with the elements, $\{\omega_{ki}\}_{i=1}^{u_k}$, being the non-zero eigenvalues of $\frac{1}{N_0}\mathbf{R}_{\mathbf{w}_k}$, and $\{\mathbf{v}_{ki}\}_{i=1}^{u_k}$ are the corresponding orthonormal eigenvectors.

Define the noise whitening matrix $\mathbf{D}_k = \mathbf{\Omega}_k^{-1/2}\mathbf{V}_k^H$. Applying $\mathbf{D}_k$ on both sides of (4.11) leads to an equivalent system

$$\bar{\mathbf{r}}_k = \sqrt{\frac{E_s}{R}}\bar{\mathbf{H}}_k \cdot \mathbf{s}_k + \bar{\mathbf{w}}_k, \tag{4.14}$$

where $\bar{\mathbf{r}}_k = \mathbf{D}_k\mathbf{r}_k$, $\bar{\mathbf{H}}_k = \mathbf{D}_k\mathbf{H}_k$, and $\bar{\mathbf{w}}_k = \mathbf{D}_k\mathbf{w}_k$. The covariance matrix of the noise vector, $\bar{\mathbf{w}}_k$, in the equivalent system can be calculated as $\mathbf{R}_{\bar{\mathbf{w}}_k} = \mathbf{D}_k\mathbf{R}_{\mathbf{w}_k}\mathbf{D}_k^H = N_0\mathbf{I}_{u_p}$. Therefore, the

original system in (4.11) with uM outputs and a colored noise is converted into an equivalent system with u_k outputs and a white noise.

From (4.14), the optimum maximum likelihood decision rule of the system can be represented as

$$\hat{\mathbf{s}}_k = \underset{\mathbf{s}_k \in \mathcal{S}^N}{\operatorname{argmin}} \left(\bar{\mathbf{r}}_k - \sqrt{\frac{E_s}{R}} \bar{\mathbf{H}}_k \mathbf{s}_k \right)^H \left(\bar{\mathbf{r}}_k - \sqrt{\frac{E_s}{R}} \bar{\mathbf{H}}_k \mathbf{s}_k \right), \tag{4.15}$$

The optimum detector in (4.15) requires the exhaustive search of a set of $|\mathcal{S}|^N$ possible signal vectors. The complexity of the optimum detector grows exponentially with the increase of the modulation level $|\mathcal{S}|$ and the number of users N.

4.4.2 Sub-optimum Detection with an Iterative Block Decision Feedback Equalizer

A low complexity sub-optimum detection algorithm is presented in this subsection to balance the trade-off between the performance and complexity. The sub-optimum algorithm is developed by employing an iterative *soft-input soft-output* (SISO) *block decision feedback equalizer* (BDFE) [20], which performs *soft successive interference cancellation* (SSIC) among the N symbols in $\mathbf{s}_k$.

The soft-input to the iterative BDFE equalizer is the *a priori* probability of the symbols, $P(s_{nk} = S_i)$, for $n = 1, \cdots, N$ and $i = 1, \cdots, |\mathcal{S}|$, where $S_i \in \mathcal{S}$. The *a priori* information is obtained from the previous detection round with an iterative detection method, and details will be given later in this subsection. The soft-output of the equalizer is the *a posteriori* probability of the symbols, $P(s_{nk} = S_i|\bar{\mathbf{r}}_k)$, for $n = 1, \cdots, N$ and $i = 1, \cdots, |\mathcal{S}|$. With the soft-output at the equalizer, define the *a posteriori* mean, $\hat{s}_{nk}$, and the extrinsic information,

$\beta_{nk}(i)$, of the symbol $s_n(k)$ as

$$\hat{s}_{nk} = \sum_{i=1}^{S} P(s_{nk} = S_i|\bar{\mathbf{r}}_k)S_i \tag{4.16a}$$

$$\beta_{nk}(i) = \log P(s_{nk} = S_i|\bar{\mathbf{r}}_k) - \log P(s_{nk} = S_i). \tag{4.16b}$$

The *a posteriori* mean, $\hat{s}_{nk}$, is used as soft decisions for the SSIC during the SISO-BDFE process. Details of the SISO-BDFE detection can be found in [20].

In the proposed sub-optimum detection, the SISO-BDFE with SSIC will be performed iteratively. At the first iteration, the *a priori* probability is initialized to $P(s_{nk} = S_i) = \frac{1}{|\mathcal{S}|}$. The extrinsic information at the output of the v-th iteration will be used as the soft-input of the $(v+1)$-th iteration as $P(s_{nk} = S_i) = c_{nk} \exp[\beta_{nk}(i)]$, where c_{nk} is a normalization constant to make $\sum_{i=1}^{S} P(s_{nk} = S_i) = 1$. At the final iteration, hard decisions will be made based on the *a posteriori* probability generated by the SISO-BDFE as

$$\hat{s}_{nk} = \underset{S_i \in \mathcal{S}}{\operatorname{argmax}}\ P(s_{nk} = S_i|\bar{\mathbf{r}}_k). \tag{4.17}$$

Simulation results show that the performance of the iterative detection algorithm usually converges after 4 iterations. The sub-optimum iterative detection algorithm can achieve a performance that is very close to its optimum counterpart, but with a much lower complexity.

4.5 Performance Analysis

The impacts of the frequency diversity and timing phase offset on the performance of the proposed FD-OOAT scheme with oversampling are studied in this section through theoretical analysis.

4.5.1 Matched Filter Bound

The matched filter bound on the *bit error rate* (BER) of the proposed frequency-domain CT-MAC scheme with *binary phase shift keying* (BPSK) is developed in this subsection. The matched filter bound is obtained by assuming that there is no interference among the users, and the obtained results serve as a lower bound on the BER of the actual system.

With the interference-free assumption, the received signal corresponding to the k-th symbol of the n-th user can be written as

$$\mathbf{r}_{nk} = \sqrt{\frac{E_s}{R}}\mathbf{g}_{nk} \cdot s_{nk} + \mathbf{w}_{nk}, \tag{4.18}$$

where $\mathbf{r}_{nk} = [\mathbf{y}_{n0}^T, \cdots, \mathbf{y}_{n(u-1)}^T]^T \in \mathcal{C}^{uR\times 1}$ with $\mathbf{y}_{nv} = [y_{_F}(vL + n_1K + k), \cdots, y_{_F}(vL + n_RK + k)]^T \in \mathcal{C}^{R\times 1}$, n_r is the r-th non-zero position in $\mathbf{p}_n$, $\mathbf{w}_{nk} = [\mathbf{z}_{n0}^T, \cdots, \mathbf{z}_{n(u-1)}^T]^T \in \mathcal{C}^{uR\times 1}$ with $\mathbf{z}_{nv} = [z_{_F}(vL + n_1K + k), \cdots, z_{_F}(vL + n_RK + k)]^T \in \mathcal{C}^{R\times 1}$, and $\mathbf{g}_{nk} = [\tilde{\mathbf{G}}_{n0}^T, \cdots, \tilde{\mathbf{G}}_{n(u-1)}^T]^T \in \mathcal{C}^{uR\times 1}$ with $\tilde{\mathbf{G}}_{nv} = [G_{nv}(n_1K + k), \cdots, G_{nv}(n_RK + k)]^T \in \mathcal{C}^{R\times 1}$ is the channel coefficient vector.

From the system model in (4.18), R repetitions of each symbol is equivalently transmitted over uR sub-carriers, which is equivalent to a *single input multiple output* (SIMO) system. The SIMO system has correlated channel taps and is corrupted by a colored noise.

The channel coefficient vector, $\mathbf{g}_{nk}$, can be represented as

$$\mathbf{g}_{nk} = \sqrt{L}\mathbf{B}_{nk} \cdot \mathbf{F}_{_{uL}} \cdot \mathbf{h}_{n,1}, \tag{4.19}$$

where $\mathbf{h}_{n,1}$ is the first column of the circulant time-domain channel matrix $\mathbf{H}_n$, and $\mathbf{B}_{nk} \in \mathcal{B}^{uR\times uL}$ is a binary matrix, with the $(vR + r, vL + n_rK + k + 1)$-th element being 1, for $r = 1, \cdots, R$, $v = 0, \cdots, u-1$, and all other elements of $\mathbf{B}_{nk}$ being zero.

The auto-correlation matrix, $\mathbf{R}_{nk} = \mathbb{E}[\mathbf{g}_{nk}\mathbf{g}_{nk}^H]$, can then be calculated as

$$\mathbf{R}_{nk} = L\mathbf{B}_{nk}\mathbf{F}_{uL}\mathbf{R}_{hn}\mathbf{F}_{uL}^H\mathbf{B}_{nk}^T, \tag{4.20}$$

where $\mathbf{R}_{hn} = \mathbb{E}(\mathbf{h}_{n,1}\mathbf{h}_{n,1}^H)$ is the auto-correlation matrix of the time-domain CIR vector. $\mathbf{R}_{hn}$ can be written as a block matrix as

$$\mathbf{R}_{hn} = \begin{bmatrix} \mathbf{0}_{l_n\times l_n} & \mathbf{0}_{l_n\times ul_c} & \mathbf{0}_{l_n\times l_r} \\ \mathbf{0}_{ul_c\times l_n} & \mathbf{R}_h & \mathbf{0}_{ul_c\times l_r} \\ \mathbf{0}_{l_r\times l_n} & \mathbf{0}_{l_r\times ul_c} & \mathbf{0}_{l_r\times l_r} \end{bmatrix}, \tag{4.21}$$

where $l_r = L - l_n - ul_c$, and the (l_1, l_2)-th element of $\mathbf{R}_h \in \mathcal{C}^{ul_c\times ul_c}$ is $c(l_1, l_2)$ defined in (4.7).

The covariance matrix $\mathbf{R}_{\mathbf{w}_{nk}}$ of the colored noise $\mathbf{w}_{nk}$ can be represented as

$$\mathbf{R}_{\mathbf{w}_{nk}} = N_0\mathbf{B}_{nk}\mathbf{F}_{uL}\mathbf{R}_p\mathbf{F}_{uL}^H\mathbf{B}_{nk}^T. \tag{4.22}$$

The covariance matrix might be rank deficient. Define the pseudo-inverse of $\frac{1}{N_0}\mathbf{R}_{\mathbf{w}_{nk}}$ as

$$\mathbf{\Phi}_{nk} = \mathbf{U}_{nk}\mathbf{\Lambda}_{nk}^{-1}\mathbf{U}_{nk}^H \in \mathcal{C}^{uR\times uR}, \tag{4.23}$$

with

$$\mathbf{U}_{nk} = [\mathbf{u}_{nk,1}, \mathbf{u}_{nk,2}, \cdots, \mathbf{u}_{nk,v_k}] \in \mathcal{C}^{uR\times v_k} \tag{4.24a}$$

$$\mathbf{\Lambda}_{nk} = \mathrm{diag}[\lambda_{nk,1}, \lambda_{nk,2}, \cdots, \lambda_{nk,v_k}] \in \mathcal{C}^{v_k\times v_k}, \tag{4.24b}$$

where v_k is the number of non-zero eigenvalues of $\frac{1}{N_0}\mathbf{R}_{\mathbf{w}_{nk}}$, $\mathbf{\Lambda}_{nk}$ is a diagonal matrix with $\{\lambda_{nk,i}\}_{i=1}^{v_k}$ being the non-zero eigenvalues of $\mathbf{R}_{\mathbf{w}_{nk}}$, and $\{\mathbf{u}_{nk,i}\}_{i=1}^{v_k}$ are the corresponding orthonormal eigenvectors.

Define the noise whitening matrix $\mathbf{D}_{nk} = \mathbf{\Lambda}_{nk}^{-1/2}\mathbf{V}_{nk}^H$. Applying $\mathbf{D}_{nk}$ on both sides of (4.23) leads to an equivalent system

$$\bar{\mathbf{r}}_{nk} = \sqrt{\frac{E_s}{R}}\bar{\mathbf{g}}_{nk}\cdot s_{nk} + \bar{\mathbf{w}}_{nk}, \tag{4.25}$$

where $\bar{\mathbf{r}}_{nk} = \mathbf{D}_{nk}\mathbf{r}_{nk}$, $\bar{\mathbf{g}}_{nk} = \mathbf{D}_{nk}\mathbf{g}_{nk}$, and $\bar{\mathbf{w}}_{nk} = \mathbf{D}_{nk}\mathbf{w}_{nk}$ with the covariance matrix of $\bar{\mathbf{w}}_{nk}$ being $\mathbf{R}_{\bar{\mathbf{w}}_{nk}} = \mathbf{D}_{nk}\mathbf{R}_{\mathbf{w}_{nk}}\mathbf{D}_{nk}^H = N_0\mathbf{I}_{v_k}$.

From (4.25), the optimum decision rule of the SIMO system can be represented as

$$\hat{s}_{nk} = \underset{s_{nk}\in\mathcal{S}}{\operatorname{argmin}} \, |\varphi_{nk} - q_{nk}s_{nk}|^2 \tag{4.26}$$

where $q_{nk} = \mathbf{g}_{nk}^H\mathbf{\Phi}_{nk}\mathbf{g}_{nk}$ and $\varphi_{nk} = \mathbf{g}_{nk}^H\mathbf{\Phi}_{nk}\mathbf{r}_{nk}$.

The SNR of (4.25) can be written as

$$\gamma = \mathbf{g}_{nk}^H\mathbf{\Phi}_{nk}\mathbf{g}_{nk}\frac{\gamma_0}{R}, \tag{4.27}$$

where $\gamma_0 = \frac{E_s}{N_0}$ is the SNR without fading. For systems with BPSK and Rayleigh fading, the error probability for s_{nk} is [12]

$$P_{nk}(E) \;=\; \frac{1}{\pi}\int_0^{\frac{\pi}{2}}\prod_{r=1}^{\tilde{L}_{nk}}\left[1+\frac{\delta_{nkr}\gamma_0}{R\sin^2\theta}\right]^{-1}d\theta, \tag{4.28}$$

where $\tilde{L}_{nk}$ is the rank of the product matrix, $\mathbf{R}_{nk}\mathbf{\Phi}_{nk}$, and δ_{nkr}, for $r = 1, \cdots, \tilde{L}_{nk}$, are the corresponding non-zero eigenvalues. The average BER can then be calculated as

$$P(E) = \frac{1}{NK}\sum_{n=1}^{N}\sum_{k=1}^{K}P_{nk}(E). \tag{4.29}$$

In the above analysis, the order of multipath diversity is quantified as $\tilde{L}_{nk}$, which is the rank of $\mathbf{R}_{nk}\mathbf{\Phi}_{nk}$. The matrix $\mathbf{R}_{nk}$ corresponds to correlation of the frequency domain channel coefficients, and $\mathbf{\Phi}_{nk}$ is the pseudo-inverse of the noise covariance matrix, $\mathbf{R}_{\mathbf{w}_{nk}}$.

The off-diagonal elements of the matrix $\mathbf{R}_{\mathbf{w}_{nk}}$ are contributed by the correlation of the colored noise. The uR elements in the noise vector, $\mathbf{w}_{nk}$, are extracted from the size-uL frequency-domain noise vector $\mathbf{z}_{_F}$ based on the transmission pattern $\mathbf{p}_n$, and there is at least K sub-channels between any two samples in $\mathbf{w}_{nk}$. As a result, the mutual correlation

Table 4.1: The metric $1-\rho$ under various values of K ($M=12$, $R=2$ and $u=2$).

K	1	10	20	50	100
$1-\rho$	4.9×10^{-3}	2.3×10^{-4}	8.9×10^{-5}	4.0×10^{-5}	1.8×10^{-5}

between the samples in $\mathbf{w}_{nk}$ is usually very small. To measure the mutual correlation of the samples in $\mathbf{w}_{nk}$, define a metric

$$\rho = \frac{1}{NK}\sum_{n=1}^{N}\sum_{k=1}^{K}\frac{\|\mathbf{R}'_{\mathbf{w}_{nk}}\|_2}{\|\mathbf{R}_{\mathbf{w}_{nk}}\|_2}, \tag{4.30}$$

where $\mathbf{R}'_{\mathbf{w}_{nk}}$ is a diagonal matrix obtained by setting all off-diagonal elements of $\mathbf{R}_{\mathbf{w}_{nk}}$ to 0, and $\|\mathbf{A}\|_2$ is the Frobenius norm of the matrix $\mathbf{A}$. The metric $0 \le \rho \le 1$ measures the percentage of energy on the diagonal of $\mathbf{R}_{\mathbf{w}_{nk}}$. The metric $\rho = 1$ means $\mathbf{R}_{\mathbf{w}_{nk}}$ is a diagonal matrix. Table 1 shows the values of $1-\rho$ with $u=2$, $M=12$, $R=2$, and various values of K. It is clear that ρ is very close to 1, and the difference between ρ and 1 decreases as K increases. The results in Table 1 demonstrate that the off-diagonal elements of $\mathbf{R}_{\mathbf{w}_{nk}}$ are negligible compared its diagonal elements. Therefore, the mutual correlation among the noise samples is very small or negligible.

If we ignore the off-diagonal elements of $\mathbf{R}_{\mathbf{w}_{nk}}$ and approximate the noise vector $\mathbf{w}_{nk}$ as white noise with correlation matrix $\mathbf{R}'_{\mathbf{w}_{nk}}$, then we can simplify the error performance analysis. With the white noise assumption, the SNR in (4.27) can be approximated by

$$\gamma'_{nk} = \frac{\gamma_0}{R}\sum_{v=0}^{u-1}\sum_{r=1}^{R}|G_{nv}(n_rK+k)|^2\phi_{nk}(vR+r), \tag{4.31}$$

where $\phi_{nk}(r) = q_{nk}^{-1}(r)$ if $q_{nk}(r) \neq 0$ with $q_{nk}(r)$ being the r-th diagonal element of $\mathbf{R}_{\mathbf{w}_{nk}}$, and $\phi_{nk}(r) = 0$ otherwise. The error probability in (4.28) and (4.29) can then be approximated by using the eigenvalues of the product matrix $\mathbf{R}_{nk}\mathbf{\Phi}'_{nk}$, where $\mathbf{\Phi}'_{nk}$ is the pseudo-inverse of the diagonal matrix $\frac{1}{N_0}\mathbf{R}'_{\mathbf{w}_{nk}}$. The BER results calculated with the white approximation

in (4.31) is slightly worse than the exact matched filter bound in (4.28). Our simulation indicate that the difference between the two is almost negligible due to the fact that ρ is very close to 1.

4.5.2 Impacts of Relative Delays

In this subsection, we study the impacts of the relative delays among the users on the performance of the proposed FD-OOAT scheme. From the analysis in the previous subsection, the performance of the system is dominated by the statistical properties of the SNR γ'_{nk} defined in (4.31), which in turn depends on the squared amplitude of the channel coefficients, $|G_{nv}(m)|^2$. It should be noted that the power and the auto-correlation of the noise components are independent of the relative delays τ_n as evident in (4.22).

The relative delay can be expressed as $\tau_n = l_n T_2 + \tau_{n0}$, where l_n represents the misalignment among the asynchronous users, and $\tau_{n0} \in [0, T_2]$ is the timing phase offset of the sampler. It is clear from (4.10) that l_n has no impact on the squared amplitude $|G_{nv}(m)|^2$. Next we will study the impact of τ_{n0} on $|G_{nv}(m)|^2$.

Define the *discrete-time Fourier transform* (DTFT) of the T_2-spaced discrete-time CIR, $h_{nT}(l)$, as

$$H_{nT}(f) = \sum_{l=0}^{ul_c-1} h_{nT}(l) e^{-j2\pi lf}, 0 \le f \le 1 \tag{4.32}$$

Since $h_{nT}(l) = h_{nc}(lT_2 - \tau_{n0})$, based on the sampling theorem, the DTFT can be expressed as

$$H_{nT}(f) = \frac{1}{T_2} \sum_{i=-\infty}^{\infty} \mathcal{H}_{nc}\left(\frac{f-i}{T_2}\right) \exp\left(-j2\pi\tau_{n0}\frac{f-i}{T_2}\right), \tag{4.33}$$

where $\mathcal{H}_{nc}\left(\frac{f}{T_2}\right)$ is the Fourier transform of the CIR $h_{nc}(t)$.

From (4.10), (4.32), and (4.33), we can write the frequency domain channel coefficient, $G_{nv}(m)$, as

$$G_{nv}(m) = \frac{\exp\left(-j2\pi\frac{l_n\cdot(vL+m)}{uL}\right)}{T_2\sqrt{u}} \sum_{i=-\infty}^{\infty} \mathcal{H}_{nc}\left(\frac{vL+m}{uLT_2} - \frac{i}{T_2}\right) \exp\left(-j2\pi\tau_{n0}\frac{vL+m-uLi}{uLT_2}\right). \tag{4.34}$$

The CIR, $h_{nc}(t)$, includes the effects of the physical channel and the transmit and receive filters. From (4.4), we have

$$\mathcal{H}_{nc}\left(\frac{f}{T_2}\right) = \mathcal{P}_1\left(\frac{f}{T_2}\right) \mathcal{G}_n\left(\frac{f}{T_2}\right) \mathcal{P}_2\left(\frac{f}{T_2}\right), \tag{4.35}$$

where $\mathcal{P}_i\left(\frac{f}{T_2}\right)$ and $\mathcal{G}_n\left(\frac{f}{T_2}\right)$ are the Fourier transforms of $p_i(t)$ and $g_n(t)$, respectively. If the roll-off factor of the transmit and receive filters is α, then the frequency domain support of $\mathcal{P}_i\left(\frac{f}{T_2}\right)$ is $\left|\frac{f}{T_2}\right| \leq \frac{1+\alpha}{2T_1}$, or $|f| \leq \frac{1+\alpha}{2u}$. All practical systems have at most 100% excessive bandwidth, *i.e.*, $\alpha \leq 1$. Therefore, $\mathcal{H}_{nc}\left(\frac{f}{T_2}\right) = 0$ for $|f| > \frac{1}{u}$.

4.5.2.1 $u = 1$

For a system without oversampling, we have $T_1 = T_2$, and the frequency domain support of $\mathcal{P}_i\left(\frac{f}{T_1}\right)$ and $\mathcal{H}_{nc}\left(\frac{f}{T_1}\right)$ are $|\frac{f}{T_1}| < \frac{1+\alpha}{2T_1}$. In this case, due to the excessive bandwidth of the transmitted signal when $\alpha > 0$, the sampling operation at the receiver causes spectrum aliasing as shown in (4.33) and (4.34). It is apparent from (4.34) that the frequency domain channel coefficient is a function of τ_{n0}. Therefore, the performance of the system with $u = 1$ will be affected by the timing phase offset τ_{n0}.

4.5.2.2 $u \geq 2$

The frequency domain support of $\mathcal{P}_i\left(\frac{f}{T_2}\right)$ and $\mathcal{H}_{nc}\left(\frac{f}{T_2}\right)$ are $|\frac{f}{T_2}| < \frac{1+\alpha}{2uT_2} \leq \frac{1}{2T_2}$ for $\alpha \leq 1$. Therefore, the sampling rate $\frac{1}{T_2}$ is at least twice as much as the signal bandwidth $B \leq \frac{1}{2T_2}$, and there is no spectrum aliasing after the sampling operation. The frequency domain channel coefficient in (4.34) can be simplified to

$$G_{nv}(m) = \frac{\exp\left(-j2\pi\frac{l_n\cdot(vL+m)}{uL}\right)}{T_2\sqrt{u}}\mathcal{H}_{nc}\left(\frac{vL+m}{uLT_2}\right)\exp\left(-j2\pi\tau_{n0}\frac{vL+m}{uLT_2}\right). \tag{4.36}$$

The squared amplitude of the channel coefficient can then be expressed as

$$|G_{nv}(m)|^2 = \frac{1}{T_2\sqrt{u}}\left|\mathcal{H}_{nc}\left(\frac{vL+m}{uLT_2}\right)\right|^2. \tag{4.37}$$

It is interesting to note that $|G_{nv}(m)|^2$ is independent of the user mis-alignments l_n or the timing phase offset τ_{n0}. Since the system performance is dominated by the squared amplitude of the channel coefficient, the user mis-alignments or timing phase offset has a very small, if any, impact on the performance of the system when $u \geq 2$. Specifically, for systems with at most 100% excessive bandwidth, an oversampling factor of 2 is sufficient to avoid spectrum aliasing at the receiver, thus removes the impacts of τ_{n0}. The above analysis is corroborated by simulation results with both the optimum and sub-optimum detectors.

4.6 Simulation Results

Simulation results are presented in this section to demonstrate the performance of the over-sampled FD-OOAT scheme with the optimum and sub-optimum detections. The effects of time-domain oversampling and the timing phase offset on the system performance are also studied in this section.

In the simulation examples, the sample period at the transmitter is set to $T_1 = 3.69$ μs, and a root-raised cosine (RRC) filter with a roll-off factor $\alpha = 1.0$ is used for both the transmit and receive filters. The relative delays among the users, τ_n, is uniformly distributed between $[0, KT_1]$ with $K = 50$ unless stated otherwise. The frequency-selective fading channel follows the *Typical Urban* (TU) *power delay profile* (PDP) [21].

Fig. 4.2 shows the BER results of the proposed CT-MAC system under various system configurations. There are $M = 12$ sub-channels per symbol and each symbol is transmitted with $R = 2$ repetitions. The sub-optimum BDFE detection is performed with 4 iterations. The analytical results are obtained with both (4.28) and the white approximation as in (4.31), and the two results overlap. Only the one obtained with (4.28) is shown in the figure. We have the following observations about the results. First, when $N = 1$, the analytical and simulation results match perfectly for both $u = 1$ and 2. Second, with the BDFE receiver, increasing N has less impacts on the oversampled system with $u = 2$ than the system with $u = 1$. At BER $= 2 \times 10^{-3}$, increasing N from 1 to 10 results in a 1.5 dB and a 0.8 dB performance loss for systems with $u = 1$ and $u = 2$, respectively. This indicates that the proposed FD-OOAT system can operate properly even when there are a large number of users and collisions. In addition, when $u = 2$ and $N = 10$, the sub-optimum BDFE receiver achieves almost the same performance as the optimum ML receiver, but with a much lower complexity. Third, the oversampled system consistently outperforms the system without oversampling. The performance improvement is contributed by the additional multipath diversity and the insensitivity to the timing phase offset due to the oversampling operation. At BER $= 2 \times 10^{-3}$ and $N = 10$, the oversampled system outperforms its non-oversampled counterpart by 5.6 dB when BDFE is used.

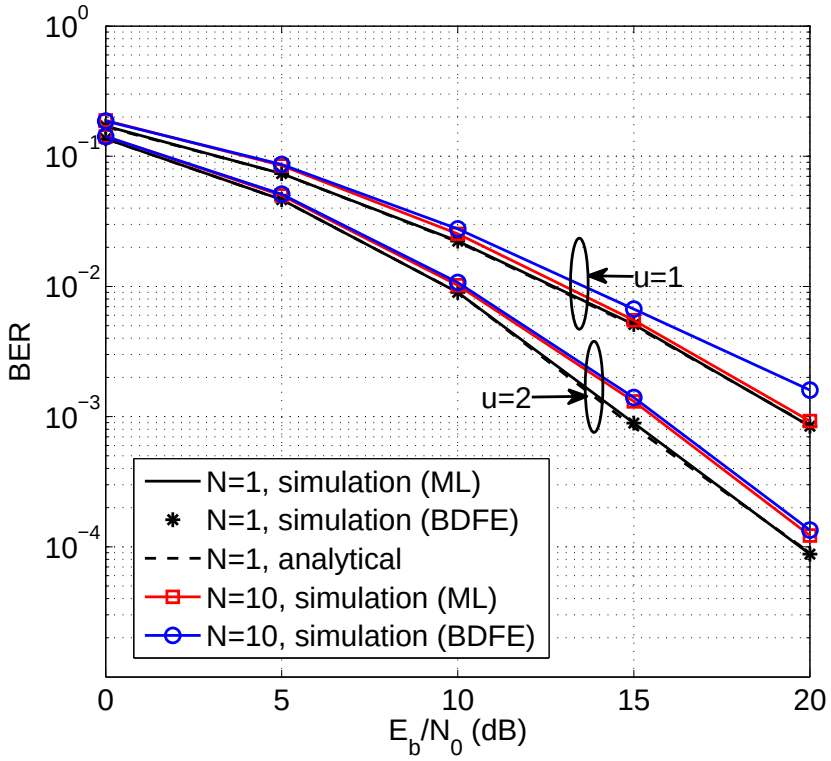

Figure 4.2: BER performance comparison of systems with $M = 12$ sub-channels per symbol, $R = 2$ repetitions, and different number of users.

The effects of the receiver timing phase offset on the system performance are studied in Fig. 4.3 for single-user systems and Fig. 4.4 for multi-user systems, respectively. In Fig. 4.3, there are $M = 12$ sub-channels per symbol, and each symbol is transmitted with $R = 2$ repetitions. To have a better understanding on the effects of timing phase offset, it is assumed that τ_{n0} is fixed at 0 or $0.5T_2$ in Fig. 4.3. The performance of the system with $u = 1$ varies as τ_{n0} changes, yet the performance of the oversampled system is independent of τ_{n0}.

A similar observation is obtained in Fig. 4.4 for systems with multiple users, where the BER is shown as a function of τ_{n0}. The mis-alignment among the asynchronous users, l_n, is uniformly distributed between $[0, uK]$. The E_b/N_0 is 10 dB. The BER of the oversampled

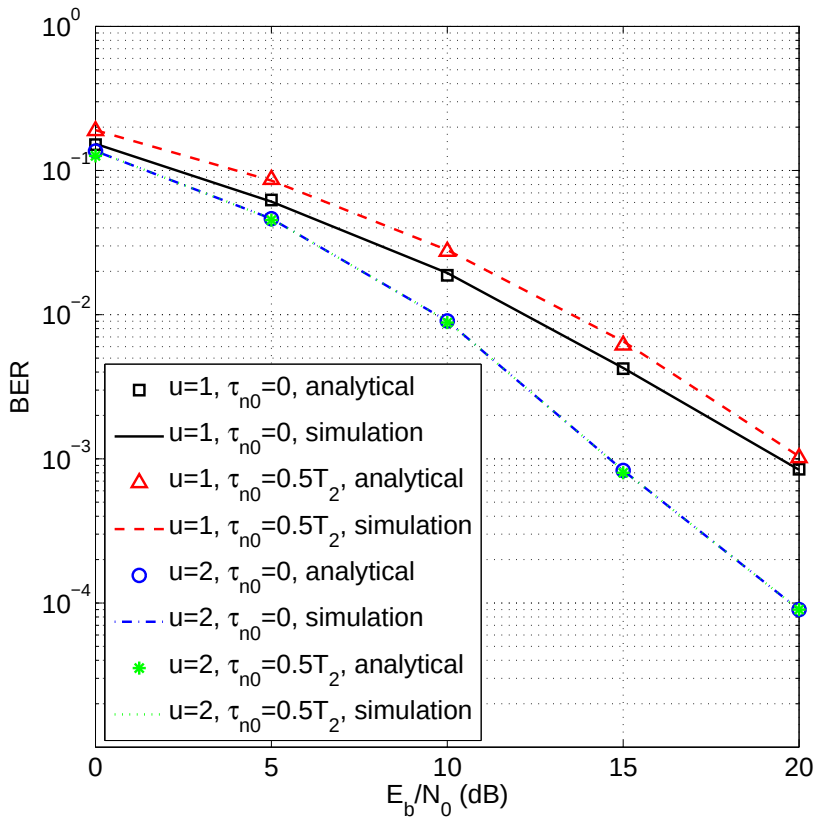

Figure 4.3: The effects of the receiver timing phase offset on the BER performance of the system (There are $N = 1$ user, $M = 12$ sub-channels per symbol, and $R = 2$ repetitions).

system stays constant regardless of the values of τ_{n0}, for both the optimum and sub-optimum algorithms with different number of users. On the other hand, the BER of the system with $u = 1$ is a function of τ_{n0}. The simulation results corroborate the theoretical analysis that twice oversampling is sufficient to remove the effects of τ_{n0} for a system with at most 100% excessive bandwidth. Therefore, the proposed oversampled FD-OOAT scheme can operate effectively at the presence of both multi-user interference, user mis-alignment, and timing phase offset.

Fig. 4.5 demonstrates the impacts of the number of iterations on the frame error rate

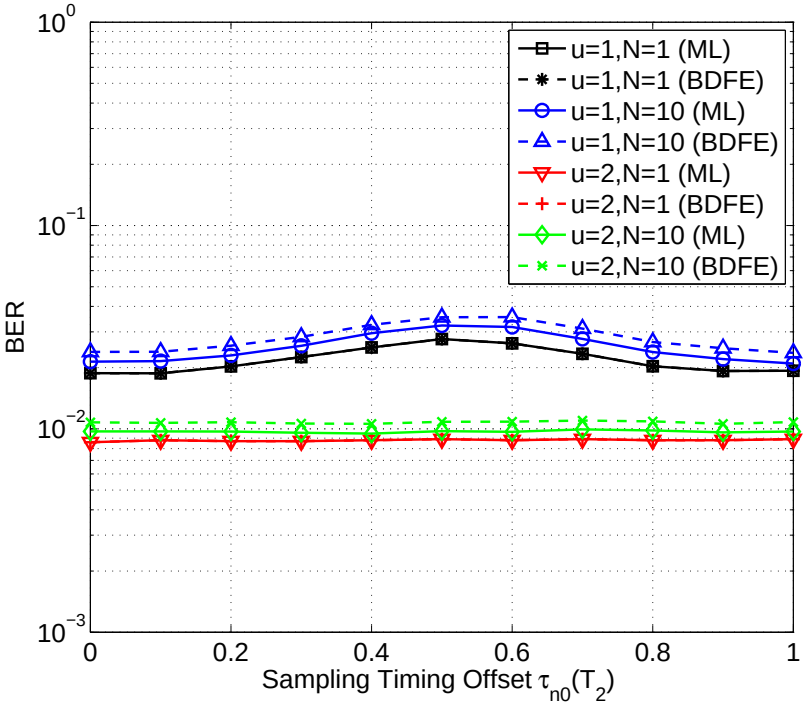

Figure 4.4: BER v.s. timing phase offset ($E_b/N_0 = 10$ dB. There are $M = 12$ sub-channels per symbol, and $R = 2$ repetitions).

(FER) with the sub-optimum BDFE detector. There are $N = 10$ active users, $M = 12$ sub-channels per symbol, $R = 2$ repetitions. As seen from the figure, the largest performance gain is achieved at the second iteration and the performance converges at the fourth iteration for systems with $u = 1$ or $u = 2$. At the fourth iteration and FER$= 4 \times 10^{-2}$, the FER performance of the oversampled system outperforms the one without oversampling by 5.6 dB, which is consistent with the BER improvement observed in Fig. 4.2.

Fig. 4.6 shows the normalized throughput as a function of the normalized offered load for various MAC schemes. For the FD-OOAT system, there are $M = 10$ sub-channels per symbol, and $R = 2$ repetitions. All other systems have $M = 10$ slots per frame. The normalized offered load of all the systems is calculated as $G = \frac{N}{M}$. The normalized throughput is defined as the amount of data successfully delivered to the receiver per unit

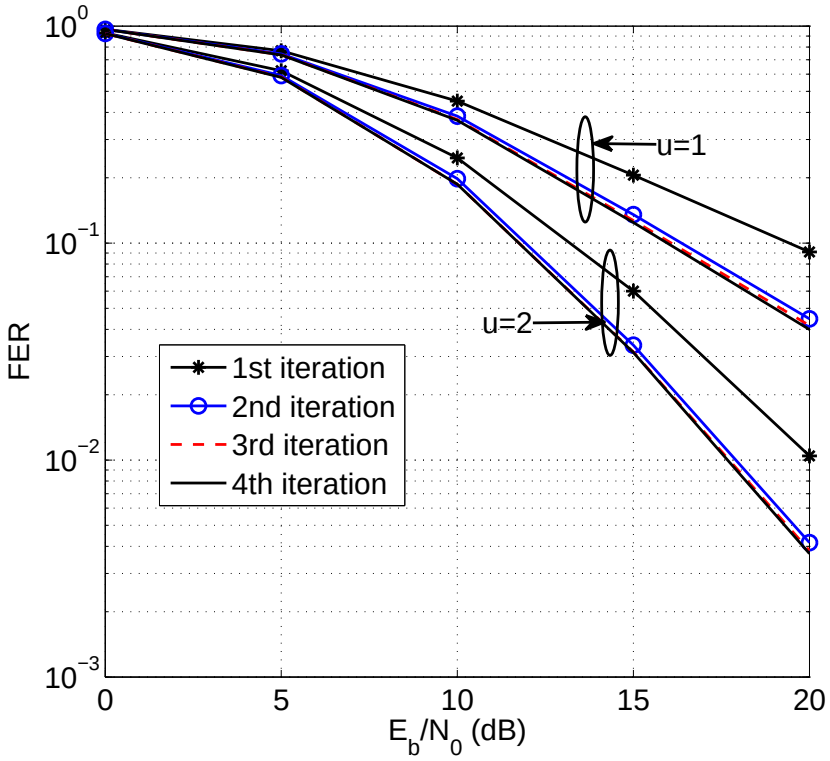

Figure 4.5: FER performance of systems with the BDFE receiver (There are $N = 10$ users, $M = 12$ sub-channels, and $R = 2$ repetitions).

time per unit bandwidth. The normalized throughput for the FD-OOAT scheme is calculated as $\frac{N}{M}(1 - \text{FER})$. Details of the calculation of the normalized offered load and normalized throughput can be found in [10]. For the slotted ALOHA, CRDSA, and IRSA systems, the simulations are performed under the assumption of noise-free communication, *i.e.*, the only source of errors for this systems is the unresolvable signal collisions among the users. Results obtained under the noise-free assumption represent the best possible performance under any channel configurations. On the other hand, the results of the proposed FD-OOAT systems are obtained in a frequency-selective fading channel with $E_b/N_0 = 15$ dB. As shown in the figure, the slotted ALOHA, CRDSA and IRSA achieve their respective peak throughputs when $G \leq 1$, and the throughputs drop dramatically when $G > 1$. The throughput of the

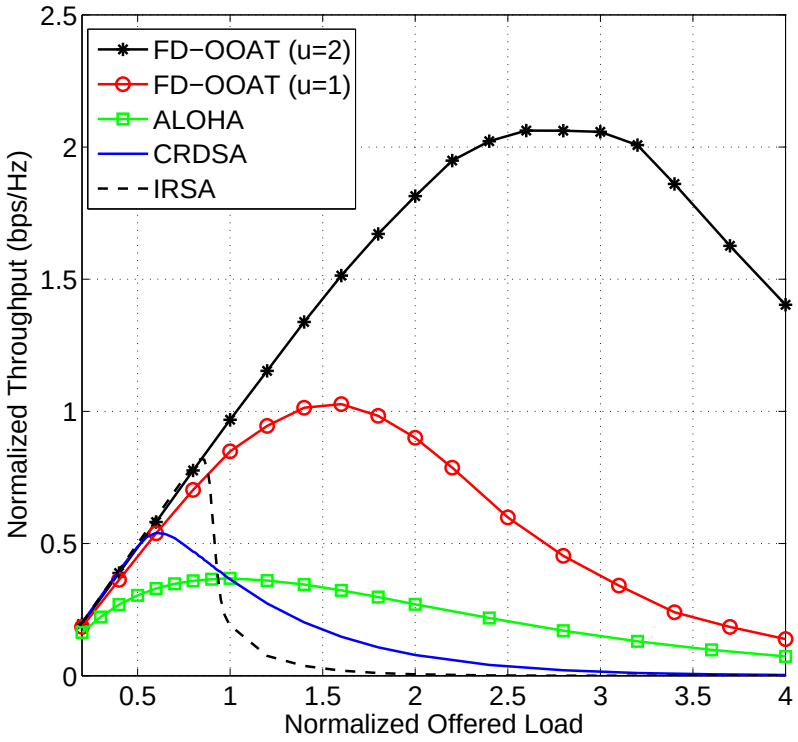

Figure 4.6: Normalized throughput v.s. normalized offered load.

proposed FD-OOAT scheme achieves the maximum throughput 1.03 bps/Hz at $G = 1.6$ when $u = 1$. For the oversampled system with $u = 2$, the maximum throughput 2.06 bps/Hz is achieved at $G = 2.6$. Therefore, the FD-OOAT system can be overloaded by supporting more users than the number of sub-channels, yet all the other MAC schemes must operate with $G < 1$. Employing FD-OOAT increases both the number of users supported and peak throughput. In addition, time domain oversampling allows the FD-OOAT system to support 60% more users than the system with $u = 1$, and improves the throughput by 100%.

4.7 Conclusions

A cross-layer CT-MAC scheme with frequency-domain OOAT and time-domain oversampling has been proposed for broadband wireless networks operating in frequency-selective

fading channels. With the help of time-domain oversampling, the proposed scheme can operate without precise synchronization, and it is insensitive to timing phase offsets between the sampling clocks at the transmitter and receiver. The collision tolerance in the MAC layer was achieved by performing MUD over the specially designed FD-OOAT signal in the PHY layer. Simulation results demonstrated that 1) the performance of the oversampled FD-OOAT system was insensitive to user mis-alignment or sampler timing phase offset; 2) significant multipath diversity gain was achieved with the oversampled FD-OOAT scheme; 3) the proposed scheme could support more users than the number of sub-channels. An oversampled FD-OOAT with M sub-channels per symbol could support up to $N = 2.6M$ simultaneous users and has a normalized throughput peak at 2.06 bps/Hz with BPSK modulation.

4.8 References

[1] G. Mergen and L. Tong, "Receiver controlled medium access in multihop ad hoc networks with multipacket reception," in *Proc. IEEE Military Commun. Conf. MILCOM 2001*, vol. 2, pp. 1014 - 1018, 2001.

[2] L. Tong, V. Naware, and P. Venkitasubramaniam, "Signal processing in random access," *IEEE Sig. processing Mag.*, vol. 21, pp. 29-39, Sept. 2004.

[3] Q. Zhao and L. Tong, "A dynamic queue protocol for multiaccess wireless networks with multipacket reception," *IEEE Trans. Wireless Communications*, vol. 3, pp. 2221 - 2231, Nov. 2004.

[4] R. Samano-Robles, M. Ghogho, and D. C. Mclernon, "An infinite user model for random access protocols assisted by multipacket reception and retransmission diversity," in *Proc.*

IEEE Sig. Processing Advances Wireless Commun. SPAWC 2008, pp. 111 - 115, 2008.

[5] E. Casini, R. De Gaudenzi, and O. del Rio Herrero, "Contention resolution diversity slotted ALOHA (CRDSA): an enhanced random access scheme for satellite access packet networks," *IEEE Trans. Wireless Commun.*, vol. 6, pp. 1408 - 1419, Apr. 2007.

[6] G. Liva, "A slotted ALOHA scheme based on bipartite graph optimization," in *Proc. Intern. ITG Conf. Source and Channel Coding SCC'10*, Jan. 2010.

[7] G. Liva, "Graph-based analysis and optimization of contention resolution diversity slotted ALOHA," *IEEE Trans. Commun.*, vol. 59, pp. 477 - 487, Feb. 2011.

[8] B. Lu, X. Wang, and J. Zhang, "Throughput of CDMA data networks with multiuser detection, ARQ, and packet combining," *IEEE Trans. Wireless Commun.*, vol. 3, pp. 1576 - 1589, Sept. 2004.

[9] Y. J. Zhang and K. B. Letaief, "An efficient resource-allocation scheme for spatial multiuser access in MIMO/OFDM systems," *IEEE Trans. Commun.*, vol. 53, pp. 107-116, Jan. 2005.

[10] J. Wu and G. Y. Li, "Collision-tolerant media access control with on-off accumulative transmission," accepted for publication in *IEEE Trans. Wireless Commun.*, 2012.

[11] D. Marabissi, R. Fantacci and S. Papini, "Robust multiuser interference cancellation for OFDM systems with frequency offset," *IEEE Trans. Wireless Commun.*, vol. 5, pp. 3068 - 3076, Nov. 2006.

[12] J. Wu and C. Xiao, "Performance analysis of wireless systems with doubly selective Rayleigh fading," *IEEE Trans. Veh. Technol.*, vol. 56, pp. 721 - 730, Mar. 2007.

[13] J. Wu, Y. R. Zheng, K. B. Letaief and C. Xiao, "On the error performance of wireless systems with frequency selective fading and receiver timing phase offset," *IEEE Trans. Wireless Commun.*, vol. 6, pp. 720 - 729, Feb. 2007.

[14] S. Tian, K. Panta, H. A. Suraweera, B. J. C. Schmidt, S. McLaughlin and J. Armstrong, "A novel timing synchronization method for ACO-OFDM based optical wireless communications," *IEEE Trans. on Wireless Commun.*, vol. 7, pp. 4958 - 4967, Dec. 2008.

[15] B. Park, H. Cheon, C. Kang, and D. Hong, "A novel timing estimation method for OFDM systems," *IEEE Commun. Lett.*, vol. 7, pp. 239-241, May 2003.

[16] M. Morelli, "Timing and frequency synchronization for the uplink of an OFDMA system," *IEEE Trans. Commun.*, vol. 52, pp. 296-306, Feb. 2004.

[17] J. Lee and S. Kim, "Time and frequency synchronization for OFDMA uplink system using the SAGE algorithm," *IEEE Trans. Wireless Commun.*, vol. 6, pp. 1176 - 1181, Apr. 2007.

[18] C. Xiao, J. Wu, S.-Y. Leong, Y. R. Zheng and K. B. Letaief, "A discrete-time model for triply selective MIMO Rayleigh fading channels," *IEEE Trans. Wireless Commun.*, vol. 3, pp. 1678 - 1688, Sept. 2004.

[19] J. Wu, and Y. R. Zheng, "Oversampled orthogonal frequency division multiplexing in doubly selective fading channels," *IEEE Trans. Wireless Commun.*, vol. 59, pp. 815 - 822, Mar. 2011.

[20] J. Wu and Y. R. Zheng, "Low complexity soft-input soft-output block decision feedback equalization," *IEEE J. Selected Areas Commun.*, vol. 26, pp. 281 - 289, 2008.

[21] ITU-R Recommendation M.1225, "Guidelines for evaluation of radio transmission techniques for IMT-2000," 1997.

Chapter 5

Cooperative Spectrum Sensing with a Progressive MAP Detection Algorithm

5.1 Abstract

In this paper, a new cooperative spectrum sensing algorithm is proposed for a cognitive radio network with multiple secondary users (SUs) sharing spectrum with one or more primary users (PUs). Unlike most previous spectrum sensing algorithms that do not consider the time domain traffic statistics of the PU, the algorithm in this paper is developed by exploiting the statistical properties of the PU's transmission pattern, which is modeled with a Markov chain with two states: busy (1) and idle (0). Each SU performs energy detection based on an observation of the Markov chain, and the detection results are forwarded to a fusion center (FC) through a noisy channel. The FC recovers the decisions of the SUs by using a new progressive maximum *a posteriori* (MAP) algorithm, where the *a priori* probability essential to the MAP detection is obtained by progressively estimating the transition probabilities of the Markov chain. Analytical expressions are derived for the probabilities of false alarm and missing detection, with both the majority data fusion rule and the OR data fusion rule. Both theoretical analysis and simulation results indicate that the proposed algorithm can provide reliable and efficient spectrum sensing over a large range of system configurations.

keywords

cooperative spectrum sensing, energy detector, MAP decision rule, OR logic data fusion rule, majority data fusion rule

5.2 Introduction

Cognitive radio, which provides flexible spectrum accesses by dynamically sensing and adapting to the surrounding radio environment, is quickly emerging as one of the most promising technologies for improving the utilization of the precious spectrum resources [1] - [3]. The proper operation of a cognitive radio network depends on the reliable and efficient spectrum sensing, with which a secondary user (SU) can detect the spectrum holes in the time-frequency plane and avoid interference to the licensed or primary users (PUs) [4].

Recently, there have been considerable efforts devoted to the development of spectrum sensing algorithms in cognitive radio networks [5] - [9]. It is shown in [5] that the energy detector is optimum in detecting weak unknown signals with zero-mean known constellations. The performance of spectrum sensing with energy detection can be significantly improved by allowing multiple SUs to cooperate with each other [6] - [9]. The cooperative spectrum sensing is usually performed in two steps: each SU performs energy detection individually, then a fusion center (FC) makes decision on the state of the channel by collecting detection results from the SUs. In [6], a noise-free channel is assumed between the SUs and the FC, and the noise-free assumption is not true in reality. Practical channel is considered in [7], where the FC detects the noisy signal from the SUs with a maximum *a posteriori* (MAP) decision rule. The MAP detector requires the knowledge of the *a priori* probability, which

is estimated assuming an infinite number of SUs. In [9], the SUs forward soft information, instead of binary hard decisions, to the FC. Soft information forwarding improves the sensing performance at the cost of significantly increased bandwidth requirement between the SUs and the FC. In addition, none of the above works consider the PUs' traffic patterns, which might be critical to the spectrum sensing performance.

In this chapter, we propose a new cooperative spectrum sensing algorithm by exploiting the statistical traffic patterns of the PU. The transmission pattern of the PU is assumed to follow a Markov chain with two states: busy (1) and idle (0) [10]. Consequently, the binary energy detection results at the SUs, which can be considered as passing the two-state Markov chain through a binary symmetric channel, form a new Markov chain. The new algorithm is motivated by the time domain correlations of the Markov chain. The FC recovers the binary energy detection results of the SUs with a new progressive MAP algorithm, where the *a priori* probabilities that are essential to the MAP detection are obtained by progressively estimating the transition probabilities of the Markov progress in the time domain. It is shown through simulations that the FC with the new algorithm can obtain a very accurate estimation of the SU detections. In most existing works [6, 7], the FC employs the OR data fusion rule over the estimated SU detections, and it is well known that the OR data fusion rule reduces missing detections at the cost of more false alarms. In this chapter, the performance of the OR data fusion rule is compared to a majority data fusion rule. Exact analytical expressions of the probability of false alarm and the probability of missing detection are derived for the majority and OR data fusion rules, and their performances are compared through both analytical and simulation results.

5.3 System Model

Consider a cooperative spectrum sensing system in a cognitive radio network with one PU and N SUs. The traffic pattern of the PU is assumed to be a Markov chain with two states: idle (0) and busy (1), with the one-step transition probabilities being p_{00} and p_{10}.

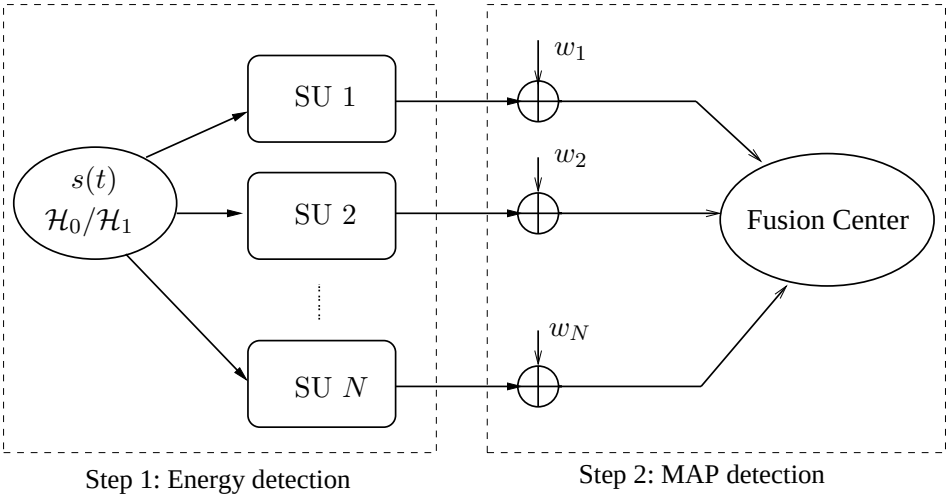

Figure 5.1: Block diagram of a cooperative spectrum sensing in cognitive radio networks

The cooperative spectrum sensing is performed with a two-step protocol as shown in Fig. 6.1. In the first step, each SU performs energy detection to sense the state of the PU, and makes a binary decision (busy or idle) based on the local sensing result. In the second step, the SUs forward their individually obtained sensing results to a FC, which will make a final decision on the state of the PU by performing data fusion over the noisy observations of the decisions from all the SUs.

In the first step, the hypothesis test of the energy detection performed by the n-th SU can be represented as [11, 12],

$$\begin{aligned} \mathcal{H}_0 : r_n(t) &= v_n(t), \\ \mathcal{H}_1 : r_n(t) &= s(t) + v_n(t), \end{aligned} \tag{5.1}$$

where $s(t)$ is a bandlimited signal from the PU with an one-sided bandwidth W, $v_n(t)$ is the additive white Gaussian noise (AWGN) with one-sided power spectral density N_{0v}, and $r_n(t)$ is the signal observed by the n-th SU.

The energy detection is performed by using signals observed during an interval of duration T. It is assumed that the state of the channel does not change within T. This assumption can be easily met by choosing a small enough T. The test statistic used by the n-th SU during the k-th detection interval, $R_n(k)$, is obtained by passing the received signal, $r_n(t)$, through an energy detector as shown in Fig. 5.2. The low pass filter (LPF) in the energy detector has a cut off frequency of W, and it is used to limit the bandwidth of the white noise. After a s square law device and a finite time integrator, the output of the energy detector can be expressed as [11],

$$R_n(k) = \frac{1}{N_{0v}} \int_{(k-1)T}^{kT} |r_n(t)|^2 dt = \sum_{i=1}^{2u} \left(\frac{s_i + v_{ni}}{\sqrt{N_{0v} W}} \right)^2, \tag{5.2}$$

where $u = TW$ denotes the time bandwidth product, with W being the one-sided bandwidth of the signal, $v_{ni} = v_n(\frac{i}{2W})$ and $s_i = s(\frac{i}{2W})$ are the noise sample and signal sample, respectively. The noise sample, v_{ni}, is a zero mean Gaussian random variable with variance, $N_{0v}W$, i,e, $v_{ni} \sim N(0, N_{0v}W)$.

The test statistic, $R_n(k)$, has the following distributions [11], [12],

$$R_n(k) \sim \begin{cases} \chi^2_{2u}, & \mathcal{H}_0, \\ \chi^2_{2u}(2\gamma_s), & \mathcal{H}_1, \end{cases} \tag{5.3}$$

where χ^2_{2u} denotes the central chi-square distribution with $2u$-degree of freedom, $\chi^2_{2u}(2\gamma_s)$ is the non-central chi-square distribution with $2u$-degree of freedom and a non centrality parameter $2\gamma_s$, $\gamma_s = \frac{E_0}{N_{0v}}$ is the signal-to-noise ratio (SNR), and $E_0 = \int_0^T s^2(t)dt$ is the signal

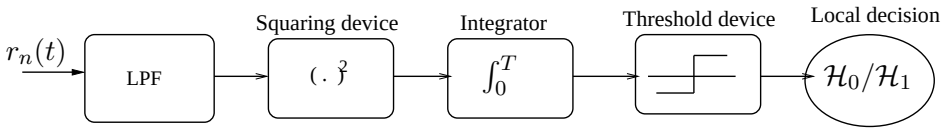

Figure 5.2: Block diagram of the energy detector employed at the SU.

energy.

During the k-th detection interval, the SU makes decision on the state of the PU by comparing $R_n(k)$ to a predefined threshold, λ, as $b_n(k) = 1$ if $R_n(k) > \lambda$, and $b_n(k) = 0$ otherwise.

Define the probability of false alarm, P_{f_n}, as the probability that a PU is detected by the n-th SU while the PU is idle. The probability of missing, P_{m_n}, is defined vice versa. With the hypotheses test defined in (6.1), we have [12]

$$\begin{aligned} P_{f_n} &= P_r(R_n > \lambda|\mathcal{H}_0) = \frac{\Gamma(u, \frac{\lambda}{2})}{\Gamma(u)}, \\ P_{m_n} &= P_r(R_n < \lambda|\mathcal{H}_1) = 1 - Q_u(\sqrt{2\gamma_s}, \sqrt{\lambda}), \end{aligned} \tag{5.4}$$

where $\Gamma(a, b)$ is the incomplete gamma function, $Q_u(a, b)$ is the generalized Marcum Q-function. The decision threshold, λ, can be chosen to meet the requirements on P_{f_n} and P_{m_n}.

The local decisions from the SUs are transmitted to the FC through an orthogonal media access control (MAC) scheme, such as frequency division multiplexing access (FDMA), to achieve a collision free communication at the FC. The signal received by the FC from the n-th SU can be represented as

$$y_n(k) = \sqrt{E_s}x_n(k) + w_n(k), \tag{5.5}$$

where $x_n(k) = 2b_n(k) - 1$, E_s is the transmission energy of one symbol, and $w_n(k)$ is the AWGN with one-sided power spectral density N_{0w}. The models in (5.1) and (5.5) can be

extended to systems with flat fading channels. The FC will make a decision on the state of the PU by collecting the information from all the SUs.

5.4 A New Cooperative Spectrum Sensing Algorithm

A new data fusion algorithm at the FC is proposed in this section to improve the performance of the cooperative spectrum sensing.

5.4.1 MAP detection with Progressively Updated A Priori Information

In this subsection, a new MAP decision rule with progressively updated *a priori* information is proposed to improve the detection performance at the FC.

The FC detects the information transmitted by the n-th SU with the MAP detection rule as

$$\hat{x}_n(k) = \underset{b\in\mathcal{B}}{\operatorname{argmax}}\, p(y_n(k)|x_n(k)=b)P(x_n(k)=b), \tag{5.6}$$

where $\mathcal{B} = \{-1, 1\}$, and $p(y_n(k)|x_n(k) = b) = \frac{1}{\sqrt{\pi N_{0w}}} \exp\left\{-\frac{1}{N_{0w}}\left|y_n(k) - \sqrt{E_s}b\right|^2\right\}$. The above detection rule can be alternatively represented as $\hat{x}_n(k) = 1$, if $y_n(k) \geq \tau_n(k)$, and $\hat{x}_n(k) = -1$ otherwise, where the threshold, $\tau_n(k)$, is

$$\tau_n(k) = \frac{N_{0w} \ln\left(\frac{1-P_n(k)}{P_n(k)}\right)}{4\sqrt{E_s}}, \tag{5.7}$$

with $P_n(k) = P(x_n(k) = 1) = P(b_n(k) = 1)$ being the probability that a PU is detected by the n-th SU.

The MAP decision rule requires the knowledge of the *a priori* probability, $P_n(k)$, which is usually not available at the receiver. We propose to progressively estimate the *a priori*

probability by using a sliding window that contains the received signal and decisions from the previous K detection intervals, as well as the statistical properties of the Markov chain.

Since $x_n(k)$ is obtained through independent observations of a Markov chain, it is easy to show that $x_n(k)$ is also a Markov chain with two states: 0 ($x_n(k) = -1$) and 1 ($x_n(k) = 1$). Define the transition probabilities of $x_n(k)$ as $q_{n00} = P(x_n(k) = -1|x_n(k-1) = -1)$ and $q_{n10} = P(x_n(k) = 1|x_n(k-1) = -1)$. When the Markov chain enters the stable state, the *a priori* probability can be expressed as [14]

$$\lim_{k\to\infty} P_n(k) = \frac{1 - q_{n00}}{1 + q_{n10} - q_{n00}}. \tag{5.8}$$

We propose to estimate the value of $P_n(k)$ by using the above relationship. Consider a sliding window with a size K, with $\{y_n(i)\}_{i=k-K}^{k-1}$ and $\{\hat{x}_n(i)\}_{i=k-K}^{K-1}$. The transition probability, q_{n00}, can be estimated as follows

$$\hat{q}_{n00}(k) = \frac{\sum_{i=k-K}^{k-2} I(\hat{x}_n(i+1) = 0 \& \hat{x}_n(i) = 0)}{\sum_{i=k-K}^{k-2} I(\hat{x}_n(i) = 0)}, \tag{5.9}$$

where $a\&b$ is the AND operation between two logic expressions a and b, and $I(a) = 1$ if the logical expression a is true, and 0 otherwise. The probability $\hat{q}_{n10}$ can be obtained similarly.

The transition probabilities are estimated by using the previous hard decisions. In order to get a better estimate, we propose to also use the soft information, $\{y_n(i)\}_{i=k-K}^{k-1}$. Define $\Delta_k = \frac{1}{K}\sum_{i=k-K}^{k-1} y_n(i)$. Then based on the strong law of large numbers, we have

$$P_n(k) = \frac{1}{2}\left(\frac{1}{\sqrt{E_s}} \lim_{K\to\infty} \Delta_k + 1\right). \tag{5.10}$$

Combining (5.8) with (5.10), we have an over-determined system with two independent equations and one unknown variable, $P_n(k)$. The system can be solved with the least squares

(LS) method, and the solution is

$$\hat{P}_n(k) = \frac{1}{4}\left[\frac{\Delta_k}{\sqrt{E_s}} + \frac{2(1-\hat{q}_{n00})}{1+\hat{q}_{n10}-\hat{q}_{n00}} + 1\right]. \tag{5.11}$$

The estimated *a priori* probability, $\hat{P}_n(k)$, can then be used in (5.6) to obtain a decision on $x_n(k)$. The simulation results show that the *a priori* probability estimated by using the progressive estimation method described in (5.11) is very close to its true value.

With this new progressive MAP detection algorithm performed at the FC, define two error probabilities between the n-th SU and the PU as, $e_{n01} = P\{\hat{x}_n(k) = 1 | x_n(k) = -1\}$, $e_{n10} = P\{\hat{x}_n(k) = -1 | x_n(k) = 1\}$. The values of e_{n01} and e_{n10} will be analyzed in the next subsection.

Once the FC obtains the estimates of the decisions from all the SUs, the results will be combined to estimate the state of the PU. Many existing cooperative spectrum sensing algorithms employ the OR data fusion rule, where the logic OR operation is performed on all the binary decisions [5], [6]. The OR data fusion rule will minimize the probability of missing at the cost of a higher probability of false alarm.

To achieve a better tradeoff between false alarm and missing detection, we will compare the performance of the OR data fusion rule with that of a majority data fusion rule, where the FC will decide in favor of the state that has the most votes from the SUs. In case there is a draw, the FC will decide in favor of the state 1 (busy) to reduce the probability of missing. Based on the above description, the FC with the majority decision rule will decide that the PU is busy during the k-th detection interval if and only if the following condition is met

$$\sum_{n=1}^{N} I(\hat{x}_n(k) = 1) \geq \lfloor N/2 \rfloor, \tag{5.12}$$

where $\lfloor a \rfloor$ returns the largest integer that is smaller than or equal to a.

5.4.2 Performance Analysis

The performance of the proposed cognitive sensing algorithm is analyzed in this subsection.

Given the noisy channel between the SU and the FC, the FC might make decision errors on the information transmitted by the SU. The following lemma gives the error probabilities at the FC during the SU signal detection.

Lemma 5.1: If the FC has ideal knowledge of the *a priori* probability, $P_n(k)$, then the error probabilities, e_{n01} and e_{n10}, can be calculated as

$$\begin{aligned} e_{n01} &= Q\left(\frac{4E_s - \eta}{\sqrt{8N_{0w}E_s^2}}\right), \\ e_{n10} &= Q\left(\frac{4E_s + \eta}{\sqrt{8N_{0w}E_s^2}}\right), \end{aligned} \tag{5.13}$$

where $Q(x) = \frac{1}{\sqrt{2\pi}}\int_x^\infty \exp\left(-\frac{u^2}{2}\right) du$ is the Gaussian-Q function, and $\eta = N_{0w} \cdot \ln\left(\frac{P_n(k)}{1-P_n(k)}\right)$.

Proof: The MAP decision rule in (5.6) will decide on $\hat{x}_n(k) = \hat{b}$ if

$$\left|y_n(k) - \sqrt{E_s}\hat{b}\right|^2 - \left|y_n(k) - \sqrt{E_s}b\right|^2 < \eta, \tag{5.14}$$

where $\eta = N_{0w} \cdot \ln\left(\frac{P(x_n(k)=\hat{b})}{P(x_n(k)=b)}\right)$, $b, \hat{b} \in \mathcal{B}$, and $b \neq \hat{b}$.

If $x_n(k) = b$ is transmitted, the above decision rule can be alternatively represented as

$$\mathbf{Z} < \eta - E_s|d|^2, \tag{5.15}$$

where $\mathbf{Z} = 2d\sqrt{E_s}\Re\{w_n(k)\}$, and $d = b - \hat{b} \in \{-2, 2\}$. The decision variable, $\mathbf{Z}$, is a Gaussian random variable, with mean $\mathbb{E}(\mathbf{Z}) = 0$, and variance $\sigma_{\mathbf{Z}}^2 = 2N_{0w}{E_s}^2|d|^2$. The error probabilities can then be calculated by using $e_{nb\hat{b}} = P\left(\mathbf{Z} < \eta - E_s|d|^2\right)$, and this leads to (5.13). ■

After the detection at the FC, the probabilities of false alarm and missing at the FC for the n-th SU can be expressed as follows

$$\begin{aligned} \hat{P}_{f_n} &= P_{f_n}(1-e_{n10}) + (1-P_{f_n})e_{n01}, \\ \hat{P}_{m_n} &= P_{mn}(1-e_{n01}) + (1-P_{mn})e_{n10}, \end{aligned} \tag{5.16}$$

where P_{f_n} and P_{mn} are defined in (5.4), and e_{n01} and e_{n10} are given in Lemma 5.1.

With the above results, we can derive the global probabilities of false alarm and missing for a system with the majority decision rule. The results are stated in the following proposition.

Proposition 5.1: If the SUs experiences independent and identical channels, then the probabilities of global false alarm, P_f, and missing, P_m, of the proposed cooperative spectrum sensing system with the majority decision rule can be calculated as

$$P_f{}^{(MJ)} = \sum_{M=\lfloor N/2 \rfloor}^{N} \binom{N}{M} \hat{P}_{f_n}^{M} (1-\hat{P}_{f_n})^{N-M}, \tag{5.17}$$

$$P_m{}^{(MJ)} = 1 - \sum_{M=\lfloor N/2 \rfloor}^{N} \binom{N}{M} \hat{P}_{m_n}^{N-M} (1-\hat{P}_{m_n})^{M}, \tag{5.18}$$

where $\binom{N}{M}$ is the binomial coefficients, $\hat{P}_{f_n}$ and $\hat{P}_{m_n}$ are given in (5.16).

Proof: With the majority decision rule, a false alarm happens if $\lfloor N/2 \rfloor$ or more SUs have false alarm after the FC detection. The number of SUs with false alarm at the FC can be modeled with a binomial distribution with parameters N and $\hat{P}_{f_n}$. Based on the probability mass function (PMF) of a binomial random variable, we can get the global false alarm probability as in (5.17). The probability of missing can be calculated in a similar manner. ■

The probabilities for the OR decision rule can be obtained by replacing $\lfloor N/2 \rfloor$ in (5.17) with 1, since a single $\hat{x}_n(k)$ is sufficient for the FC to make a decision in favor of 1. The results are summarized as follows.

Corollary 5.1: If the SUs experiences independent and identical channels, then the probabilities of global false alarm, P_f, and missing, P_m, of the proposed cooperative spectrum sensing system with the OR data fusion rule can be calculated as

$$P_f{}^{(OR)} = 1 - (1 - \hat{P}_{f_n})^N, \tag{5.19}$$

$$P_m{}^{(OR)} = \hat{P}_{m_n}^N, \tag{5.20}$$

where $\binom{N}{M}$ is the binomial coefficients, $\hat{P}_{f_n}$ and $\hat{P}_{m_n}$ are given in (5.16).

5.5 Numerical Results

Numerical results are presented in this section to evaluate the performance of the proposed cooperative sensing algorithm. In the simulation, the time-bandwidth product is $u = 5$. The traffic pattern of the PU follows a two-state Markov chain with transition probabilities $\{p_{00} = 0.8 \text{ and } p_{10} = 0.3\}$. The SNR between the PU and the SU is assumed to be $\gamma_s = 10$ dB. In the progressive MAP decision rule, the size of the sliding window is $K = 100$.

Fig. 5.3 shows the global P_f and P_m as a function of the normalized threshold. There are $N = 5$ SUs in the network. The SNR between the SU and the FC is $\gamma_T = 5$ dB. The FC performs detection of the signals from the SUs with the new progressive MAP algorithm. Both the OR and majority data fusion rules are applied to the detection results. Excellent agreement is observed between the analytical and simulation results. It should be noted that the analytical results are obtained under the assumption of perfect *a priori*

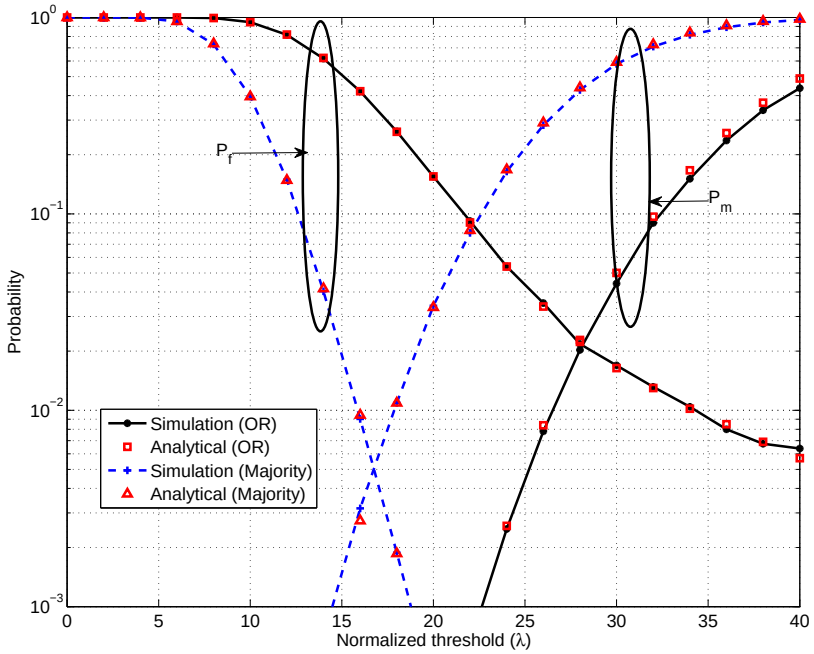

Figure 5.3: Comparison between the analytical and simulated P_f and P_m.

information. The results indicate the newly proposed progressive algorithm can obtain a very accurate estimation of the *a priori* probabilities. In addition, as expected, the majority rule is better than the OR rule in terms of P_f, and the relationship is reversed for P_m.

Fig. 5.4 compares the performance of the newly proposed progressive MAP algorithm, with the algorithm presented in [6], where the *a priori* probability is estimated by averaging the signals from all the SUs in the spatial domain. The results are presented in Fig. 5.4 in the form of receiver operating characteristics (ROC). There are two SUs in the network, thus the OR fusion rule and the majority fusion rule are the same. The SNR at the second step, γ_T, varies from -10 dB to 10 dB. When the second step SNR is less than or equal to 0 dB, the newly proposed progressive MAP algorithm outperforms the spatial MAP in most of the P_m/P_f regions, except the region with $P_m \approx P_f$, where the spatial MAP slightly outperforms the progressive MAP. As γ_T increases, the differences between the two algorithms gradually

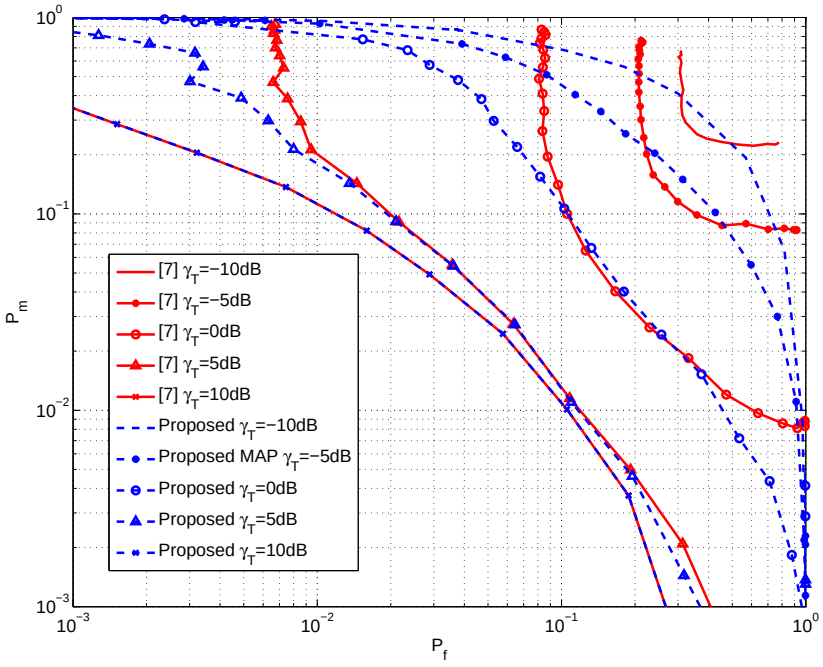

Figure 5.4: ROC performance of the systems with the progressive MAP algorithm.

diminishes. In order to reduce the interference to the PU, the SUs usually have very low transmission power, it is expected that the second step SNR is usually low. Therefore, the proposed progressive MAP algorithm can achieve a better P_m/P_f tradeoff in most of the operation regions.

The performances of the majority and OR data fusion rules are compared in Fig. 5.5. There are three SUs in the network. The FC employs the new progressive MAP algorithm to detect the signals from the SUs. For a given value of the second step SNR γ_T, when the P_f is smaller than a certain threshold (or P_m is larger than a certain threshold), the majority decision rule is better than the OR decision rule. The relationship is reversed when P_f is larger than the threshold. Therefore, the choice between the OR and the majority fusion rules depends on the targeted P_f (or P_m). If the targeted P_f is small, then the majority fusion rule is preferred. The OR fusion rule is preferred when the targeted P_m is small. In

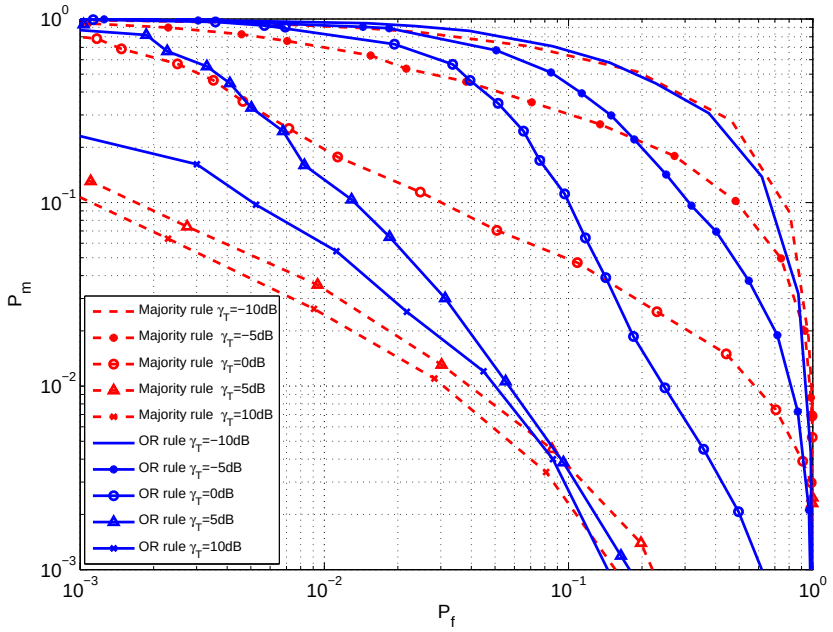

Figure 5.5: ROC performances of the systems with the OR data fusion rule and the majority data fusion rule.

addition, the P_f threshold decreases as γ_T increases. At $\gamma_T = 10$ dB, the majority fusion rule outperforms the OR fusion rule over all the operation ranges shown in the figure. Therefore, when the second step SNR is high, the majority decision rule can usually lead to a better performance.

5.6 Conclusions

A new cooperative spectrum sensing algorithm was proposed for a cognitive radio network. The algorithm was developed by exploiting the PU's statistical transmission pattern, which was modeled with a two-state Markov chain. With the new algorithm, the *a priori* probabilities of the information from the SUs were obtained at the FC by progressively estimating the transition probabilities of a Markov chain, and this led to a progressive MAP detection algorithm. Analytical expressions were derived for the error probabilities of the progressive

MAP detection, and the global probabilities of false alarm and missing detection with the majority and OR data fusion rules. It was observed through numerical results that the new progressive MAP detection improved the performance of existing spectrum sensing algorithms. In addition, when the SNR at the FC was high, the majority data fusion rule outperformed the OR data fusion in terms of both probabilities of false alarm and missing.

5.7 References

[1] Federal Communications Commission, "Spectrum policy task force report,"Nov. 2002

[2] J. Mitola and G. Maguire, "Cognitive radio: Making software radios more personal," *IEEE J. Personal Commun.*, vol. 6, no. 4, pp. 13 - 18, Aug. 1999.

[3] J. Mitola, "Cognitive radio: An integrated agent architecture for software defined radio," Doctor of Technology, Royal Inst. Technol. (KTH), Stockholm, Sweden, 2000.

[4] S. Haykin, "Cognitive radio: Brain-empowered wireless communications," *IEEE J. Selected Areas Commun.*, vol. 23, no. 2, pp. 201 - 220, Feb. 2005.

[5] A. Sahai, N. Hoven and R. Tandra "Some fundamental limits on cognitive radio," in *Proc. Allerton Conf. Commun., Control, and Computing*, pp. 131 - 136, Oct. 2004.

[6] A. Ghasemi and E. S. Sousa "Collaborative spectrum sensing for opportunistic access in fading environments," in *Proc. IEEE Sym. New Frontiers in Dynamic Spectrum Access Networks*, pp. 131 - 136, Nov. 2005.

[7] T. C. Aysal, S. Kandeepan and R. Piesiwicz "Cooperative spectrum sensing over imperfect channels," in *Proc. IEEE Global Telecommun. Conf. Workshops*, pp. 1 - 5, Dec. 2008.

[8] D. Cabric, A. Tkachenko and R. W. Brodersen, "Experimental study of spectrum sensing based on energy detection and network cooperation," in *Proc. ACM 1st Int. Workshop on Tech. and Policy for Accessing Spectrum (TAPAS)*, Aug. 2006.

[9] Z. Quan and S. Cui, "Optimal linear cooperation for spectrum sensing in cognitive radio networks," *IEEE J. Selected Topics in Signal Processing*, vol. 2, no. 1, Feb. 2008.

[10] K. Liu and Q. Zhao, "Indexability of restless bandit problems and optimality of white index for dynamic multichannel access," *IEEE Trans. Infor. Theory*, vol. 56, no. 11, Nov. 2010.

[11] H. Urkowitz, "Energy detection of unknown deterministic signals," in *Proc. IEEE*, vol. 55, No. 4, pp. 523 - 531, Apr. 1967.

[12] F. F. Digham, M. S. Alouini, and M. K. Simon "On the energy detection of unknown signal over fading channels," in *Proc. IEEE Conf. on Commun.*, pp. 3575 - 3579, May 2003.

[13] J. Wu and G. Zhou, "A new Ultra-low power wireless sensor network with integrated energy harvesting, data sensing, and wireless communication," in *Proc. IEEE Inter. Conf. on Commun.*, June 2011.

[14] S. M. Ross, *Introduction to Probability Models*, 7th Ed., Academic Press, 2007.

Chapter 6

Cooperative Spectrum Sensing with Slepian-Wolf Coded Cooperations

6.1 Abstract

A new Slepian-Wolf coded cooperation scheme is proposed for a cognitive radio network with two secondary users (SUs) performing cooperative spectrum sensing through a fusion center (FC). Instead of making a hard decision based on the local sensing results, the SUs quantize the measured energy statistics with a Lloyd-Max quantizer, and forward the quantized information to the FC. Due to the wireless nature of the channel, signals transmitted by one SU to the FC will also be observed by the other SU, which can cooperate with the transmitting SU by relaying the observed signals to the FC. Motivated by the fact that the signals observed at the FC and the relay SU are strongly correlated, we propose to perform an asymmetric Slepian-Wolf code at the SU to reduce the amount of cooperation information, thus to improve the cooperation efficiency. To compensate the energy loss due to the redundancy introduced by the coded cooperation, we propose to unequally allocate energy among the coded bits, and this yields better performance compared to conventional equal energy coding schemes. The FC makes a decision of the status of the primary user (PU) by

performing soft combining over the quantized energy statistics from the two SUs. Simulation results demonstrate that the proposed cooperative spectrum sensing scheme operating in practical fading channels can achieve a performance that is almost identical to the ideal case that the SUs can directly perform soft combining of the distortion-free energy statistics.

6.2 Introduction

Cognitive radio (CR) is emerging as one of the most promising techniques for efficient utilization of the precious spectrum resources [1]–[3]. In a CR network, secondary users (SUs) can coexist with primary users (PUs) by sensing the presence of PU signals and only transmitting at time-frequency holes with no PU activities. Therefore, Efficient and reliable spectrum sensing is critical to the proper operation of a CR network [4].

Energy detection is one of the most commonly used spectrum sensing methods given that it does not require the *a priori* knowledge of the PU and has a low complexity. The performance of the energy detection can be improved with the cooperative spectrum sensing, where multiple SUs can cooperate with each other by transmitting their local sensing results to a fusion center (FC) [5]–[9]. In most existing cooperative spectrum sensing schemes [5]–[7], the FC combines hard decisions from the SUs with an OR or majority data fusion rule. The hard combining is simple to implement, but the soft information in the energy statistics is lost due to the 1-bit hard decision at the SUs. A soft combining scheme that directly combines the analog energy statistics from the multiple SUs is proposed in [8], where it is assumed that the FC can have ideal distortion-free observations of the the analog energy statistics. Soft combining with practical channel is considered in [9], where the SUs forward soft analog information to the FC through an additive white Gaussian noise (AWGN) channel. The soft

combining scheme outperforms the hard combining ones at the cost of significantly increased bandwidth requirement between the SUs and the FC.

In this chapter, we propose a new cooperative spectrum sensing scheme with a practical coded cooperation for a CR network with two SUs and one FC. There are three main contributions of the proposed scheme. First, different from existing hard combining or the analog information-based soft combining schemes, the SUs will quantize the measured energy statistics with a Lloyd-Max quantizer, and forward the quantized information to the FC, which then performs soft combining over the quantized information. Second, the SUs forward the quantized information to the FC with a new Slepian-Wolf coded cooperation, where the two SUs transmit not only their own information but also relay each other's information through a coded cooperation. The Slepian-Wolf theorem states that two sources with correlated information can perform encoding separately and still achieve the same performance as the two sources are encoded jointly [10]. The signal transmitted by one SU will be observed by both the FC and the other SU, and this yields two strongly correlated signals at the FC and the receiving SU. The signal correlation can be exploited by an asymmetric Slepian-Wolf code, where the receiving SU can encode the signal from the transmitting SU and relay a compressed version of the signal to the FC. Such a coding scheme can significantly improve the cooperation efficiency by reducing the amount of relay information. Third, we propose to allocate unequal amount of energy among the coded bits to compensate the energy loss due to the redundancy introduced by the coded cooperation. Fading channels are used to model all the communication links in the network. Simulation results show that the proposed scheme can achieve almost the same performance as the analog information-based soft combining scheme with distortion-free SU-FC links.

6.3 System Model

Consider a CR network with one PU and two SUs as shown in Fig. 6.1. Signals transmitted by the PU are received by the SUs. There are two hypotheses about the state of the PU: idle ($\mathcal{H}_0$) or busy ($\mathcal{H}_1$). Correspondingly, the signals observed by the n-th SU can be represented as

$$\begin{aligned} \mathcal{H}_0 &: r_n(t) = v_n(t), \quad n = 1, 2, \\ \mathcal{H}_1 &: r_n(t) = h_{pn}(t)s(t) + v_n(t), \quad n = 1, 2, \end{aligned} \tag{6.1}$$

where $s(t)$ is the band-limited signal from the PU with an one-sided bandwidth W, $v_n(t)$ is the additive white Gaussian noise (AWGN) with an one-sided power spectral density N_{nv}, $r_n(t)$ is the signal received by the n-th SU, and $h_{pn}(t)$ represents the fading coefficient between the PU and the n-th SU.

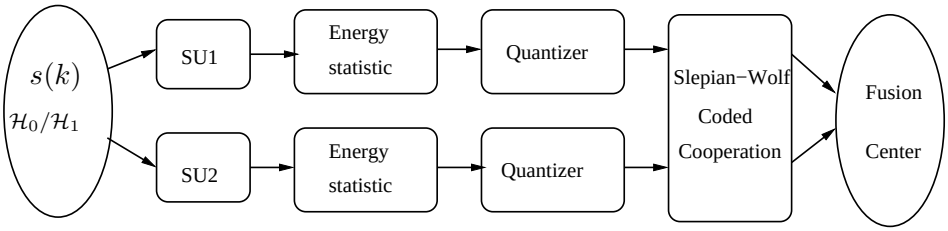

Figure 6.1: System model of a cooperative spectrum sensing in cognitive radio networks

The SU performs energy measurement of the received signals during an interval of duration T. It is assumed that the state of the channel does not change within T. The n-th SU can obtain an energy statistic during the k-th detection interval by passing the received signal, $r_n(t)$, through a square law device and a finite time integrator, which yields

$$S_n(k) = \frac{1}{N_{0v}} \int_{(k-1)T}^{kT} |r_n(t)|^2 dt = \sum_{i=1}^{2u} \left(\frac{r_{ni}}{\sqrt{N_{0v}W}} \right)^2, \tag{6.2}$$

where $u = TW$ denotes the time bandwidth product, with W being the one-sided bandwidth of the signal, and $r_{ni} = r_n(\frac{i}{2W})$ is the received signal sample.

The energy statistic has the following distributions [12]

$$S_n(k) \sim \begin{cases} \chi^2_{2u}, & \mathcal{H}_0, \\ (1+\gamma_{sn})\chi^2_{2u}, & \mathcal{H}_1, \end{cases} \tag{6.3}$$

where χ^2_{2u} denotes the central chi-square distribution with $2u$-degree of freedom, $\gamma_{sn} = \frac{E_0}{N_{nv}}$ is the signal-to-noise ratio (SNR) at the SU, and $E_0 = \int_0^T |h_{pn}(t)s(t)|^2 dt$ is the signal energy.

Most existing cooperative sensing schemes make a hard decision of the PU's state at the SU by comparing $S_n(k)$ to a predefined threshold. The hard decision is then modulated and transmitted to the FC, which makes a final decision on the state of the PU by collecting hard decisions from all the SUs. Making binary decisions at the SU will lose the soft information contained in $S_n(k)$. The soft information can be used by the FC to further improve the sensing performance.

A soft combining scheme has been proposed in [8], which combines $S_n(k)$ from all the SUs, as

$$S(k) = \sum_{n=1}^{N} \frac{\gamma_{sn}}{1+\gamma_{sn}} S_n(k), \tag{6.4}$$

where γ_{sn} is the SNR of the signal observed by the n-th SU, and N is the number of SUs. The soft combining scheme assumes a distortion-free channel between the SUs and the FC, such that the FC can have ideal knowledge of the analog energy statistics, $S_n(k)$.

In practical systems, the SUs usually communicate with the FC through wireless links, which introduce fading and noise to the signals received by the FC. The fading and noise in the channel will introduce significant distortions to the signals observed at the FC. Therefore, it is undesirable to directly transmit the analog information, $S_n(k)$, to the FC.

In order to take advantage of the soft combining in a system with practical channels between the SUs and the FC, we propose to quantize the energy statistics, $S_n(k)$, at the SUs, and then deliver the quantized digital information to the FC. A new Slepian-Wolf Cooperation scheme is proposed in this chapter for the efficient transmission and detection of the quantized energy statistics, and details are given in the next section. It will be shown with simulation that the proposed method with quantized information transmission in a wireless link can achieve a performance that is almost identical to a system with analog information transmitted in a distortion-free link.

The quantization of $S_n(k)$ is performed through a Lloyd-Max quantizer [11] at the SU. The construction of the Lloyd-Max quantizer requires the *a priori* knowledge of the distribution of $S_n(k)$. If the *a priori* probability of the state of the PU is known, then the average probability density function (pdf) of $S_n(k)$ can be expressed by

$$f_{_{S_n}}(x) = P_0 f(x; 2u) + (1-P_0)\frac{1}{1+\gamma_{sn}} f\left(\frac{x}{1+\gamma_{sn}}; 2u\right), \tag{6.5}$$

where P_0 is the probability that the PU is idle, $f(x; 2u)$ is the pdf of a χ^2-distributed random variable (RV) with $2u$-degree of freedom. The pdf in (6.5) can then be used to formulate the Lloyd-Max quantizer.

The pdf in (6.5) requires the knowledge of the *a priori* probability P_0, which might not be readily available at the SU. Simulations indicate that quantizing with $f(x; 2u)$ lead to a performance that is very close to the optimum result obtained by using the true pdf $f_{_{S_n}}(x)$. Therefore, the pdf $f(x; 2u)$ under the null hypothesis is used in this chapter to quantize the signal.

Assume the quantization level is 2^m. The quantized information at the n-th SU can

be represented by $Q[S_n(k)] = \mathbf{b}_n(k) = [b_{n1}(k), \cdots, b_{nm}(k)]^T \in \mathcal{B}^{m\times 1}$, where $Q[x]$ is the Lloyd-Max quantization operator, $\mathbf{a}^T$ is the transpose of the vector $\mathbf{a}$, and $\mathcal{B} = \{0, 1\}$. The FC obtains an estimate of the quantized information, $\hat{\mathbf{b}}_n(k)$. The quantized information recovered at the FC is converted back to the analog domain as $\hat{S}_n(k) = Q^{-1}[\hat{\mathbf{b}}_n(k)]$, which can then be used in (6.4) to obtain the soft combined energy statistic $\hat{S}(k)$.

The hard decision on the PU's state is obtained at the FC by comparing $\hat{S}(k)$ to a predefined threshold, $\mu(k)$. The PU is detected as busy if $\hat{S}(k) > \mu(k)$ and idle otherwise. Similar to [8], the threshold, $\mu(k)$, is calculated for a given probability of false alarm. The soft combining described in (6.4) maximizes the probability of detection under a fixed false alarm probability.

6.4 A New Slepian-Wolf Coded Cooperation for Spectrum Sensing

In this section, we present a new Slepian-Wolf coded cooperation scheme for the efficient and reliable delivery of the quantized information to the FC. The coded cooperation is developed by taking advantage of the wireless links between the SUs.

Due to the wireless nature of the channel and the relative proximity between the two SUs, signals transmitted by one SU to the FC will also be observed by the other SU. Without loss of generality, consider the case that SU n transmits a modulated codeword, $\mathbf{x}_n$, to the FC. The signal is also observed by SU $m \neq n$, which gets an estimate of the signal as $\hat{\mathbf{x}}_n$. The signals, $\mathbf{x}_n$ and $\hat{\mathbf{x}}_n$ are usually not identical due to the distortions of the wireless channel between the two SUs. However, they are strongly correlated. Motivated by this fact, we propose to perform coded cooperation between the two SUs by applying an asymmetric Slepian-Wolf code at the SU m. Therefore, SU m can cooperate with SU n by including a

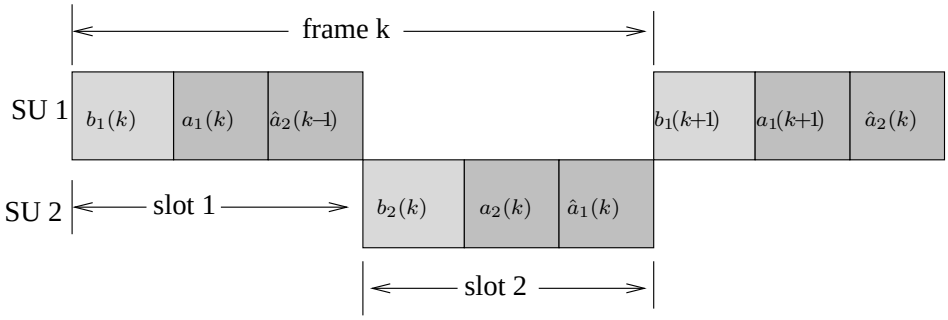

Figure 6.2: The codewords of a practical Slepian-Wolf coded cooperation.

compressed version of $\hat{\mathbf{x}}_n$ in its own signal to the FC. Such a scheme will reduce the amount of information that needs to be delivered to the FC and still achieve a diversity gain due to the cooperation. It should be noted that the Slepian-Wolf theorem is non-constructive, *i.e.*, it only states the existence of the coding scheme, but does not specify how the coding should be performed. In this chapter, we propose a practical Slepian-Wolf cooperation scheme by employing linear block codes on the SUs. The details of the encoding, transmission, and decoding processes are given as follows.

6.4.1 Encoding

The encoding scheme is illustrated in Fig. 6.2 for a system with two SUs. The two SUs transmit to the FC through time division multiple access (TDMA), where each frame of a duration T is divided into two slots with a duration of $\frac{T}{2}$ each. The SU n transmits at the n-th slot of the frame, with $n = 1, 2$. The codewords formed by SUs 1 and 2 at the k-th frame can be represented, respectively, as

$$\mathbf{c}_1(k) = [\mathbf{b}_1^T(k), \mathbf{a}_1^T(k), \hat{\mathbf{a}}_2^T(k-1)]^T, \tag{6.6a}$$

$$\mathbf{c}_2(k) = [\mathbf{b}_2^T(k), \mathbf{a}_2^T(k), \hat{\mathbf{a}}_1^T(k)]^T. \tag{6.6b}$$

In the equations above, $\mathbf{b}_n(k) \in \mathcal{B}^{m\times 1}$ is the quantized energy statistic at the n-th SU, $\mathbf{a}_n(k) = \mathbf{P} \cdot \mathbf{b}_n(k) \in \mathcal{B}^{p\times 1}$ is the parity vector of $\mathbf{b}_n(k)$, with $\mathbf{P} \in \mathcal{B}^{p\times m}$ being a parity generation matrix of a linear block code with a coding rate $m/(p+m)$, and $\hat{\mathbf{a}}_n(k)$ is the cooperation information.

In the proposed Slepian-Wolf cooperation scheme, the cooperation information transmitted by node n is a distorted observation of the parity vector from node $m \neq n$ from the previous slot, *i.e.*, the cooperation information from SU 1 is the estimated parity vector, $\hat{\mathbf{a}}_2(k-1)$, transmitted by SU 2 at the second slot of the $(k-1)$-th frame, and the cooperation information from SU 2 is $\hat{\mathbf{a}}_1(k)$, an estimate of the parity vector transmitted by SU 1 at the first slot of the k-th frame. Even though node n has a distorted observation of the entire codeword from node m, it does not need to forward the entire codeword due to the strong correlation between the distorted codeword and the original information. In the proposed scheme, only the estimated parity bits are forwarded to the FC, and such a scheme reduces the number of bits required for cooperation.

The FC can perform decoding by combining the information from the two SUs. The information vector $\mathbf{b}_n(k)$ can be decoded by using the received signals $\mathbf{b}_n(k)$, $\mathbf{a}_n(k)$, and $\hat{\mathbf{a}}_n(k)$.

6.4.2 Transmission with Unequal Energy Allocation

The cooperation codeword, $\mathbf{c}_n(k)$, will be modulated and amplified before transmitting to the FC. Denote the modulated version of the information vector and parity vector as $\mathbf{s}_n(k) = M[\mathbf{b}_n(k)]$, $\mathbf{p}_n(k) = M[\mathbf{a}_n(k)]$, and $\hat{\mathbf{p}}_n(k) = M[\hat{\mathbf{a}}_n(k)]$, with $M[\mathbf{b}]$ representing the the binary phase shift keying (BPSK) modulation of the binary vector $\mathbf{b}$.

We propose to allocate different energy per bit to the information vector, $\mathbf{s}_n(k)$, and the parity vectors, $\mathbf{p}_n(k)$ and $\hat{\mathbf{p}}_n(k)$. The unequal energy allocation between the information and parity vectors is motivated by the fact that the FC has two distorted observations of the same parity vector due to the Slepian-Wolf cooperation, yet it receives only one copy of the information vector. Therefore, we can allocate less energy to the parity bits to account for the cooperative transmission. The codewords after modulation and energy allocation are

$$\mathbf{x}_1(k)=\left[\sqrt{E_s}\mathbf{s}_1^T(k), \sqrt{E_p}\mathbf{p}_1^T(k), \sqrt{E_p}\hat{\mathbf{p}}_2^T(k-1)\right]^T, \tag{6.7a}$$

$$\mathbf{x}_2(k)=\left[\sqrt{E_s}\mathbf{s}_2^T(k), \sqrt{E_p}\mathbf{p}_2^T(k), \sqrt{E_p}\hat{\mathbf{p}}_1^T(k)\right]^T, \tag{6.7b}$$

where E_s is the energy per information bit, $E_p = \delta E_s$ is the energy per parity bit, with $0 \leq \delta \leq 1$ being the energy allocation factor.

With the energy allocation scheme in (6.7), the effective uncoded energy per information bit can be calculated as

$$E_b = \frac{mE_s + 2pE_p}{m} = E_s\left(1 + \delta\frac{2p}{m}\right). \tag{6.8}$$

The energy allocation factor, δ, can be changed between 0 and 1 to adjust the energy allocation between the information and parity bits. When $\delta = 0$, the scheme degrades to a regular uncoded non-cooperative system.

The codeword, $\mathbf{x}_n(k)$, is transmitted to the FC through a wireless link, and the signal received from the n-th SU is

$$\mathbf{y}_n(k) = h_{nF}(k)\mathbf{x}_n(k) + \mathbf{z}_n(k), \tag{6.9}$$

where $h_{nF}(k)$ is the fading coefficient between the n-th SU and the FC, $\mathbf{z}_n(k)$ is the AWGN with a single-sided power spectral density N_{0z}. The received signal vector at the FC can

be expressed as $\mathbf{y}_n(k) = [\mathbf{y}_{bn}^T(k), \mathbf{y}_{an}^T(k), \mathbf{y}_{\hat{a}n}^T(k_n)]^T$, where $\mathbf{y}_{bn}(k)$, $\mathbf{y}_{an}(k)$, $\mathbf{y}_{\hat{a}n}(k_n)$ are the received signal vectors corresponding to the coded sequence $\mathbf{b}_n(k)$, $\mathbf{a}_n(k)$, and $\hat{\mathbf{a}}_n(k_n)$, respectively, with $k_1 = k-1$ and $k_2 = k$.

6.4.3 Decoding

The FC recovers the quantized information vector, $\mathbf{b}_n(k)$, by decoding over two consecutive slots. The vector $\mathbf{b}_1(k)$ is decoded by using the received information corresponding to $\mathbf{b}_1(k)$, $\mathbf{a}_1(k)$, and $\hat{\mathbf{a}}_1(k)$ from the two slots in the k-th frame. The vector $\mathbf{b}_2(k)$ is decoded by using the received information corresponding to $\mathbf{b}_2(k)$, $\mathbf{a}_2(k)$, and $\hat{\mathbf{a}}_2(k)$, which are from the second slot of frame k and the first slot of frame $k+1$.

The decoding is performed at the FC with a modified message passing algorithm for graph-based codes.

For the received signals corresponding to the information vector, $\mathbf{b}_n(k)$, and the parity vector, $\mathbf{a}_n(k)$, the log-likelihood ratio (LLR) calculated from the channel observations is

$$\boldsymbol{\lambda}_{bn}(k) = -2\frac{\sqrt{E_s}\Re[\mathbf{y}_{bn}(k)h_{nF}^*]}{N_{0z}}, \tag{6.10}$$

$$\boldsymbol{\lambda}_{an}(k) = -2\frac{\sqrt{E_p}\Re[\mathbf{y}_{an}(k)h_{nF}^*]}{N_{0z}}, \tag{6.11}$$

where $\Re[x]$ is the real part operator, and a^* denotes complex conjugate.

The LLR of the parity vector, $\mathbf{a}_n(k)$, can also be calculated from the cooperation information received from SU $m \neq n$, $\mathbf{y}_m(k_m)$, where $k_1 = k-1$ and $k_2 = k$. The LLR calculation of the cooperation information needs to take into consideration of the distortion introduced by the channel between the two SUs. If the bit error rate of the channel between the two

SUs is ϵ, then the LLR of $\mathbf{a}_n(k)$ based on $\mathbf{y}_{\hat{a}m}(k_m)$ can be calculated as

$$\hat{\boldsymbol{\lambda}}_{an}(k) = \ln \frac{\epsilon + (1-\epsilon)\exp\left[-2\frac{\sqrt{E_p}\Re\left[\mathbf{y}_{\hat{a}m}(k_m)h^*_{mF}\right]}{N_{0z}}\right]}{(1-\epsilon) + \epsilon\exp\left[-2\frac{\sqrt{E_p}\Re\left[\mathbf{y}_{\hat{a}m}(k_m)h^*_{mF}\right]}{N_{0z}}\right]}, \tag{6.12}$$

The LLRs of $\mathbf{a}_n(k)$ from both the direct transmission and the cooperative transmission can be combined to obtain an enhanced parity LLR vector, as

$$\tilde{\boldsymbol{\lambda}}_{an}(k) = \boldsymbol{\lambda}_{an}(k) + \hat{\boldsymbol{\lambda}}_{an}(k). \tag{6.13}$$

The initial LLR vector of the linear block code can then be written as $\boldsymbol{\lambda}_n(k) = [\boldsymbol{\lambda}^T_{bn}(k), \tilde{\boldsymbol{\lambda}}^T_{an}(k)]^T \in \mathcal{R}^{(m+p)\times 1}$. The iterative message passing algorithm [13] can be applied by combining the initial LLR vector, $\boldsymbol{\lambda}_n(k)$, and the Tanner graph formulated from the parity check matrix, $\mathbf{H} = [\mathbf{P}, \mathbf{I}_p] \in \mathcal{B}^{p\times(m+p)}$. Details of the iterative message passing algorithm are referred to [13].

The iterative message passing decoding algorithm will be terminated when the syndrome of the codeword becomes 0. The decoded information vector is denoted as $\hat{\mathbf{b}}_n(k)$, which is then converted back to the analog domain as $\hat{S}_n(k) = Q^{-1}[\hat{\mathbf{b}}_n(k)]$ and used in the soft combining operation described in (6.4).

6.5 Simulation Results

Simulation results are presented in this section to demonstrate the performance of the proposed cooperative sensing schemes. In the simulation, the time-bandwidth product is $\mu = 3$. The probability of detection is maximized at a fixed false alarm probability of 0.05.

We first study the impact of energy statistic quantization on the detection probability in

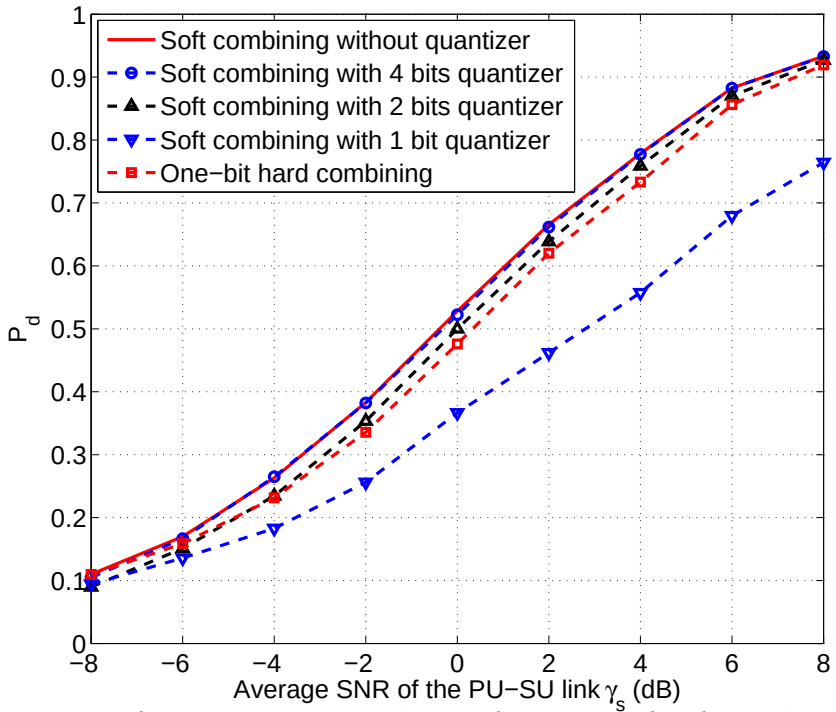

Figure 6.3: Impacts of quantization on the performance of soft combining (ideal SU-FC links).

Fig. 6.3. The probability P_d is shown as a function of γ_s, the SNR of PU-SU links. Error-free communications between the SUs and the FC are assumed in this example to highlight the impacts of quantization, and the effects of channel distortions between the SU-FC links will be considered later. The traditional one-bit hard decision at the SU is also shown for comparison. The simulation results indicate that the soft combining with quantized energy statistics outperforms the traditional hard decision except the 1-bit quantization case. A 4-bit quantization of the energy statistic can achieve exactly the same performance as combining the analog information without quantization. This demonstrates the effectiveness of the Lloyd-max quantizer for the soft combining. Therefore, the 4-bits quantizer is used for the remaining examples.

The next example is used to verify the proposed Slepian-Wolf cooperation with unequal

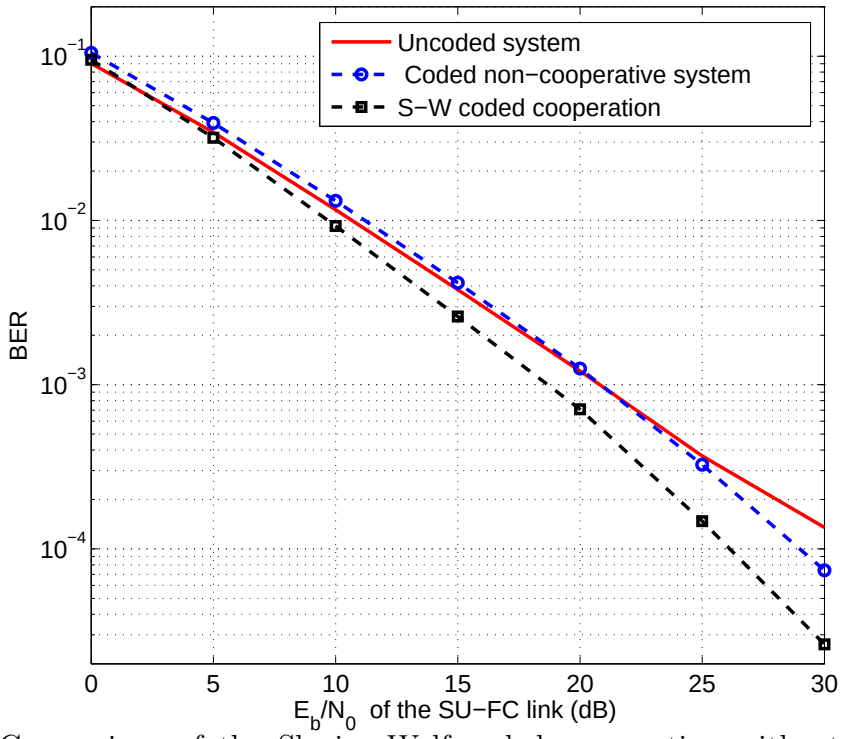

Figure 6.4: Comparison of the Slepian-Wolf coded cooperation with other transmission schemes.

energy allocation. Fig. 6.4 shows the bit error rate (BER) of various system configurations as a function of E_b/N_0 of the SU-FC links. The BER curves of the uncoded systems and the linear block code without cooperation are also shown in the figure for comparison. The (7, 4) Hamming code is used as the linear block code for both the cooperative and coded non-cooperative systems. Rayleigh fading channel is assumed for both the SU-SU link and the SU-FC links. The SNR between the two SUs is 0 dB, which corresponds to an error probability of $\epsilon = 0.08$ for the cooperative link. The energy allocation factor is $\delta = 2/9$. The performance of the coded non-cooperative system is slightly worse than the uncoded system when $E_b/N_0 < 25$ dB because the coding gain is not enough to compensate the energy loss due to the parity bits, and the coding gain is only obvious after $E_b/N_0 \geq 25$ dB. The Slepian-Wolf cooperation with unequal energy allocation has a superior performance than

both the uncoded system and the coded non-cooperative system for all the E_b/N_0 considered. It outperforms the coded non-cooperative system by 2.5 dB at BER = 10^{-4}.

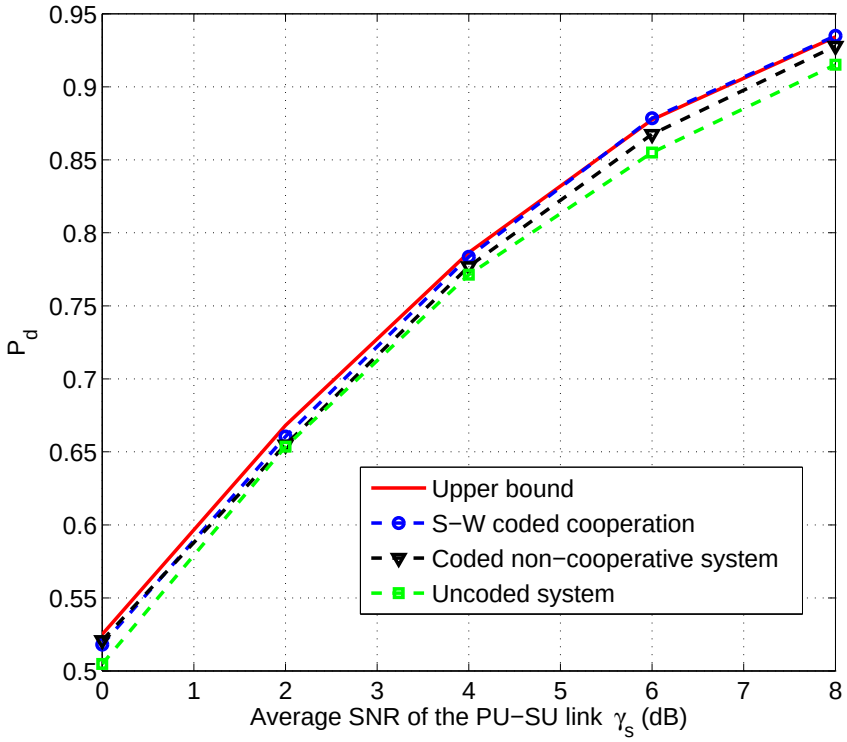

Figure 6.5: Probability of detection with various cooperative spectrum sensing schemes (E_b/N_0 of the SU-FC link is 10 dB).

Fig. 6.5 shows the detection probability at the FC as a function of γ_s, the SNR of the PU-SU link. The E_b/N_0 between the SU-FC link is fixed at 10 dB. The rest of the simulation parameters are the same as in Fig. 6.4. The upper bound shown in the figure is obtained by performing soft combining over unquantized, distortion-free energy statistics. As expected, the proposed Slepian-Wolf cooperation with unequal energy allocation outperforms both the uncoded system and the coded non-cooperative system. The performance of the proposed scheme achieves the upper bound for γ_s>4 dB.

6.6 Conclusion

A new Slepian-Wolf coded cooperation scheme with unequal energy allocation among the coded bits was proposed for a cooperative cognitive radio network. The energy statistics measured at the SUs were quantized with a Lloyd-Max quantizer, and then forwarded to the FC by utilizing the SU-SU link as a cooperation channel. The newly proposed unequal energy allocation among the coded bits can compensate the energy loss due to parity bits introduced by the coded cooperation. A soft combining scheme was employed at the FC to improve the detection probability by combining an estimate of the quantized energy statistics. Simulation results demonstrated that the proposed scheme in practical system configurations with fading and noise in the SU-FC links can achieve a performance that is almost identical to the ideal soft combining with distortion-free SU-FC links and no quantization. The scheme is proposed for a CR network with two SUs, but can be easily extended to networks with more than two SUs by grouping two SUs together for cooperation.

6.7 References

[1] Federal Communications Commission, "Spectrum policy task force report," Nov. 2002

[2] J. Mitola and G. Maguire, "Cognitive radio: Making software radios more personal," *IEEE J. Personal Commun.*, vol. 6, no. 4, pp. 13 - 18, Aug. 1999.

[3] J. Mitola, "Cognitive radio: An integrated agent architecture for software defined radio," Doctor of Technology, Royal Inst. Technol. (KTH), Stockholm, Sweden, 2000.

[4] S. Haykin, "Cognitive radio: Brain-empowered wireless communications," *IEEE J. Selected Areas Commun.*, vol. 23, no. 2, pp. 201 - 220, Feb. 2005.

[5] A. Ghasemi and E. S. Sousa "Collaborative spectrum sensing for opportunistic access in fading environments," in *Proc. IEEE Sym. New Frontiers in Dynamic Spectrum Access Networks*, pp. 131 - 136, Nov. 2005.

[6] T. C. Aysal, S. Kandeepan and R. Piesiwicz "Cooperative spectrum sensing over imperfect channels," in *Proc. IEEE Global Telecommun. Conf. Workshops*, pp. 1 - 5, Dec. 2008.

[7] G. Zhou and J. Wu , "Cooperative spectrum sensing with a progressive MAP detection algorithm," in *Proc. IEEE Global Telecommun. Conf.*, Dec. 2011.

[8] J. Ma, G. Zhao and Y. Li, "Soft combination and detection for cooperative spectrum sensing in cognitive radio networks," *IEEE Trans. on Wireless Commun.*, vol. 7, no. 11, pp. 4502 - 4507, Nov. 2008.

[9] Z. Quan and S. Cui, "Optimal linear cooperation for spectrum sensing in cognitive radio networks," *IEEE J. Selected Topics in Signal Processing*, vol. 2, no. 1, Feb. 2008.

[10] D. Slepian and J. K. Wolf, "Noiseless coding of correlated information sources," *IEEE Tran. Inform. Theory*, vol. 19, no. 4, pp. 471 - 480, July 1973.

[11] S. Lloyd, "Least squares quantization in PCM," *IEEE Trans. on Information Theory*, vol. IT-28, no. 2, pp. 129 - 137, Mar. 1982.

[12] H. Urkowitz, "Energy detection of unknown deterministic signals," in *Proc. IEEE*, vol. 55, No. 4, pp. 523 - 531, Apr. 1967.

[13] A. Goldsmith, *Wireless communications*, 2nd Ed., Cambridge University Press, 2005.

Chapter 7

Conclusions

In this chapter, the main contributions of this dissertation are summarized and the future work directions are proposed and discussed.

7.1 Contributions

In this dissertation, I mainly focused on the energy and spectral efficient wireless communication design and the main contributions can be summarized as follows.

First, in order to improve the energy efficiency in the wireless sensor network designed for SHM system, a unified energy harvesting, sensing, and communication scheme was proposed for the ULP SHM. The IHSC scheme was designed by exploiting the correlation between the harvested energy and vibration intensity. Both the theoretical and simulation results indicated that the proposed system can operate effectively at a SNR as low as -10 dB without battery or external energy sources. As a result, an energy efficient SHM system was realized through the unified process.

Second, a cross layer CT-MAC with message passing detection scheme was proposed in chapter 3. The proposed scheme can effectively resolve the collisions in the MAC layer

by utilizing message passing detection in the PHY layer. Therefore, cross layer design can improve the energy efficiency with multiuser detection in the wireless communication system.

Third, a new cross-layer CT-MAC scheme that operates in frequency-selective fading was proposed. It does not require either MUS or SPS, and is insensitive to timing phase offsets. The collision tolerance is achieved by employing a FD-OOAT. Such a configuration renders a special signal structure that enables multiuser detection (MUD) in the physical layer to resolve the collisions at the MAC layer. Most MUDs in the literature require precise symbol level synchronizations among the users. The proposed scheme, on the other hand, can operate with asynchronous users, and it is insensitive to the timing phase offset between the sampling clocks at the transmitter and receiver with a new time-domain oversampling detector. In addition, oversampling in the time domain and spreading the signal in the frequency domain enable multipath diversity that further improves the system performance. Theoretical analysis is performed to quantify the impacts of multipath diversity and relative user delays on the performance of the system. Both analytical and simulation results demonstrated that significant performance gains are achieved with the proposed scheme, in terms of both the number of users supported and the normalized throughput.

Fourth, to address the spectral efficiency problem, two cooperative spectrum sensing methods were proposed in this dissertation. One was the cooperative spectrum sensing with a progressive MAP detection algorithm. Unlike most previous spectrum sensing algorithms that do not consider the time domain traffic statistics of the PU, the algorithm in this method was developed by exploiting the statistical properties of the PU's transmission pattern. Analytical expressions were derived for the probabilities of false alarm and missing detection, with both the majority data fusion rule and the OR data fusion rule. Both theoretical

analysis and simulation results indicated that the proposed algorithm can provide reliable and efficient spectrum sensing over a large range of system configurations. The other method was cooperative spectrum sensing with Slepian-Wolf coded cooperations. The energy statistics measured at the SUs were quantized with a Lloyd-Max quantizer, and then forwarded to the FC by utilizing the SU-SU link as a cooperation channel. The newly proposed unequal energy allocation among the coded bits can compensate the energy loss due to parity bits introduced by the coded cooperation. A soft combining scheme was employed at the FC to improve the detection probability by combining an estimate of the quantized energy statistics. Simulation results demonstrated that the proposed cooperative spectrum sensing scheme operating in practical fading channels can achieve a performance that is almost identical to the ideal case that the SUs can directly perform soft combining of the distortion-free energy statistics.

7.2 Future Works

Based on the research I have been done so far, some of the future research works are discussed in this section.

First, to further improve the energy efficiency in WSNs, multi-hop transmission should be considered instead of single hop transmission. In [1], they proposed that the most fundamental question for the energy constraint network communication is how to utilize the limited energy to efficiently transmit all the information to the FC such that the energy required to transmit one unit information is minimized. Nodes in the multi-hop WSN need not only to transmit their own information, but also need to relay other nodes' information to the FC. Therefore, the first problem is how to divide the limited power between one's own information and the relay information. Second, how to choose the optimum path for

multi-hop to minimize the routing energy cost. Hence, the efficiency of the entire WSN can be optimized based on solving these two problems.

Second, in cooperative spectrum sensing, a common control channel is used by CR users to transmit their local sensing data to the FC. In most of the literatures, the common control channel is usually assumed to be always available. However, as the number of the CR users in the cognitive networks increases, the bandwidth required by the control channel increases dramatically because CR users need to use an orthogonal media access control (MAC) scheme to transmit their data [2]. Therefore, how to efficiently utilize the limited bandwidth of the control channel to report the local sensing data to the FC is a new challenge in cooperative spectrum sensing.

Finally, another important direction of study is the development of a test bed for cognitive radio systems. The results we have in this dissertation so far are either theoretical analysis or computer simulation. However, the results from test bed will be more practical than what we have so far. Moreover, the problems we will meet in the design of the test bed or algorithm testing period can in turn help modify the developed algorithm. This iteration process will make the design more practical in the applications.

7.3 References

[1] Jingxian Wu and Yahong R. Zheng, "Optimum multi-hop transmission strategies for energy constrained wireless sensor networks," in *Proc. IEEE Intern. Conf. Commun. ICC'12,* Jun. 2012.

[2] X. Zhou, G. Li, D. Li, and C. K. Soong, "Bandwidth efficient combination for cooperative spectrum sensing in cognitive radio networks," in *Proc. IEEE Acoustic Speech and Signal Processing (ICASSP) Conf.*, Mar. 2010.

Vita

Guoqing Zhou received the B.S. (EE) degree from the Shandong University of Science and Technology (SDUST), Qingdao, China, in 2002, the M.S. (EE) from Soongsil University, Seoul, South Korea, in 2008. He is currently a PhD candidate in the Department of Electrical Engineering, University of Arkansas, Fayetteville, USA.

From 2002 to 2006, he was a research engineer in Science & Technology Company of SDUST, Qingdao, China. His research interests include wireless communications, wireless sensor networks and underwater acoustic communications.